Spring 5-2-2018

Characterizing the Heme Uptake Proteins HtaB and ChtB in Corynebacterium diphtheriae

Brandon L. Ferrell
Georgia State University, ferrell.bran2011@gmail.com

CHARACTERIZING THE HEME UPTAKE PROTEINS HTAB AND CHTB IN *CORYNEBACTERIUM DIPHTHERIAE*

by

BRANDON LEE FERRELL

Under the Direction of Dabney K. W. Dixon, PhD

ABSTRACT

Corynebacterium diphtheriae is a Gram-positive, pathogenic bacterium. Pathogenic bacteria require iron as a key nutrient for survival. *C. diphtheriae* utilizes a direct heme uptake system in which the heme binds to a receptor protein that transfers the heme along the pathway to an ABC transporter, which facilitates the transfer of heme into the bacterial cell. This heme uptake pathway is encoded by the *hmu* and *cht* gene loci, which includes the genes for the surface-anchored proteins HtaB and ChtB. HtaB is proposed to have a function in transporting the heme obtained by HtaA to HmuT. ChtB is proposed to have a similar function to that of HtaB. Bioinformatics analysis shows that both HtaB and ChtB contain conserved tyrosine and histidine residues that are consistent with that of HtaA domains. A combination of UV-visible, circular dichroism, resonance Raman, and fluorescence spectroscopy have been used to characterize these proteins further.

INDEX WORDS: Gram-positive bacteria, Heme, HtaA domains, *Corynebacterium diphtheriae*, *Streptococcus pyogenes,* Homology Model, UV-visible, circular dichroism

CHARACTERIZING THE HEME UPTAKE PROTEINS HTAB AND CHTB IN *CORYNEBACTERIUM DIPHTHERIAE*

by

BRANDON LEE FERRELL

A Thesis Submitted in Partial Fulfillment of the Requirements for the Degree of

Master of Science

in the College of Arts and Sciences

Georgia State University

2018

CHARACTERIZING THE HEME UPTAKE PROTEINS HTAB AND CHTB IN *CORYNEBACTERIUM DIPHTHERIAE*

by

BRANDON LEE FERRELL

Committee Chair: Dabney W. Dixon

Committee: Donald Hamelberg

Kathryn Grant

Electronic Version Approved:

Office of Graduate Studies

College of Arts and Sciences

Georgia State University

Spring 2018

DEDICATION

I dedicated this thesis to my family, especially my mother and father. Without their support and constant motivation, I would not have been able to achieve this type of accomplishment.

ACKNOWLEDGEMENTS

I would like to acknowledge my lab mates: Stephanie Thompson, Dr. Elizabeth Draganova, Cyrianne Ketchua, Carly Wieting, Robby Kirby, Amaris Aguillon, Catherine Odhiambo, and Naema Daino. All of your encouragement and support has encouraged me to keep pushing and strive for success. I could not have asked for better lab mates. I would also like to acknowledge Dr. Rizvan Uluisik. I truly appreciate the way you pushed me to learn and develop into the lab member that I have become. Lastly, I would like to acknowledge my mentor, Dr. Dabney White Dixon. I have never had a professor that was so involved with his or her students. I truly appreciate all the knowledge and values that you have taught to not only me but also all the members of the lab. I am a better student and scientist because of your constant pushing and telling us how much potential we have. Thank you for always believing in me.

TABLE OF CONTENTS

DEDICATION ..... **VIII**

ACKNOWLEDGEMENTS ..... **V**

LIST OF TABLES ..... **XI**

LIST OF FIGURES ..... **XII**

1 CHAPTER 1: INTRODUCTION **1**

1.1 Heme and Heme Sources **1**

1.2 Heme Uptake in Gram-positive Bacteria **4**

1.3 Heme Uptake in *Streptococcus pyogenes* **4**

1.4 Heme Uptake in *C. diphtheriae* **6**

1.4.1 C. diphtheriae hmu Gene Cluster ***6***

1.4.2 Proposed Mechanism of hmu Heme Uptake ***7***

1.4.3 C. diphtheriae Heme Source Utilization ***7***

1.5 Lac Promoter and Protein Expression **9**

1.6 Thesis Goals **11**

2 CHAPTER 2: BIOINFORMATIC STUDIES OF HTAB AND CHTB **16**

2.1 Introduction **16**

2.1.1 Bioinformatics Studies of Corynebacterium diphtheriae ***16***

2.1.2 Literature Studies of HtaA Domains ***16***

2.1.3 Structure of NEAT Domains ***17***

2.2 Materials and Methods 19

2.2.1 Sequence Alignments 19

2.2.2 Gram-Positive Bacteria BLAST Search 19

2.2.3 Homology Modeling 19

2.3 Results and Discussion 19

2.3.1 Sequence Alignments 19

2.3.2 SXXXY Conserved Motif 21

2.3.3 FXGH Conserved Motif 22

2.3.4 FXXXY Conserved Motif 22

2.3.5 Gram-Positive Bacteria BLAST Search 23

2.3.6 Homology Modeling 23

3 CHAPTER 3: EXPERIMENTAL CHARACTERIZATION OF THE HTAB HEME UPTAKE PROTEIN IN CORYNEBACTERIUM DIPHTHERIAE 34

3.1 HtaB 34

3.2 Materials and Methods 35

3.2.1 General 35

3.2.2 Expression and Purification 35

3.2.3 HtaB-WT Sire Directed Mutagenesis 37

3.2.4 UV-visible Absorption Spectroscopy 38

3.2.5 Determination of Percent Heme-loaded and Soret Extinction Coefficients 39

3.2.6 CD Spectroscopy of HtaB-WT and Mutants 40

3.2.7 Heme Transfer Between Y56A and Hemoglobin 40

3.2.8 Heme Titration of HtaB and Mutants 40

3.2.9 Resonance Raman Spectroscopy 41

3.2.10 Thermal Unfolding in the Presence of GdnHCl 42

3.2.11 Time Scale Unfolding of HtaB in the Presence of 4.0 M GdnHCl 42

3.3 Results and Discussion 43

3.3.1 HtaB and Mutants Growth and Expression 43

3.3.2 UV-visible Spectroscopy of HtaB-WT and Mutants 44

3.3.3 Determination of Percent Heme Loading and Soret Extinction Coefficient 44

3.3.4 CD Spectroscopy of HtaB-WT and Mutants 45

3.3.5 Hemoglobin Heme Transfer to HtaB-Y56A 46

3.3.1 HtaB Hemin Titration 46

3.3.2 Resonance Raman of Ferric HtaB-WT 48

3.3.3 Resonance Raman of Ferrous Carbonyl HtaB-WT 49

3.3.4 Thermal Unfolding in the Presence of GdnHCl 50

3.3.5 Time Scale Unfolding of HtaB in the Presence of 4.0 M GdnHCl 51

***4* CHAPTER 4: EXPERIMENTAL CHARACTERIZATION OF THE CHTB HEME UPTAKE PROTEIN IN *CORYNEBACTERIUM DIPHTHERIAE* 82**

4.1 *ChtB in Corynebacterium diphtheriae* 82

4.2 Materials and Methods 83

4.2.1 Expression and Purification 83

4.2.2 Spectroscopy: UV-visible and Circular Dichroism 84

4.2.3 Determining Percent Heme Loading 84

4.2.4 Resonance Raman Spectroscopy 85

4.2.5 ChtB pH Titration 85

4.2.6 Heme Transfer between ChtB and HtaB 86

4.2.7 Thermal Unfolding in the Presence of GdnHCl 86

4.2.8 Time Scale Unfolding in the Presence of 4.0 M GdnHCl 87

4.2.9 Fluorescence of GdnHCl-induced Unfolding of ChtB 87

4.3 Results and Discussion 89

4.3.1 ChtB Expression and Purification 89

4.3.2 UV-Visible Spectroscopy of ChtB 89

4.3.3 Determination of Percent Heme Loading 89

4.3.4 Resonance Raman of ferric ChtB 90

4.3.5 Resonance Raman of ferrous ChtB 91

4.3.6 Resonance Raman of ferrous carbonyl ChtB 91

4.3.7 pH Titration of ChtB 92

4.3.8 Heme Transfer between ChtB and HtaB 92

4.3.9 CD Spectroscopy 93

4.3.10 Time Scale Unfolding in the Presence of GdnHCl..... 93

4.3.11 Thermal Unfolding in the Presence of GdnHCl..... 94

4.3.12 GdnHCl-induced Unfolding of ChtB 95

5 GENERAL CONCLUSIONS 109

REFERENCES..... 111

LIST OF TABLES

Table 3.1 HtaB Mutant Primers 80

Table 3.2 PCR reaction mixtures of lanes 1-5 from HtaB-Y56A agarose gel. 81

LIST OF FIGURES

Figure 1.1 Structure of heme b. 12

Figure 1.2 Overview of the S. pyogenes Sia/Hts heme uptake pathway. 13

Figure 1.3 Schematic of the hmu and cht gene clusters in C. diphtheriae. Taken from {Allen, 2009 #3638;Allen, 2013 #232}..... 14

Figure 1.4 Heme uptake pathway in C. diphtheriae..... 15

Figure 2.1 Blast search showing which strains of C. diphtheriae contain the proteins encoded in the hmu and cht gene loci. Data from columns HtaA-CR1, HtaA-CR2, and ChtB-CR are from {Allen, 2013 #232}. The asterisk (*) the presence of HtaA that contains point mutations with unknown functional status. 25

Figure 2.2 Crystal structure of IsdX2 NEAT-5 domain from B. anthracis. Protein Data Bank code 4H8P {Honsa, 2013 #1135}..... 26

Figure 2.3 Multiple sequence alignment of the conserved regions of HtaA proteins from related species with the conserved regions of HtaB, ChtB, and ChtA. The diagram includes C. ulcerans (Cu), C. tuberculostearicum (Ctb), C. jeikeium (Cj), C. pseudodiphtheriticum (Cpd), C. propinquum (Cp), C. striatum (Cst), C. singular (Csi), C. aurimucosum (Ca), C. glutamicum (Cg). 28

Figure 2.4 Circular phylogenetic tree demonstrating the relationship of 20 HtaA domains with those of HtaB, ChtB, and ChtA. The tree was run from HtaA-CR1. The diagram includes C. ulcerans (Cu), C. tuberculostearicum (Ctb), C. jeikeium (Cj), C. pseudodiphtheriticum (Cpd), C. propinquum (Cp), C. striatum (Cst), C. singular (Csi), C. aurimucosum (Ca), C. glutamicum (Cg). 29

Figure 2.5 The signature sequence characteristics of HtaA and NEAT domains are shown below. The residues that are both underlined and bolded are the respective heme axial ligands. 30

Figure 2.6 Overview of medically important gram-positive bacteria and their heme uptake strategies. The numbers in parenthesis refer to the number of results obtained from the BLAST search with a HtaA (red) or NEAT (blue) sequence. 31

Figure 2.7 Homology model of WT HtaB-CR. The model was constructed from gp39 in marine virus Syn5 (PDB: 4BML). 32

Figure 2.8 Homology model of WT ChtB-CR. The model was constructed from UspA1 in Moraxella catarrhalis (PDB: 4BML). 33

Figure 3.1 Hemoglobin binding to various hmu gene proteins. Taken from {Allen, 2011 #2147}. 52

Figure 3.2 Heme transfer between HtaA and HtaB. Taken from {Allen, 2011 #2147}..... 53

Figure 3.3 The sequence of the conserved domain of HtaB as supplied by Dr. Michael Schmitt. The strep tag sequence is underlined and bolded..... 54

Figure 3.4 Comparing the protein yield of HtaB-WT, HtaB-Y56A, and HtaB-H121A..... 55

Figure 3.5 Agarose gel of the PCR reaction of HtaB Y56A. Lanes corresponding to the five reactions in Table A are shown..... 56

Figure 3.6 DNA sequence alignment of wild type HtaB-CR and the HtaB-CR H121A mutant in the forward direction. The missing stars represent the mutation in the seventh row (CAT = His, GCG = Ala). Clustal Omega was used for the alignment {Sievers, 2011 #24708;Li, 2015 #24686}..... 57

Figure 3.7 The optical densities at 600 nm for the growth of HtaB-containing cells with no glucose are plotted as a function of time. The three data points represent triplicate runs. 58

Figure 3.8 The optical densities at 600 nm for the growth of HtaB-containing cells with 0.3% glucose are plotted as a function of time. The three data points represent triplicate runs. 59

Figure 3.9 Absorbance as fraction collected of strep-tagged HtaB-WT purified on a StrepTactin column. HtaB-WT is seen as a peak between 42-50 mL. The FPLC was run at 4 °C with a linear gradient of buffer B (0-100%). 60

Figure 3.10 Absorbance as fraction collected of strep-tagged HtaB Y56A purified on a StrepTactin column. HtaB Y56A is seen as a peak between 84-92 mL. The FPLC was run at 4 °C with a linear gradient of buffer B (0-100%). 61

Figure 3.11 Absorbance as fraction collected of strep-tagged HtaB H121A purified on a StrepTactin column. HtaB H121A is seen as a peak between 56-66 mL. The FPLC was run at 4 °C with a linear gradient of buffer B (0-100%). 62

Figure 3.12 SDS PAGE gel of WT HtaB-CR confirms a molecular weight of ~ 32 kDa. The first two lanes consist of protein ladders, and lanes 3-5 consist of purified strep-tagged HtaB. The big bands in the second lane represent proteins with masses of 68 kDa and 26 kDa. 63

Figure 3.13 The UV-visible spectra of HtaB-WT, Y56A, and H121A. The absorbances at 280 nm have been normalized to 1.0. All spectra were taken in buffer A. 64

Figure 3.14 Comparing the heme-loading of HtaB-WT, HtaB-Y56A, and HtaB-H121A. 65

Figure 3.15 Circular dichroism spectra of HtaB-WT, Y56A, and H121A. All spectra were an average of 20 scans in buffer A. 66

Figure 3.16 The UV-visible spectra of 40 μM HtaB Y56A are shown before and after incubation overnight at 4 °C with 100 μM hemoglobin. The spectra were normalized to 1.0 at 280 nm. 67

Figure 3.17 Absorbance versus wavelength of a solution of HtaB-WT with the indicated ratio of hemin added. The spectra were taken in buffer A. 68

Figure 3.18 The ratio of the absorbances at 365 nm and 406 nm of WT HtaB as a function of the ratio of hemin to WT HtaB. 69

Figure 3.19 Absorbance versus wavelength for the two cuvette heme titration of HtaB Y56A up to a heme:protein of 0.74. The spectra are normalized to 1.0 at 280 nm. All spectra were taken in buffer A. 70

Figure 3.20 The absorbance at the Soret is plotted as a function of the ratio of the concentration of heme to the concentration of HtaB-Y56A. The titration is performed until a heme:protein of 0.74. 71

Figure 3.21 Absorbance versus wavelength of the two cuvette heme titration of HtaB-H121A with the indicated ratio of hemin added. The spectra were normalized to 1.0 at 280 nm. The spectra were taken in buffer A. 72

Figure 3.22 The Abs_{365}:Abs_{Soret} is plotted as a function of the ratio of the concentration of heme to the concentration of HtaB-H121A. The titration is performed until a heme:protein of 0.65..... 73

Figure 3.23 UV-visible spectra of as-isolated His-tagged HtaB overlaid with increasing titrations of hemin. The spectra represent the different equivalents of heme. All spectra are normalized to 1.0 at 280 nm and taken in buffer A. 74

Figure 3.24 Ferric high-frequency rR of HtaB as a function of pH. Glycine (pH 9.6, black), Tris-HCl (pH 8.8, red and 8.0, blue), and phosphate (pH 5.8, green) buffers at 100 mM were used. Resonance Raman scattering was excited with 413.1-nm emission from a Kr^+ laser

using ten mW of power. The assignments are made by analogy with other heme proteins. 75

Figure 3.25 Resonance Raman spectra of the heme carbonyls of HtaB-WT. Raman scattering was excited using 413.1-nm emission from a Kr+ laser; 5.7 mW. Natural-abundance HtaB−CO (top), HtaB−13CO (middle) and 12CO−13CO difference (blue, bottom) spectra are shown in the νFe−CO, δFeCO, and νC−O regions. Bands in the low-frequency region were fit using Gaussian peak functions (gray). These bands were used to calculate the red difference spectrum superimposed on the blue points in the bottom left spectrum. The bands sensitive to 13CO substitution are labeled with their respective mode designations. Spectra were recorded at pH 8.8. Inset: UV-visible absorbance spectrum of HtaB−CO. 76

Figure 3.26 Resonance Raman correlation plot showing the frequency of the iron-carbon bond stretching as a function of the frequency of the carbon-oxygen bond stretching. Data courtesy of Dr. Kenton Rodgers and Dr. Gudrun Lukat-Rodgers. The two forms of HtaB-CO are shown as filled red stars while the two forms of ChtB-CO are shown as filled green stars. HmuT and mutants of HmuT are shown as unfilled blue stars {Draganova, 2015 #35;Draganova, 2016 #24521}; catalase as a blue hexagon {Hu, 1992 #2357}; SmHasA(WT), SmHasA(H83A), SmHasA(H32A) as magenta circles {Lukat-Rodgers, 2008 #1866}. The data for HRP (grey triangle) and globins (grey squares) have been previously compiled {Lukat-Rodgers, 2008 #1866}. The dotted line is the least squares fit for six-coordinate heme carbonyls in which the proximal ligands is a neutral imidazole from a histidine residue {Smulevich, 1988 #207;Lukat-Rodgers, 2008 #1866;Streit, 2010 #1629}. The solid blue line represents a compilation of heme proteins in which the ligand

trans to CO is coordinated through an oxygen atom that is hydrogen bonded to an arginine residue via two hydrogen bonds {Hu, 1992 #2357;Draganova, 2015 #35}. The solid magenta line is the least squares fit for six-coordinate Fe-CO adducts which are coordinated through an O atom having a single hydrogen bond to histidine or tyrosine {Lukat-Rodgers, 2008 #1866}..... 77

Figure 3.27 Absorbance at 410 nm as a function of temperature for the ChtB and HtaB conserved regions (CR). Experiments were performed in 1 M GdnHCl in buffer A. The line is a fit to the equation described in Section 3.2.10. 78

Figure 3.28 Absorbance at 409 nm versus time of the ChtB and HtaB conserved regions (CR) at 25 °C. Experiments were performed in 4 M GdnHCl in buffer A pH 8.0. The line is a fit to the equation described in Section 3.2.11. 79

Figure 4.1 The sequence of the conserved domain of ChtB as supplied by Dr. Michael Schmitt. The strep tag sequence is underlined and bolded..... 96

Figure 4.2 Absorbance as fraction collected of strep-tagged ChtB-WT purified on a StrepTactin column. ChtB-WT is seen as a peak between 85-95 mL. The FPLC was run at 4 °C with a linear gradient of buffer B (0-100%). 97

Figure 4.3 SDS PAGE of ChtB-WT after purification. Lane 1 consists of the protein ladder. Lane 2 contains both BSA (67 kDa) and myoglobin (17 KDa). Lanes 3-4 consist of varying concentrations of ChtB after purification. 98

Figure 4.4 The spectra of as-isolated HtaA-CR2, HtaB-CR, and ChtB-CR overlaid. These spectra are normalized to 1.0 at the Soret. The spectra were taken buffer A at room temperature. 99

Figure 4.5 Ferric high-frequency rR of ChtB as a function of pH. Tris-HCl (pH 8.8, blue and 8.0, red) and phosphate (pH 5.8, green) buffers at 100 mM were used. The excitation wavelength from 413.1 nm from Kr ion laser with 11.4 mW of power. The $\nu_{C=C}$ band shifts under the ten band as the pH is decreased indicating a change in the interactions between the vinyl groups and the heme pocket. 100

Figure 4.6 Resonance Raman spectra of the ferrous carbonyls of WT ChtB with conditions and interpretation as described in the legend of Figure 3.25. 101

Figure 4.7 SDS PAGE of HtaB-WT and ChtB-WT after the heme transfer experiment. ChtB-WT is in lanes 2-3, and HtaB is in lanes 4-5. 102

Figure 4.8 Absorbance versus wavelength of a solution of heme-loaded ChtB-WT before and after incubation with as-isolated HtaB-WT. The spectra were taken in buffer A. 103

Figure 4.9 Absorbance versus wavelength of a solution of as-isolated HtaB-WT before and after incubation with heme-loaded ChtB-WT. The spectra were taken in buffer A. 104

Figure 4.10 Circular dichroism spectra of as-isolated ChtB-WT and HtaB-WT normalized to -20 mdeg at 215 nm. The spectra are an average of 20 scans taken in buffer A. 105

Figure 4.11 CD spectra of ChtB-WT before and after heme loading. The spectra are an average of 20 scans taken in buffer A. 106

Figure 4.12 Tryptophan emission of as-isolated ChtB (30% heme loaded) as a function of GdnHCl concentration. The reaction was in 100 mM Tris-HCl, 150 mM NaCl, pH 8.0. The data points were recorded after chemical equilibration (10 min). Solid points represent the fluorescence intensity at the respective concentration of GdnHCl. The data were fit using the equation described in Section 4.2.9. 107

Figure 4.13 Tryptophan emission of fully heme-loaded ChtB as a function of GdnHCl concentration. The reaction was in 100 mM Tris-HCl, 150 mM NaCl, pH 8.0. The data points were recorded after chemical equilibration (10 min). Solid points represent the fluorescence intensity at the respective concentration of GdnHCl. The data were fit using the equation described in Section 4.2.9. 108

1 CHAPTER 1: INTRODUCTION

1.1 Heme and Heme Sources

Heme plays an important part in pathogenic bacterial life (Anzaldi and Skaar, 2010; Braun and Hantke, 2011; Benson and Rivera, 2013). The iron coordinated within the tetrapyrrole ring gives heme its reactivity and enables utilization of this transition metal as a cofactor for enzymes involved in various processes including cellular respiration, signal transduction, and oxygen transport (Farrand and Skaar, 2014). Although necessary for cellular growth, free heme can be damaging to many components of the cell. Free heme can oxidize lipids, which leads to the damage of membrane bilayers and organelles (Farrand and Skaar, 2014). Hydrogen peroxide may interact with free heme to generate reactive oxygen species that can oxidize proteins, causing protein degradation. Binding of heme to proteins prevents free heme from causing cellular damage.

Three main types of heme are biologically relevant: heme *a*, heme *b*, and heme *c*. The core structure of these heme molecules is the same. They each have a protoporphyrin ring system composed of four aromatic pyrrole rings connected by methine bridges. Each pyrrole contains a single methyl group extending outwards. All hemes have two propionic acids attached to two of the pyrrole groups. The groups attached to the remaining two pyrrole groups determined the identity of the heme. Heme *a* contains a methyl group on one of the pyrrole rings that has been oxidized to a formyl group and an isoprenoid chain group attached to one of the vinyl side chains. Heme *b*, the most common (Figure 1.1), contains a methyl group on one of the remaining pyrrole rings and a vinyl group on the other. Heme *c* differs from both heme *a* and *b* in that it is covalently linked to a protein through two thioester linkages on two of the pyrrole rings. Heme *b*, is found in myoglobin and hemoglobin (Edelstein et al., 1970; Antonini and Brunori, 1971;

Fermi and Perutz, 1981). The iron found chelated in the heme molecule exists most commonly in its ferric (3^+) and ferrous (2^+) states.

For pathogenic bacteria, heme can be a rich source of iron that is essential for cellular growth of the pathogen during infection. Most bacterial pathogens contain extensive systems dedicated to the capture and uptake of heme as an iron source (Nobles and Maresso, 2011; Smith and Wilks, 2012; Benson and Rivera, 2013; Contreras et al., 2014; Farrand and Skaar, 2014; Rodgers and Lukat-Rodgers, 2014; Wilks and O'Neill, 2014; Naoe et al., 2017). Once captured, the heme can be incorporated into hemoproteins or degraded to release the iron (Farrand and Skaar, 2014; Wilks and Ikeda-Saito, 2014).

Bacteria are becoming increasingly more resistant to commonly-used antibiotics (Bassetti et al., 2013). Bacterial that have developed resistance continue to multiply, resulting in a resistant population that is then transmitted from person to person. Bacteria use various biochemical mechanisms to counter antibiotic pressure: antibiotic-degrading enzymes, antibiotic-altering enzymes, and antibiotic efflux pumps. Alternatively, eliminating the nutritional sources of these pathogens, such as iron in the form of heme, could be effective in deterring the growth of these bacteria. Therefore, heme uptake studies in pathogenic bacteria may allow development of an alternative approach to combat antibiotic resistance (Rodgers and Lukat-Rodgers, 2014; Wilks and Ikeda-Saito, 2014).

Within the human body, there are various proteins which use heme as a cofactor. The total amount of iron in the body, approximately four grams, consists of heme bound to hemoglobin, myoglobin, a few heme enzymes, and ferric ions found in ferritin (Tong and Guo, 2009).

The most abundant heme source is hemoglobin. Upon being liberated from the red blood cells by hemolysis, hemoglobin dimers are bound by haptoglobin, a serum heterotetrameric glycoprotein, to form a hemoglobin-haptoglobin complex (Hb-Hp) (Tong and Guo, 2009). The two bind with a $K_d \sim 10^{-12}$ M (Tong and Guo, 2009). The hemoglobin-haptoglobin complex is transported to the reticuloendothelial system by CD163 receptor-mediated endocytosis (Kristiansen et al., 2001). This system is responsible for the formation of red blood cells, the formation of plasma proteins, and the storage of iron in the liver and bone marrow. Not all bacterial pathogens can use the Hb-Hp complex as an iron source. However, some species, such as *Hemophilus influenza* and *Porphyromonas gingivalis* are capable of obtaining iron through receptors specific for the Hb-Hp complex.

Free heme in plasma is bound by hemopexin, a 60 kDa protein plasma glycoprotein with a $K_d \sim 10^{-13}$ M (Tong and Guo, 2009). Hemopexin helps to prevent heme-mediated oxidative stress (the production of oxygen free radicals) and heme-bound iron loss. Once hemopexin binds to heme, the complex is transported to the liver. Apo-hemopexin is regenerated, and the heme is released inside the liver cells.

Human serum albumin (HSA) is the most abundant protein found in the plasma, and serves to both sequester and transport free hemin (Zunszain et al., 2003). HSA it is a monomer that consists of three homologous domains (I, II, and II), each of which is made up of two separate subdomains (A and B) that are connected to one another by random coils. HSA binds heme with a $K_d \sim 10^{-8}$ M. The heme binds to a hydrophobic, narrow D-shaped cavity in the IB subdomain. The propionate groups of heme are bound to a group of three basic residues at the entrance of the heme-binding pocket (Wardell et al., 2002; Zunszain et al., 2003). The iron in heme is ligated to a Tyr161.

Both low and high-density lipoproteins also can bind heme with high affinity, having K_d values of 10^{-11} M and 10^{-10} M, respectively (Grinshtein et al., 2003). The binding of heme to these molecules is kinetically faster than that of serum albumin and hemopexin.

1.2 Heme Uptake in Gram-positive Bacteria

Gram-positive and Gram-negative bacteria show many similarities in their heme uptake systems (Nobles and Maresso, 2011; Smith and Wilks, 2012; Benson and Rivera, 2013; Contreras et al., 2014; Farrand and Skaar, 2014; Rodgers and Lukat-Rodgers, 2014; Wilks and O'Neill, 2014). The key difference between the two is that Gram-positive bacteria must remove heme from host hemoproteins in solution or at the bacterial surface. They must then transport heme through the thick peptidoglycan layer and the plasma membrane (Farrand and Skaar, 2014). Most Gram-positive bacteria employ cell surface receptors to bind heme from the host. Gram-positive bacteria are classified into two phyla: Actinobacteria and Firmicutes. Actinobacteria are classified by having high G + C content in their genome; Firmicutes contain low G + C content. Some Actinobacteria of medical importance include the genera *Corynebacterium*, *Mycobacterium*, and *Actinomyces*. Likewise, some examples of Firmicutes include the genera *Streptococcus*, *Staphylococcus*, and *Clostridium*.

1.3 Heme Uptake in *Streptococcus pyogenes*

S. pyogenes, also known as Group A streptococcus (GAS), is a pathogenic, Gram-positive bacterium that causes a variety of infections such as pharyngitis, impetigo, and toxic shock syndrome in more serious cases (Cunningham, 2008; Eichenbaum, 2012). *S. pyogenes* requires iron as a key nutrient and utilizes heme-containing proteins as sources of this iron (Bates et al., 2003; Sachla et al., 2014). Hemoglobin acts as an iron source for this pathway. The heme

uptake pathway for *S. pyogenes* is a very well-studied example from the Firmicutes phylum and is discussed below in some detail.

S. pyogenes contains the *sia* iron-regulated ten-gene operon (Bates et al., 2003; Lei et al., 2003; Sun et al., 2010). Suppression of the *sia* locus results in reduced iron uptake and decreased hemoglobin binding, suggesting that the genes in the operon are responsible for both iron uptake and hemoglobin binding. A schematic of the heme uptake pathway for *S. pyogenes* is shown in Figure 1.2 (Akbas et al., 2016). The *sia* locus encodes a hemoprotein receptor, Shr, a heme-binding protein, Shp, SiaA, and an ABC transporter SiaBC. Shr is found on the outer surface, interacts with host hemoproteins, and transfers heme to Shp. SiaA is a heme-binding lipoprotein. Once SiaA binds a heme molecule, it then transfers it to SiaB, the membrane permease. SiaC, on the inside of the membrane, is the ATPase. ATP hydrolysis serves as the energy source to transport the heme into the cell. The heme is degraded inside the cell, and the iron is extracted.

Hemoglobin binds to the membrane-bound protein Shr (Ouattara et al., 2010). Shr contains two NEAT (NEAr iron Transporter) domains (Honsa et al., 2014), NEAT1 and NEAT2 (Nygaard et al., 2006; Ouattara et al., 2010). Under high heme conditions, Shr-NEAT2 is thought to receive heme from Shr-NEAT1 and store the heme until the cell enters a low heme state, upon which Shr-NEAT2 transfers the heme back to Shr-NEAT1 (Ouattara et al., 2013). Holo Shr-NEAT1 transfers heme to apo-Shp with a rate constant of $18.7 \pm 3.8\ s^{-1}$ and $0.60 \pm 14\ s^{-1}$, indicating a biphasic kinetic system (Lu et al., 2012). Holo Shr-NEAT2 shows only minimal and slow transfer of heme to apo-Shp (Ouattara et al., 2013).

Shp is a membrane-bound protein that contains only one domain that binds heme (Aranda et al., 2007). Shp has an immunoglobulin-like β-sandwich fold with eight β-strands and one α-helix. The eight β-strands are divided into three and four-stranded antiparallel β-sheets that form

a twisted β-sandwich with the eighth β-strand connecting the two β-sheets. The heme-bound to Shp has bis-methionyl coordination. Met66 and Met153, located on the α-helix and between the B7 and B8 β-strands, respectively, bind the heme on opposite sides. The sulfur atoms from both Met66 and Met153 are located 2.4 Å from the iron atom of heme. Met66 is more solvent exposed than Met153. Holo Shp transfers heme to apo SiaA with a rate constant of 43 ± 3 s^{-1} (Nygaard et al., 2006).

Homology modeling of SiaA shows that SiaA contains a bisligated heme center (Grigg et al., 2007). The low-spin heme is hexacoordinated by methionine and histidine residues (Sook et al., 2008; Akbas et al., 2016). The model structure of SiaA contains the classic two-lobe organization in the superfamily of bacterial periplasmic binding proteins, with a specific topology characteristic of the metal-binding receptor family (Tam and Saier, 1993). Each of the lobes is composed of a central β-sheet surround with α-helices. One long α-helix serves as a linker between the N- and C-terminal domains. SiaA has a pI value of 9.7 (Sook et al., 2008). Its reduction and oxidative midpoints are 83.3 ± 3 and 64 ± 3, respectively.

1.4 Heme Uptake in *C. diphtheriae*

1.4.1 *C. diphtheriae hmu* Gene Cluster

Heme transport in *C. diphtheriae* is encoded by the *hmu* gene cluster, shown in Figure 1.3 (Allen and Schmitt, 2009). The *hmu* cluster contains a six-gene cluster that contains three distinct iron- and DtxR (diphtheria toxin repressor)-regulated transcriptional regions (Bibb et al., 2005; Allen and Schmitt, 2009). The genes encoded in this region include *htaA*, *htaB*, *htaC*, and *hmuTUV*. The *hmuTUV* and *htaA* genes comprise a single operon, while *htaB* and *htaC* are independently transcribed. The *htaA* gene encodes a 61 kDa protein that is known to be a surface-anchored heme binding protein (Drazek et al., 2000; Schmitt and Drazek, 2001). HtaA

contains an N-terminal leader peptide sequence and a hydrophobic C-terminal region that is predicted to anchor the protein to the cytoplasmic membrane. There are two conserved repeats of approximately 150 amino acids in HtaA that are designated CR-1 (conserved region 1) and CR-2 (conserved region 2). The *htaB* gene encodes a 35 kDa protein that contains a C-terminal hydrophobic region, similar to the conserved regions of HtaA. The *htaC* gene encodes a 30 kDa protein that is predicted to be membrane-associated but has an undefined function. The *hmuTUV* gene produces three proteins identified as the lipoprotein HmuT (37 kDa), the permease HmuU (37 kDa), and the ATPase HmuV (30 kDa). The three proteins function as an iron-regulated ABC-type transporter.

1.4.2 *Proposed Mechanism of hmu Heme Uptake*

The heme uptake pathway in the *C. diphtheriae* involves the use of the iron-regulated *hmu* and *cht* hemin uptake loci (Allen and Schmitt, 2009; Allen et al., 2013). The schematic of the *hmu* and *cht* heme uptake pathways is shown in Figure 1.4. It is proposed that HtaA binds hemoglobin and takes a heme. HtaA can transfer heme to HtaB. HtaB is a surface-anchored protein found in the peptidoglycan layer of the cell wall that may transfer the heme to the lipoprotein HmuT. HmuT transfers the heme to the ABC transporter comprised of the permease HmuU and the ATPase HmuV. This protein complex will then facilitate the transport of heme into the bacterial cell. Figure 1.3 shows the schematic of the hmu and cht heme uptake pathway is C. diphtheriae.

1.4.3 *C. diphtheriae Heme Source Utilization*

ELISA analysis showed that HtaA, ChtA, ChtC, and ChtB could all bind hemoglobin (Allen et al., 2013). HtaB did not show significant binding to hemoglobin (Allen and Schmitt,

2011). HtaA, ChtA, ChtB, and ChtC had hemoglobin binding K_d values within a factor of two of one another (0.28 μM, 0.41 μM, 0.51 μM, 0.52, respectively).

C. diphtheriae also can use the hemoglobin-haptoglobin (Hb-Hp) complex as a heme source (Allen and Schmitt, 2015). Growth analysis with Hb-Hp as the only iron source has shown that *C. diphtheriae* can utilize the heme from this protein in the presence of HtaA-WT. Nonpolar deletions of *htaA* and *hmuTUV* abolish the use of Hb-Hp as the sole iron source, suggesting that these proteins are necessary for Hb-Hp utilization. Separate nonpolar deletions of *chtA*, *chtC*, and a *chtA/chtC* double mutant were constructed, and growth was measured with Hb-Hp as the sole iron source. The single *chtA* and *chtC* deletions showed no change in growth in comparison to WT. The *chtA/chtC* double mutant showed a significant reduction in growth. This may suggest that ChtA and ChtC could be interchangeable for one another when Hb-Hp is the iron source. The deletion of *htaA*, *chtA*, and *chtC* abolished the ability of the organism to use Hb-Hp. Growth analysis suggested that HtaA and either ChtA or ChtC are necessary for the use of Hb-Hp as the sole iron source. The data may also suggest that there is no other uptake pathway available for the use of Hb-Hp.

HtaA binds the Hb-Hp complex (Allen and Schmitt, 2015). An in vitro ELISA assay of various HtaA derivatives showed that full-length HtaA and HtaA-CR2 bind Hb-Hp the most strongly with K_d values of 210 nM and 200 nM, respectively. HtaA-CR1 had a Hb-Hp binding K_d value that was approximately two-fold weaker than that of both full-length HtaA and HtaA-CR2. The full-length Y361A derivative (altering the conserved tyrosine in CR2) showed reduced binding to Hb-Hp (K_d = 870 nM), while the HtaA-CR2 domain showed no evidence of binding. The Y49A derivative (altering the conserved tyrosine in CR1) had only slightly smaller Hb-Hp binding (K_d = 270 nM) than HtaA-WT. The results from the in vitro ELISA assay provide

evidence in the importance of the conserved tyrosine found in the second conserved region of HtaA when Hb-Hp is the iron source. HtaA showed background levels of binding to haptoglobin in comparison to that of Hb-Hp, indicating that the interaction between HtaA and Hb-Hp is primarily through the hemoglobin subunit.

Hb-Hp binding studies with Strep-tagged proteins showed that HtaA bound Hb-Hp more tightly than did ChtA and ChtC (Allen and Schmitt, 2015). Full-length ChtA and ChtC showed reduced binding in comparison to HtaA with K_d values greater than 2 μM each. The ChtA-CR (K_d = 890 nM) showed enhanced Hb-Hp binding in comparison with the full-length ChtA (K_d > 2 μM).

Myoglobin (Mb), human serum albumin (HSA), and hemopexin (Hpx) may also serve as heme sources for *C. diphtheriae* (Allen and Schmitt, 2015). Growth studies were performed on *C. diphtheriae* using Mb, HSA, and Hpx in separate experiments. *C. diphtheriae* grew with HAS-heme as the sole iron source. Deleting either htaA or hmuTUV significantly reduced organism growth. Similar results were shown when Mb was the only iron source. There was no growth in the presence of Hpx. These studies provided evidence that HtaA and HmuTUV could be involved in HSA or Mb utilization.

1.5 Lac Promoter and Protein Expression

A staple in prokaryotic research and protein expression is the *lac* promoter from the *lac* operon (Müller-Hill, 1996). The *lac* operon encodes for the proteins that are required to import and digest lactose. The genes found within the operon consist of *lacI*, *lacZ*, *lacY*, and *lacA*. The lac repressor is encoded by *lacI*. *LacI* is transcribed separately, while *lacZYA* are all expressed on a polycistronic mRNA. The lac repressor is transcribed within the bacteria under normal conditions. The repressor then binds to the operator that exists partially within the promoter to

prevent the expression of the other *lac* operon products until needed. In the absence of lactose, the repressor remains bound to the operator, and the full *lac* operon transcription does not occur. In the presence of lactose, β-galactosidase, the product of *lacZ*, catalyzes the intramolecular isomerization of lactose to allolactose, which is the lac operon inducer. Allolactose binds to the Lac repressor, which causes a conformational change in the repressor. This change in conformation causes the repressor to be no longer able to bind to the operator sequence. RNA polymerase is then able to transcript the remaining *lac* genes.

Glucose is the most common carbon source used by prokaryotes. Under normal conditions, glucose inhibits adenylyl cyclase, which converts ATP to cyclic AMP (cAMP). When glucose levels are low, the organism needs to utilize an alternate carbon source. Cyclic AMP levels rise when the amount of glucose in the cell depletes. The catabolite activator protein (CAP) binds two cAMP molecules under these conditions. The CAP/cAMP complex then binds in a region on the DNA upstream of the lac repressor, enhancing the ability of RNA polymerase to transcribe the *lac* genes.

The T7 promoter system in pET vectors is commonly used in recombinant protein expression (Silverstone et al., 1970). In the pET system, the gene of interest in cloned behind a promoter sequence specifically recognized by T7 RNA polymerase (Rosano and Ceccarelli, 2014). This polymerase is most frequently placed into the bacterial genome in a prophage (λDE3) encoding for the T7 RNA polymerase under the transcriptional control of a *lac*UV5 promoter (Studier and Moffatt, 1986). This system can be induced by the non-hydrolysable analog of lactose, β-D-thiogalactopyranoside (IPTG). Basal expression of the target protein is controlled by *lac*I^Q or by T7 lysozyme co-expression. T7 lysozyme inhibits premature

transcription by binding to T7 RNA polymerase (Stano and Patel, 2004). After induction, the amount of T7 RNA polymerase exceeds that of T7 lysozyme.

1.6 Thesis Goals

Characterization studies of the use of pathogenic heme uptake pathways has steadily been on the rise. Most of the heme uptake work has been performed Gram-negative bacteria. Our studies focus mainly on the strategies used by Gram-positive bacteria for heme uptake. In this study, we will work to characterize the relatively new heme-binding proteins HtaB and ChtB from *C. diphtheriae*. We will use a combination of techniques to determine some biochemical and biophysical characteristics of these proteins. A bioinformatics study will be performed in Chapter 2 to determine more information about the HtaA domains and which types of Gram-positive bacteria prefer the HtaA system or NEAT system. Chapters 3 and 4 will focus on the studies involving HtaB and ChtB, respectively.

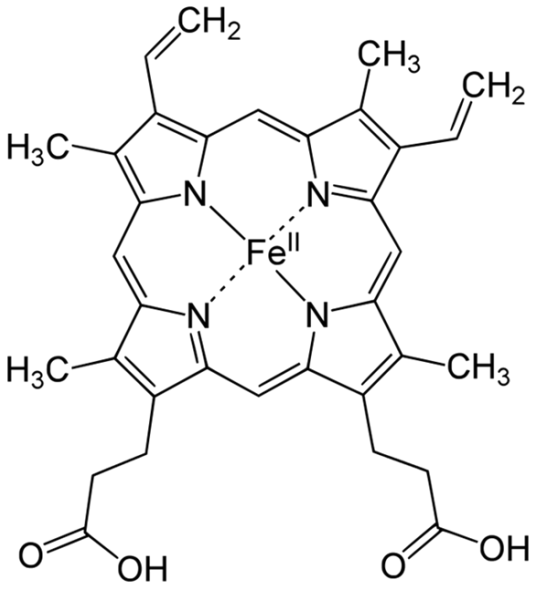

Figure 1.1 Structure of heme b.

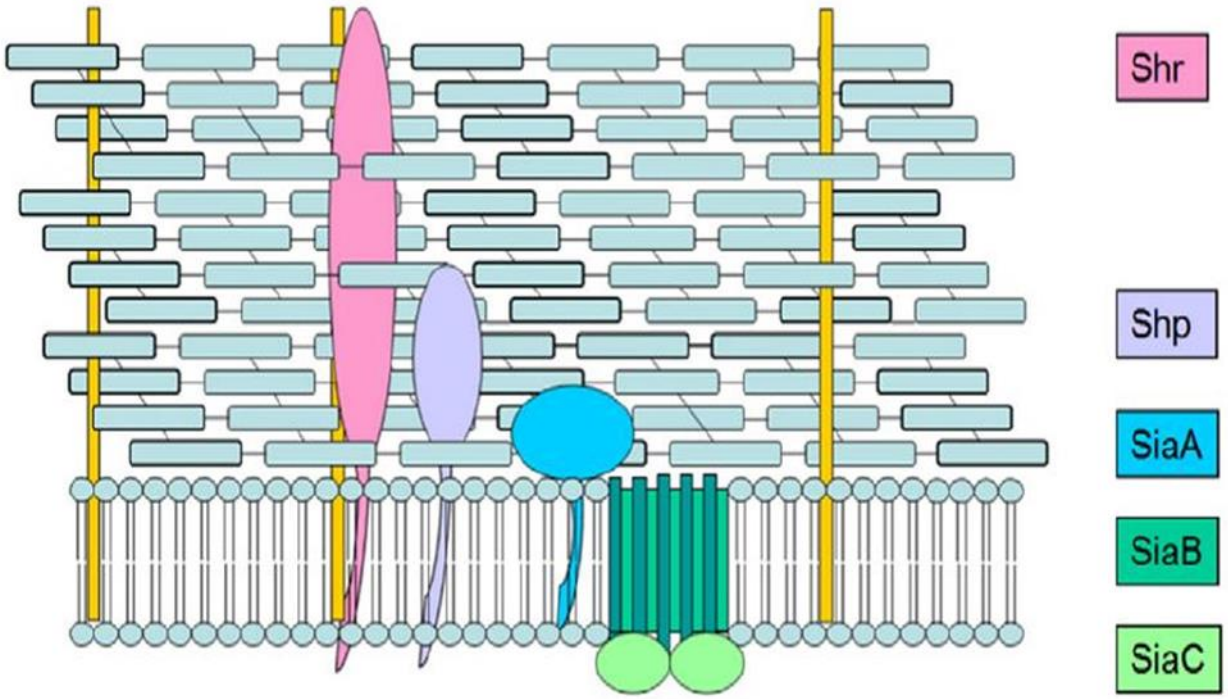

Figure 1.2 Overview of the S. pyogenes Sia/Hts heme uptake pathway.

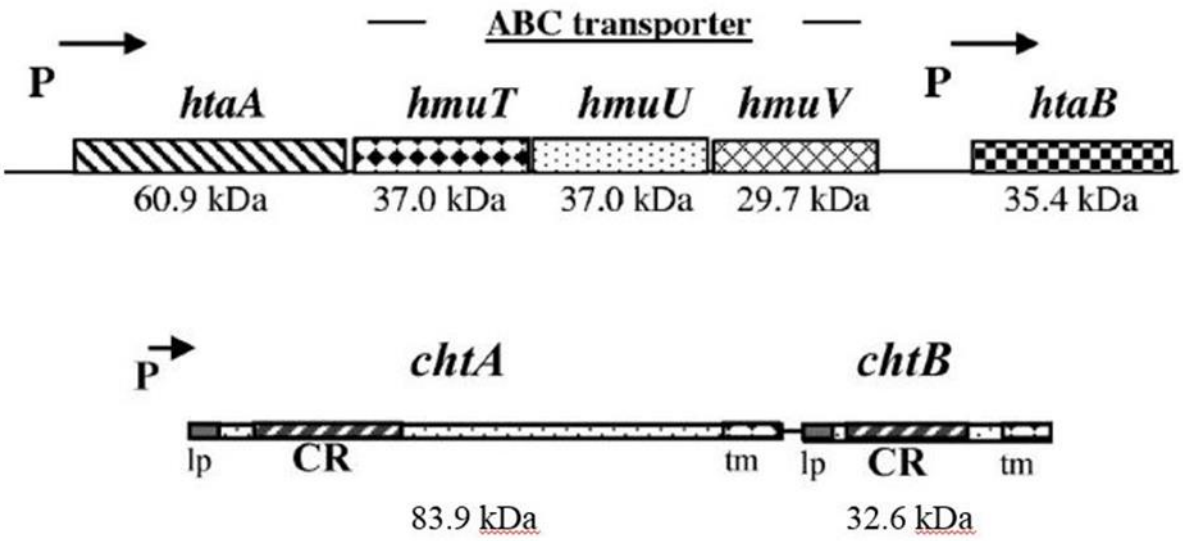

Figure 1.3 Schematic of the hmu and cht gene clusters in C. diphtheriae. Taken from (Allen and Schmitt, 2009; Allen et al., 2013)

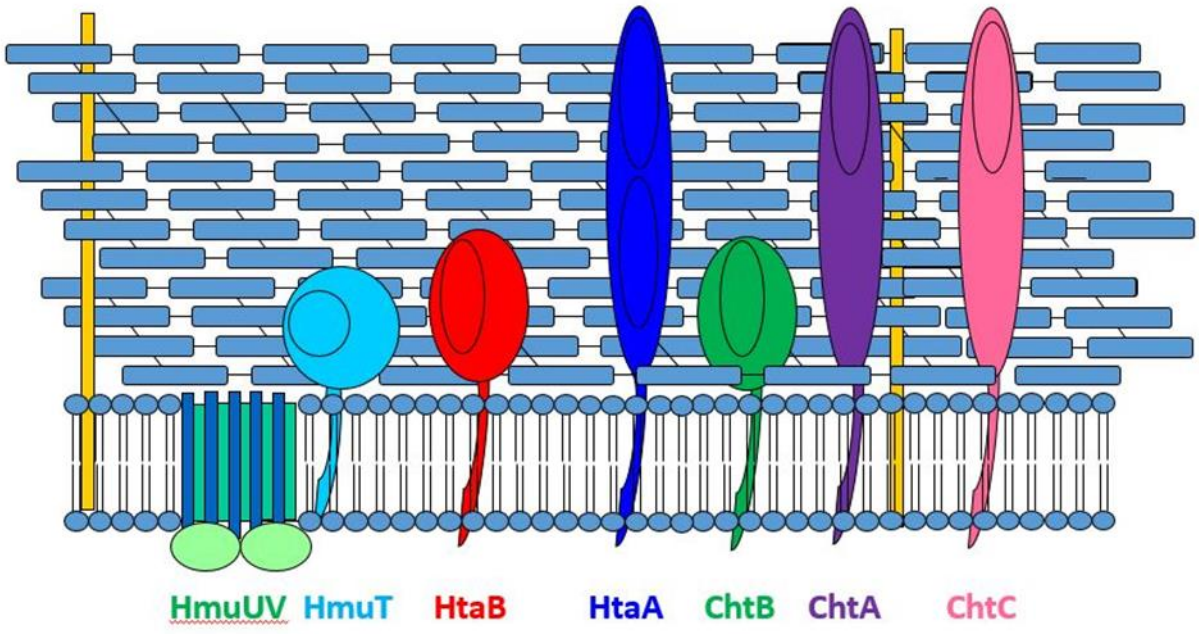

Figure 1.4 Heme uptake pathway in C. diphtheriae.

2 CHAPTER 2: BIOINFORMATIC STUDIES OF HTAB AND CHTB

2.1 Introduction

The goal of this work was to extend literature bioinformatic studies on HtaA domains to gain a deeper understanding of the similarities and differences in this class of proteins. In addition, we performed a comparison of the HtaA and NEAT domains to probe the structural motifs involved in readily reversible heme binding and develop an overall picture of heme uptake in Gram-positive bacteria.

2.1.1 *Bioinformatics Studies of Corynebacterium diphtheriae*

A sequence alignment of the conserved regions of HtaA was performed previously by Allen and Schmitt (Allen and Schmitt, 2011). The sequence alignment compared the two conserved regions of HtaA and the conserved region of HtaB with other HtaA homologs from various *Corynebacterium* species. The sequence alignment showed two conserved tyrosines and one conserved histidine (Y49, H107, and Y197 in CR1 and Y361, H412, and Y490 in CR2 of HtaA). The conserved region of HtaB contained two conserved tyrosines at positions 56 and 222 and a conserved histidine at position 121. The conserved region of ChtB contained two conserved tyrosine residues at positions 30 and 202 and a histidine at position 95 (Allen et al., 2013). Tyrosine and histidine residues are known to coordinate the iron atom of heme in other well-characterized heme binding proteins (Grigg et al., 2007; Pilpa et al., 2009; Rodgers and Lukat-Rodgers, 2014; Wilks and O'Neill, 2014; Sheldon and Heinrichs, 2015; Brewitz et al., 2016).

2.1.2 *Literature Studies of HtaA Domains*

A pan-genomic study was performed on various *C. diphtheriae* strains to determine which ones contained the HtaA-CR genes (Trost et al., 2012; Allen et al., 2013). Figure 2.1

shows the results of this study. Not all *C. diphtheriae* strains contain a fully functioning HtaA sequence. Allen and Schmitt (2013) found that some of the strains from Brazil have the genes present which code for HtaA, but that these genes contain point mutations predicted to result in premature termination of HtaA (e.g., without the membrane-anchoring sequence). Most sequences of the full genome available at the time of that study contained the genes for HtaB but not ChtB. The C7 strain, the most widely used in laboratory research in the United States, does not contain HtaA, HtaB, or ChtB. The C7 strain does, however, contain the sequence for what would be expected to be a fully functioning hemin-specific ABC transporter encoded by hmuTUV. The C7 strain only shows a slight defect in the ability to use hemin and Hb as iron sources. This shows that there may be other mechanisms present for utilizing heme iron.

2.1.3 *Structure of NEAT Domains*

The second heme-binding paradigm in Gram-positive heme uptake proteins is the NEAr-iron Transport (NEAT) domain (Andrade et al., 2002; Honsa et al., 2014; Sheldon and Heinrichs, 2015). Examples of bacteria using this system include *Bacillus anthracis*, *Staphylococcus aureus*, *Streptococcus pyogenes*, and *Listeria monocytogenes*.

NEAT domains are composed of eight β-strands that form a β-barrel (Sharp et al., 2007). As an example, the crystal structure of the NEAT-5 domain of IsdX2 from *B. anthracis* is shown in Figure 2.2 (Honsa et al., 2013a). This NEAT domain has a small 3_{10}-helix (lip-region) that folds to form a hydrophobic heme-binding pocket. The 3_{10}-helix has an SXXXXY motif, where X represents any amino acid. The serine residue of the helix hydrogen bonds with the propionate group of the heme, which may help to increase binding affinity. At the other end of the helix, the tyrosine can undergo π-stacking interactions with the heme ring (Li et al., 2011; Ekworomadu et al., 2012).

In a 2014 study, approximately 70% of NEAT domains analyzed contained the SXXXXY motif (Honsa et al., 2014). Another 11% (39 examples) had either Phe (38 examples) or His (1 example) in place of the tyrosine (SXXXXF/H). These domains may have a similar heme-binding environment to those with an SXXXXY motif, using the aromatic Phe or His for π-stacking instead of tyrosine. Another 17% of the NEAT domains studied did not have the conserved SXXXXY motif. It appears that only NEAT domains with the conserved 3_{10}-helix motif bind heme (Honsa et al., 2013b). It was proposed that the NEAT domains without the 3_{10}-helix motif may help other NEAT domains within the same protein to bind heme, as seen in IsdB-N1, IsdH-N1, and IsdH-N2 (Pilpa et al., 2006; Watanabe et al., 2008; Honsa et al., 2013b).

Across the heme from the SXXXXY region is a five-amino acid motif on the eighth β-strand that generally begins with a Tyr and ends with Tyr, His, or Phe [YXXXY(H/F)] (Honsa et al., 2014). It was found that approximately 50% of the NEAT domains contain the YXXXY motif, utilizing a tyrosine in the last position (Honsa et al., 2014). The first tyrosine in the YXXXY motif often forms a coordinate covalent bond with the iron atom of the heme, with the second tyrosine hydrogen bonding to the first (Pilpa et al., 2009; Grigg et al., 2010; Honsa et al., 2011). Approximately 10% of the NEAT domains possess the first tyrosine but have another aromatic amino acid in the place of the second tyrosine YXXX(H/F), with 9% having His and 1% having Phe. The NEAT domains that do not contain this motif lack any other noticeable heme-binding motifs, suggesting that either these NEAT domains play a structural role, as in the NEAT domains of IsdB and IsdH of *S. aureus*, or there is a yet unidentified heme-coordinating axial ligand in these proteins (Pilpa et al., 2009).

2.2 Materials and Methods

2.2.1 *Sequence Alignments*

Sequence alignments were performed using the Clustal Omega software from the European Bioinformatics Institute (EMBL-EBI) database (Sievers et al., 2011; Li et al., 2015). The conserved regions (CR1 and CR2) of HtaA proteins of various *Corynebacterium* species were aligned with the conserved regions of HtaA (CR1 and CR2), HtaB, and ChtB.

Clade diagrams were constructed using the DrawGram program from the Phylip package. The tree was run from HtaA-CR1 (http://evolution.genetics.washington.edu/phylip/credits.html).

2.2.2 *Gram-Positive Bacteria BLAST Search*

The CR2 sequence of HtaA from *C. diphtheriae* (Accession: AEX48107.1) (Trost et al., 2012) and the NEAT domain of IsdA from *Staphylococcus aureus* (PDB: 2ITE) (Grigg et al., 2010), were used with the Basic Local Alignment Search Tool (BLAST) from the National Center for Biotechnology Information (NCBI). The protein sequence from each domain was blasted into various Gram-positive genera of medical importance.

2.2.3 *Homology Modeling*

Homology models were constructed using the I-TASSER software (Yang et al., 2015). PyMol was used for further visualization (DeLano, 2015).

2.3 Results and Discussion

2.3.1 *Sequence Alignments*

The results from the sequence alignment are shown in Figure 2.3. Similar to previous alignments (Allen and Schmitt, 2011; Allen et al., 2013), two conserved Tyr residues and one conserved His residue are seen, typical of HtaA domains. There is a highly-conserved Phe

residue three residues before the conserved His and another almost fully-conserved Phe residue four residues before the second conserved Tyr residue. There are conserved Ser and Trp residues four and nine residues before the first conserved Tyr.

The first conserved Tyr has been proposed to be the axial ligand for HtaA in *C. diphtheriae* (Allen and Schmitt, 2011; Uluisik et al., 2017), largely because the mutation of the first Tyr has a larger effect on heme uptake than the mutation of the second Tyr. A higher level of conservation in the residues surrounding the first conserved Tyr compared with the second is also consistent with the first Tyr as the axial ligand (Allen and Schmitt, 2011). However, absent a published crystal structure, the identity of the axial tyrosine cannot be firmly assigned.

Biochemical studies on the conserved His residue have shown that it also plays an important role in the heme pocket (Allen and Schmitt, 2011). The His residue may be acting as a hydrogen-bonding partner to the axial Tyr. His hydrogen bonding to an axial Tyr has been shown in HasA from various species (Arnoux et al., 1999; Alontaga et al., 2009; Kumar et al., 2013).

The sequence alignments of CR1 and CR2 can be visualized in a circular phylogenetic tree. Figure 2.4 shows that all CR1 domains are grouped, and all CR2 domains are grouped. HtaA is closest in sequence to the sister group (closest relatives of another given unit in an evolutionary tree) Cu-CR1 and Ctb-CR1. The alignment (Figure 2.3) shows that these two proteins contain a Thr residue in place of the Ser residue that is found in all other HtaA domains in the diagram.

The CR regions of HtaB, ChtB, and ChtA appear between the CR1 and CR2 sequences. HtaB and ChtB are a sister group, consistent with the idea that HtaB and ChtB may be able to substitute for one another in vivo (Allen et al., 2013). ChtA contains a common ancestor with all CR1 domains, HtaB, and ChtB but does not have any immediately related proteins. The

alignment in Figure 2.3 shows that ChtA has a Tyr in the place of the conserved His found in other HtaA domains. It is relatively common for tyrosine to serve as a hydrogen partner to an axial Tyr in heme proteins, as shown in a recent data compilation (Draganova et al., 2015).

Alanine mutations constructed of the conserved residues in HtaA (Y49A, H107A, and Y197A in CR1; Y361A, H412A, and Y490 in CR2) were shown to decrease the ability of the protein to bind heme with respect to wild type (Allen and Schmitt, 2011). Alanine replacement of the conserved residues also showed a decrease in the ability of the proteins to bind hemoglobin.

2.3.2 *SXXXY Conserved Motif*

Our analysis of the HtaA domains reveals a highly-conserved SXXXY motif. Figure 2.3 shows that most HtaA domains contain a conserved serine residue four residues before the first conserved tyrosine, shown at positions 52 and 26 in HtaB and ChtB, respectively. Of the tested sequences, 90% contained this motif. The first conserved HtaA regions from *C. ulcerans* and *C. tuberculostearicum* contained a Thr residue in place of the serine. The Ser and Thr residues may act in the same manner since both side chains contain a hydroxyl group. Of the HtaA domains tested, all contain an aromatic amino acid directly following the Ser, with CR1 domains having 50% Tyr and 50% Phe and all CR2 domains having Phe. Following the aromatic residue, 100% of CR1 domains possess an Arg residue after the aromatic residue. Of the CR2 domains tested, 70% possess an Arg residue at the same position, while the other 30% possess a Gln residue. The third amino acid between the Ser and Tyr residue of both CR1 and CR2 domains does not appear to follow an obvious pattern.

At first glance, the SXXXY motif found herein seems similar to the SXXXXY motif (Honsa et al., 2014) found in the 3_{10}-helix portion of NEAT domains (71% of the sequences

studied) (Figure 2.5). In the NEAT domain motif, the serine is a hydrogen-bond partner of one of the propionates and the tyrosine π-stacks with the heme. In contrast, the HtaA data to date have been interpreted in terms of the tyrosine in the SXXXY motif being the heme-bound axial ligand (Allen and Schmitt, 2011) (although the absence of a published crystal structure means that this assignment could be open to reinterpretation). Therefore, as of this writing, it seems that these SXXXY (HtaA) and SXXXY (NEAT) motifs, while appearing similar, seem to have different roles in heme binding.

2.3.3 *FXGH Conserved Motif*

A highly conserved FXGH motif involving the signature His residue is seen in all HtaA sequences in Figure 2.3. The His residue in HtaA is proposed to be the hydrogen-bonding partner to the heme axial tyrosine (Uluisik et al., 2017). The Phe residue may be involved in helping stabilize the heme in the pocket as seen in other heme binding proteins (Schneider et al., 2007; Smith et al., 2010). The "X" residues following immediately after the Phe are all polar residues. Of the polar residues, approximately 80% of those contain side chains that have at least one oxygen atom (Asn, Asp, Glu, Ser, and Thr). Directly before the His is a fully conserved Gly residue. The combination of these specific residues could serve as another fingerprint in combination with the other conserved motifs to identify future HtaA domain-containing proteins.

2.3.4 *FXXXY Conserved Motif*

Most of the CR2 domains investigated show a conserved FXXXY motif towards the N-terminal region. Some CR1 domains have this motif, and some have an FXXY motif in the same position. Maresso and colleagues have discussed the possible role of Phe in terms of stabilizing heme binding by π-stacking with the heme (Balderas et al., 2012). For Hal from *B. anthracis*, is it proposed that the tyrosine in the YXXXF motif binds to the heme while the Phe stacks with the

heme pyrrole rings. The *Clostridium* NEAT domains also lack the classic YXXXY NEAT signature (Honsa et al., 2014). Most of the NEAT domains from this group contain a Phe residue on the eighth β strand comparable to the position of the second Tyr residue in the YXXXY motif previously described. It is proposed that this Phe residue may function in heme binding by forming π-stacking interactions with the pyrrole units of the heme (Schneider et al., 2007; Smith et al., 2010).

2.3.5 *Gram-Positive Bacteria BLAST Search*

A goal of this research was to determine if there were an overall species pattern for bacterial use of either the HtaA or NEAT domain. Results of the domain-specific BLAST search are shown in Figure 2.6. *Enterococci* have neither the HtaA nor NEAT sequences. Beyond this, for the major medically-important Gram-positive bacteria, Actinobacteria utilize the HtaA system and Firmicutes use the NEAT system in their heme uptake pathways. None of the listed bacteria are shown to possess both methods for heme uptake. This is the first demonstration of this pattern. We note that two of the approximately 1300 *Bacillus* genes seems to indicate the presence of an HtaA sequence. However, as pointed out in a previous study on HtaA alignments (Allen et al., 2013), the observation of sequence homology does not necessarily correlate with viable proteins; truncation and frame-shift mutations can produce peptides that are not functional in heme uptake.

2.3.6 *Homology Modeling*

The I-TASSER structure prediction program can give good models for proteins if structures of sufficient sequence homology have been structurally characterized. For HtaB-CR and ChtC-CR, the closest sequences were gp39 for the former and UspA1 for the latter (only 7.4% and 9.4% sequence identity, respectively). Possible models for the conserved regions of

HtaB-CR and ChtB-CR are shown in Figure 2.7 and Figure 2.8, respectively. In addition to the low sequence identity, the large amount of unstructured protein and the very large difference between the proposed structures for HtaB and ChtB (which are very similar in terms of biophysical characteristics and ability to substitute for one another in vivo) indicate that these are novel proteins, whose structure is not as yet well-described by homology modeling.

Strains	HtaA-CR1	HtaA-CR2	HtaB-CR	ChtB-CR	Additional Information
241					Brazil/Tox^{+}
31A	*	*			Brazil/Tox^{+}
BH8	*	*			Brazil
C7 (beta)					USA/lab strain
CDCE 8392	*	*			CDC
HC01					Brazil/endocarditis
HC02					Brazil/endocarditis
HC03					Brazil/endocarditis
HC04					Brazil/endocarditis
INCA 402	*	*			Brazil/pneumonia
NCTC 13129					FSU/epidemic clone
PW8	*	*			USA/vaccine strain
VA01					Brazil/Tox^{-}

Figure 2.1 Blast search showing which strains of C. diphtheriae contain the proteins encoded in the hmu and cht gene loci. Data from columns HtaA-CR1, HtaA-CR2, and ChtB-CR are from (Allen et al., 2013). The asterisk (*) the presence of HtaA that contains point mutations with unknown functional status.

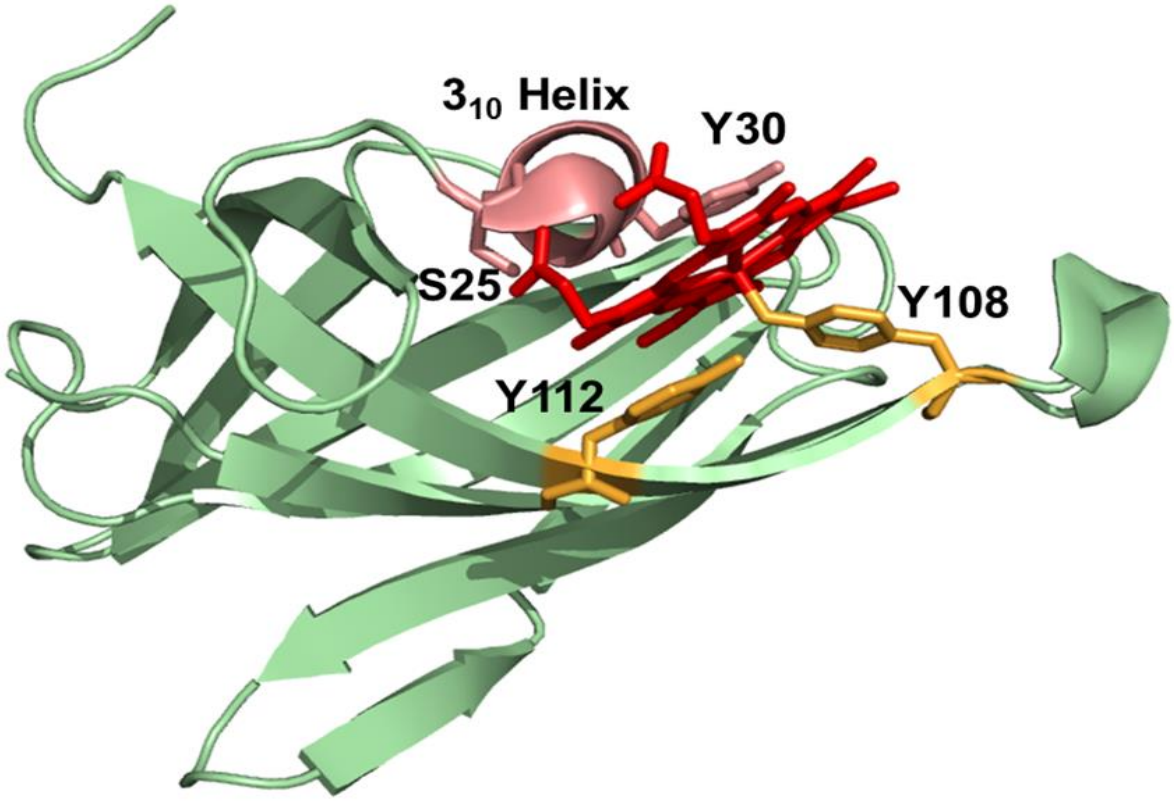

Figure 2.2 Crystal structure of IsdX2 NEAT-5 domain from B. anthracis. Protein Data Bank code 4H8P (Honsa et al., 2013b).

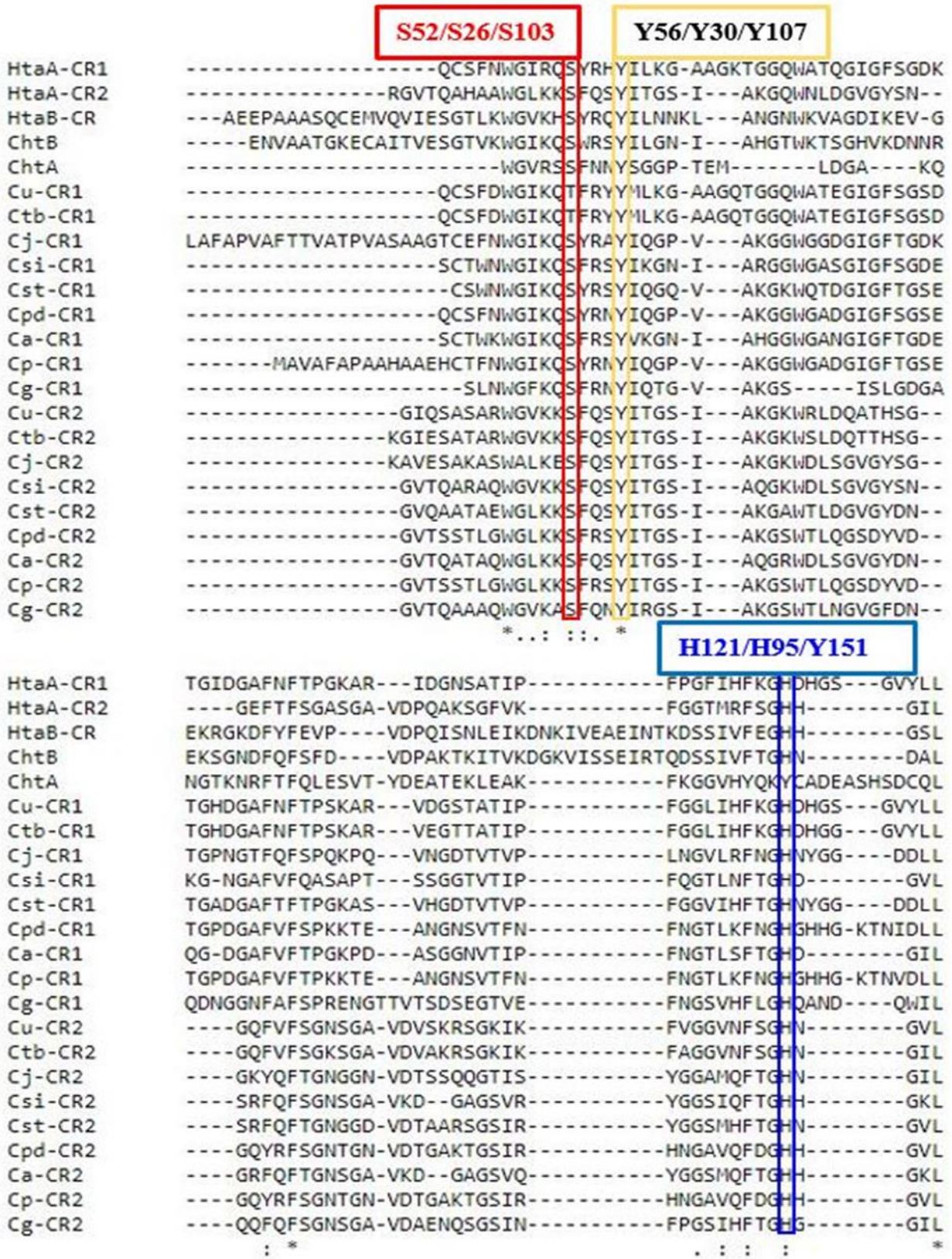
S52/S26/S103
Y56/Y30/Y107
H121/H95/Y151
HtaA-CR1 ----------QCSFNWGIRQSYRHYILKG-AAGKTGGQWATQGIGFSGDK
HtaA-CR2 ----------RGVTQAHAAWGLKKSFQSYITGS-I---AKGQWNLDGVGYSN--
HtaB-CR ---AEEPAAASQCEMVQVIESGTLKWGVKHSYRQYILNNKL---ANGNWKVAGDIKEV-G
ChtB -----ENVAATGKECAITVESGTVKWGIKQSWRSYILGN-I---AHGTWKTSGHVKDNNR
ChtA ----------WGVRSSFNNYSGGP-TEM-------LDGA----KQ
Cu-CR1 ----------QCSFDWGIKQTFRYYMLKG-AAGQTGGQWATEGIGFSGSD
Ctb-CR1 ----------QCSFDWGIKQTFRYYMLKG-AAGQTGGQWATEGIGFSGSD
Cj-CR1 LAFAPVAFTTVATPVASAAGTCEFNWGIKQSYRAYIQGP-V---AKGGWGGDGIGFTGDK
Csi-CR1 ----------SCTWNWGIKQSFRSYIKGN-I---ARGGWGASGIGFSGDE
Cst-CR1 ----------CSWNWGIKQSYRSYIQGQ-V---AKGKWQTDGIGFTGSE
Cpd-CR1 ----------QCSFNWGIKQSYRNYIQGP-V---AKGGWGADGIGFSGSE
Ca-CR1 ----------SCTWKWGIKQSFRSYVKGN-I---AHGGWGANGIGFTGDE
Cp-CR1 -------MAVAFAPAAHAAEHCTFNWGIKQSYRNYIQGP-V---AKGGWGADGIGFTGSE
Cg-CR1 ----------SLNWGFKQSFRNYIQTG-V---AKGS-----ISLGDGA
Cu-CR2 ----------GIQSASARWGVKKSFQSYITGS-I---AKGKWRLDQATHSG--
Ctb-CR2 ----------KGIESATARWGVKKSFQSYITGS-I---AKGKWSLDQTTHSG--
Cj-CR2 ----------KAVESAKASWALKESFQSYITGS-I---AKGKWDLSGVGYSG--
Csi-CR2 ----------GVTQARAQWGVKKSFQSYITGS-I---AQGKWDLSGVGYSN--
Cst-CR2 ----------GVQAATAEWGLKKSFQSYITGS-I---AKGAWTLDGVGYDN--
Cpd-CR2 ----------GVTSSTLGWGLKKSFRSYITGS-I---AKGSWTLQGSDYVD--
Ca-CR2 ----------GVTQATAQWGLKKSFQSYITGS-I---AQGRWDLSGVGYDN--
Cp-CR2 ----------GVTSSTLGWGLKKSFRSYITGS-I---AKGSWTLQGSDYVD--
Cg-CR2 ----------GVTQAAAQWGVKASFQNYIRGS-I---AKGSWTLNGVGFDN--
HtaA-CR1 TGIDGAFNFTPGKAR---IDGNSATIP----------FPGFIHFKGHDHGS---GVYLL
HtaA-CR2 ----GEFTFSGASGA-VDPQAKSGFVK----------FGGTMRFSGHH--------GIL
HtaB-CR EKRGKDFYFEVP----VDPQISNLEIKDNKIVEAEINTKDSSIVFEGHH--------GSL
ChtB EKSGNDFQFSFD----VDPAKTKITVKDGKVISSEIRTQDSSIVFTGHN--------DAL
ChtA NGTKNRFTFQLESVT-YDEATEKLEAK----------FKGGVHYQKYCADEASHSDCQL
Cu-CR1 TGHDGAFNFTPSKAR---VDGSTATIP----------FGGLIHFKGHDHGS---GVYLL
Ctb-CR1 TGHDGAFNFTPSKAR---VEGTTATIP----------FGGLIHFKGHDHGG---GVYLL
Cj-CR1 TGPNGTFQFSPQKPQ---VNGDTVTVP----------LNGVLRFNGHNYGG----DDLL
Csi-CR1 KG-NGAFVFQASAPT---SSGGTVTIP----------FQGTLNFTGHD--------GVL
Cst-CR1 TGADGAFTFTPGKAS---VHGDTVTVP----------FGGVIHFTGHNYGG----DDLL
Cpd-CR1 TGPDGAFVFSPKKTE---ANGNSVTFN----------FNGTLKFNGHGHHG-KTNIDLL
Ca-CR1 QG-DGAFVFTPGKPD---ASGGNVTIP----------FNGTLSFTGHD--------GIL
Cp-CR1 TGPDGAFVFTPKKTE---ANGNSVTFN----------FNGTLKFNGHGHHG-KTNVDLL
Cg-CR1 QDNGGNFAFSPRENGTTVTSDSEGTVE----------FNGSVHFLGHQAND----QWIL
Cu-CR2 ----GQFVFSGNSGA-VDVSKRSGKIK----------FVGGVNFSGHN--------GVL
Ctb-CR2 ----GQFVFSGKSGA-VDVAKRSGKIK----------FAGGVNFSGHN--------GIL
Cj-CR2 ----GKYQFTGNGGN-VDTSSQQGTIS----------YGGAMQFTGHN--------GIL
Csi-CR2 ----SRFQFSGNSGA-VKD--GAGSVR----------YGGSIQFTGHH--------GKL
Cst-CR2 ----SRFQFTGNGGD-VDTAARSGSIR----------YGGSMHFTGHN--------GVL
Cpd-CR2 ----GQYRFSGNTGN-VDTGAKTGSIR----------HNGAVQFDGHH--------GVL
Ca-CR2 ----GRFQFTGNSGA-VKD--GAGSVQ----------YGGSMQFTGHH--------GKL
Cp-CR2 ----GQYRFSGNTGN-VDTGAKTGSIR----------HNGAVQFDGHH--------GVL
Cg-CR2 ----QQFQFSGNSGA-VDAENQSGSIN----------FPGSIHFTGHG--------GIL

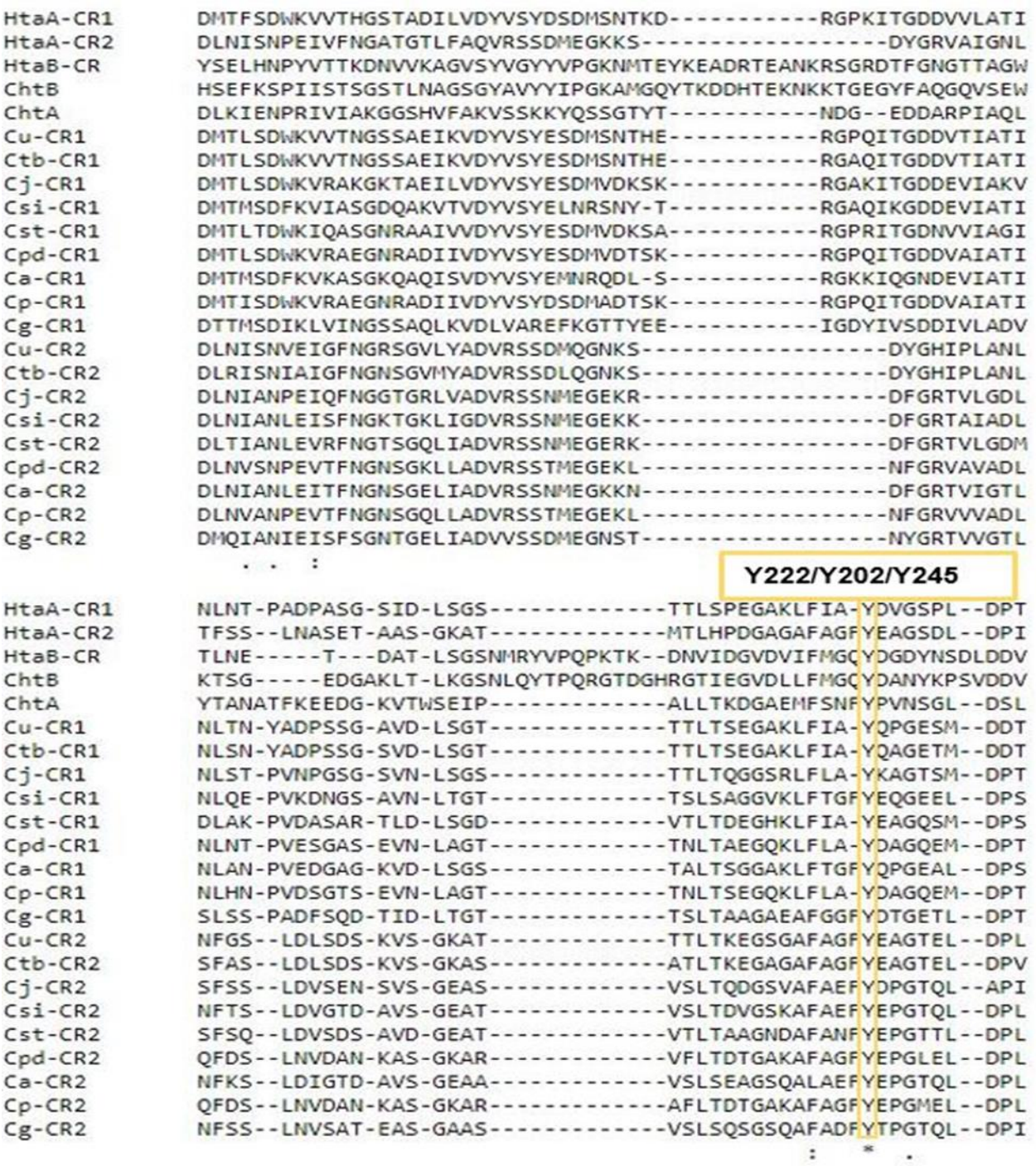

Figure 2.3 Multiple sequence alignment of the conserved regions of HtaA proteins from related species with the conserved regions of HtaB, ChtB, and ChtA. The diagram includes C. ulcerans (Cu), C. tuberculostearicum (Ctb), C. jeikeium (Cj), C. pseudodiphtheriticum (Cpd), C. propinquum (Cp), C. striatum (Cst), C. singular (Csi), C. aurimucosum (Ca), C. glutamicum (Cg).

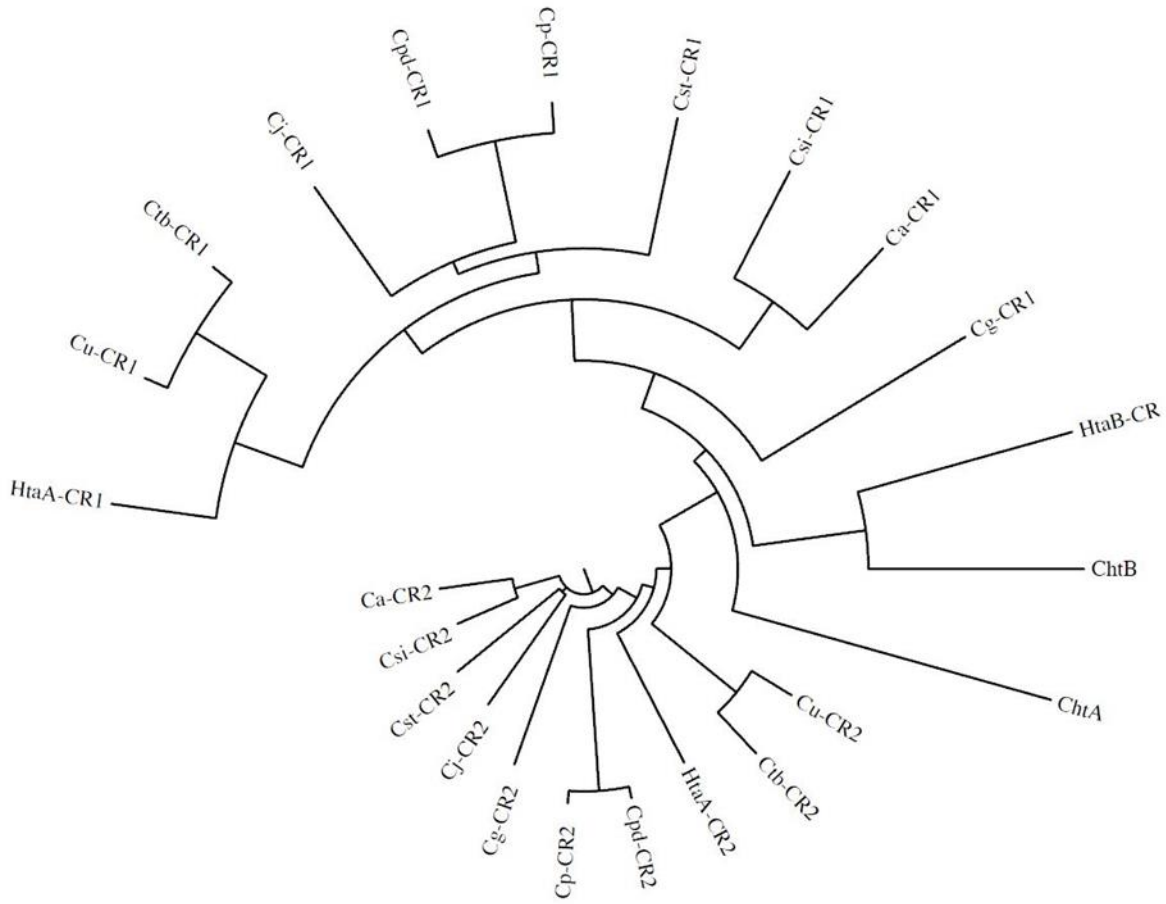

Figure 2.4 Circular phylogenetic tree demonstrating the relationship of 20 HtaA domains with those of HtaB, ChtB, and ChtA. The tree was run from HtaA-CR1. The diagram includes C. ulcerans (Cu), C. tuberculostearicum (Ctb), C. jeikeium (Cj), C. pseudodiphtheriticum (Cpd), C. propinquum (Cp), C. striatum (Cst), C. singular (Csi), C. aurimucosum (Ca), C. glutamicum (Cg).

HtaA			NEAT		
Motif	**Position**	**Role**	**Motif**	**Position**	**Role**
SXXX**<u>Y</u>**	N-terminal	S: Hydrogen bonding to heme propionate? **<u>Y</u>**: Axial ligand	SXXXXY	N-terminal	S: Hydrogen bonding to heme propionate Y: π-stacking with heme
FXGH	N-terminal	H: Hydrogen bonding to axial Tyr	-	-	-
FXXXY	C-terminal	Y: Hydrogen bonding or π-stacking with heme? F: π-stacking with heme?	**<u>Y</u>**XXXY(H/F)	C-terminal	**<u>Y</u>**: Axial ligand Y: Hydrogen bonding to axial Y

Figure 2.5 The signature sequence characteristics of HtaA and NEAT domains are shown below. The residues that are both underlined and bolded are the respective heme axial ligands.

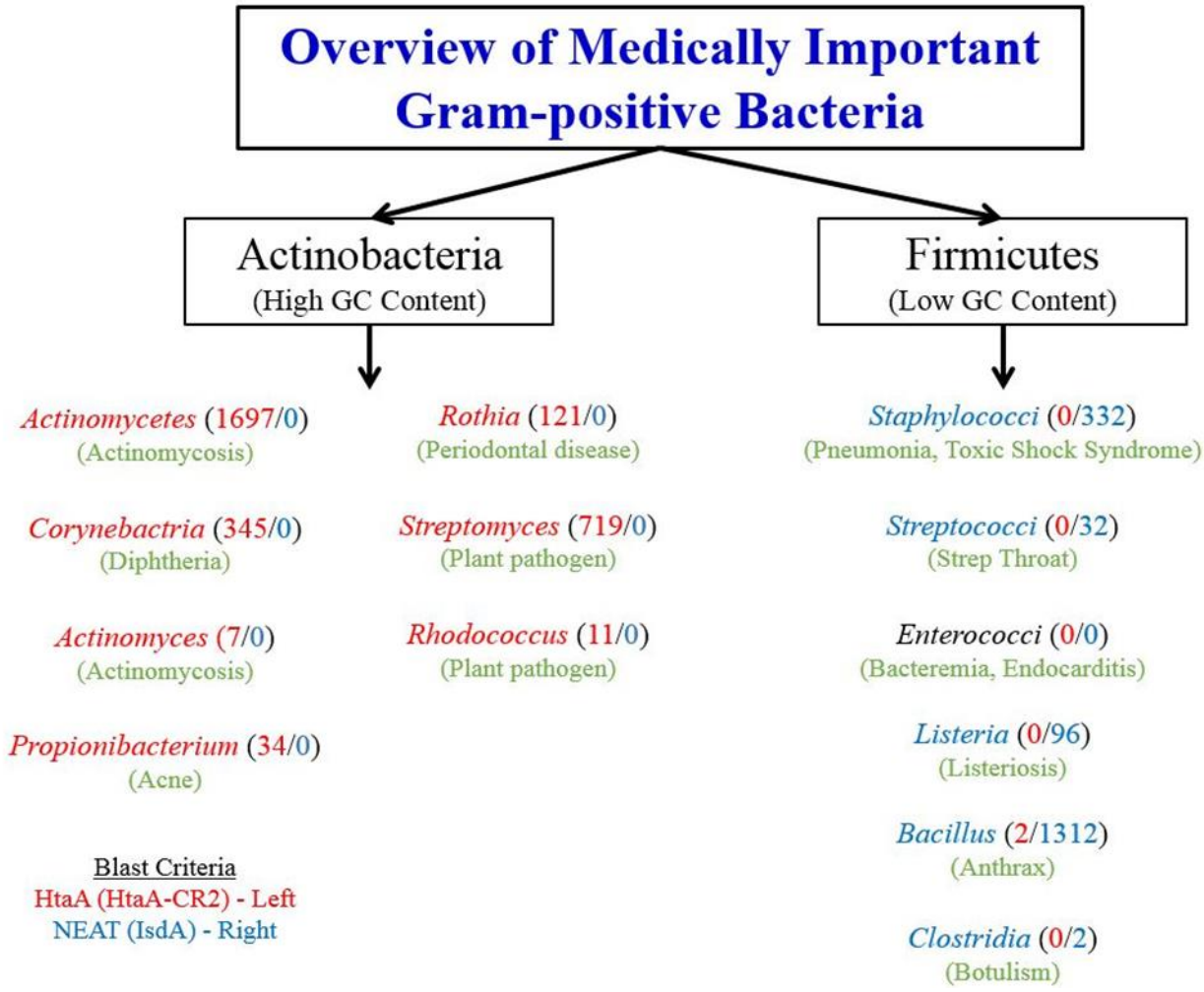

Figure 2.6 Overview of medically important gram-positive bacteria and their heme uptake strategies. The numbers in parenthesis refer to the number of results obtained from the BLAST search with a HtaA (red) or NEAT (blue) sequence.

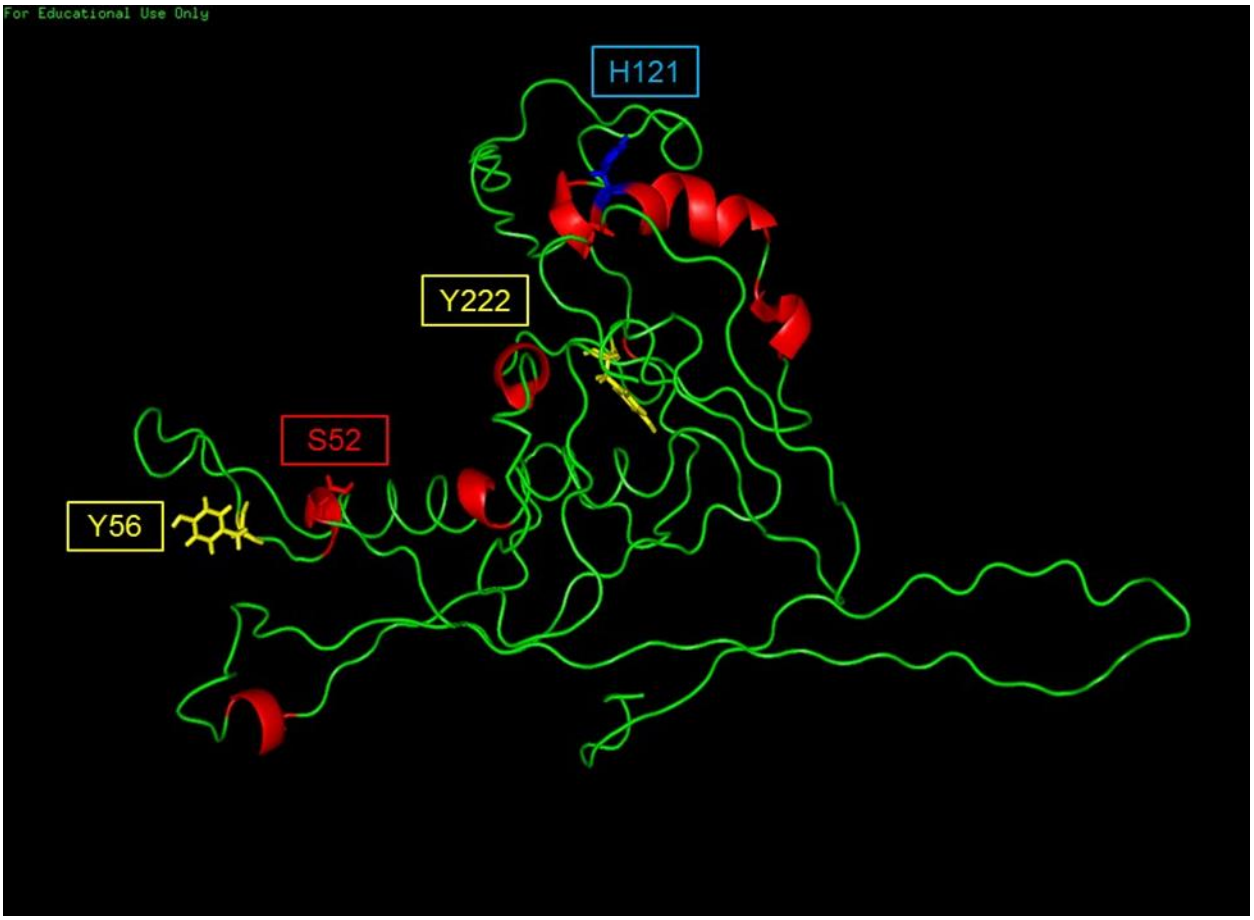

Figure 2.7 Homology model of WT HtaB-CR. The model was constructed from gp39 in marine virus Syn5 (PDB: 4BML).

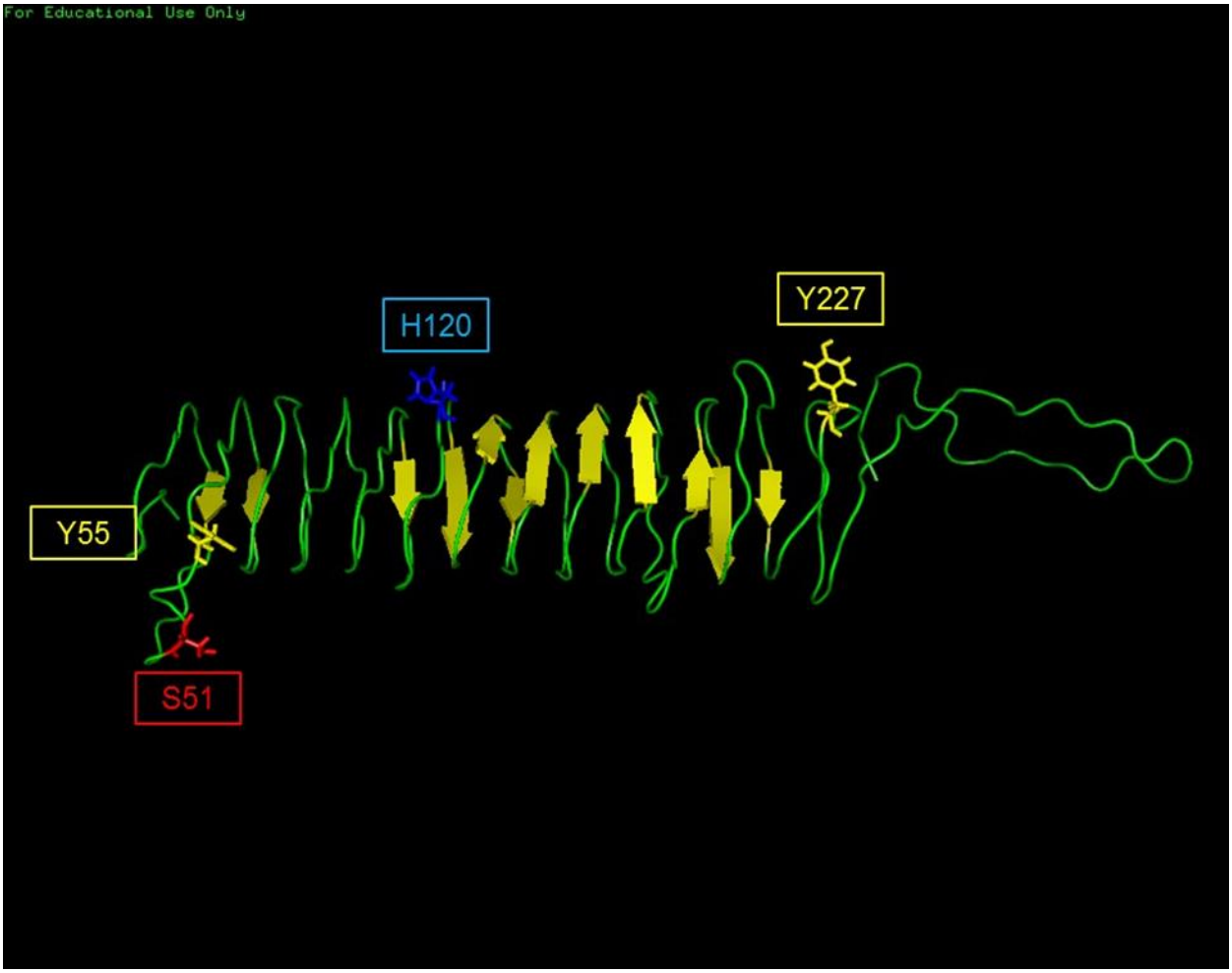

Figure 2.8 Homology model of WT ChtB-CR. The model was constructed from UspA1 in Moraxella catarrhalis (PDB: 4BML).

3 CHAPTER 3: EXPERIMENTAL CHARACTERIZATION OF THE HTAB HEME UPTAKE PROTEIN IN CORYNEBACTERIUM DIPHTHERIAE

The Raman spectroscopy sections are intended for publication verbatim in Rizvan C. Uluisik, Brandon L. Ferrell, Gudrun S. Lukat-Rodgers, Courtni E. Allen, Michael P. Schmitt, Kenton R. Rodgers, and Dabney W. Dixon.

3.1 HtaB

HtaB is a heme-binding protein encoded in the *hmu* operon, which is involved in the heme uptake pathway in *C. diphtheriae* (Allen and Schmitt, 2009). Unlike the other *hmu* genes, the *htaB* gene has a separate promoter and is transcribed separately from the other gene products. The expression of HtaB is both iron-regulated and DtxR-regulated. HtaB contains a conserved region of approximately 200 amino acid residues that shares almost 50% sequence similarity to HtaA-CR2. HtaB contains a predicted signal peptide sequence and a putative transmembrane region towards the C-terminal, which is followed by two positively charged residues (Lys and Arg).

HtaB does not bind hemoglobin (Allen and Schmitt, 2011). As shown in Figure 3.1, when HtaB was added to a hemoglobin-enriched plate using the ELISA method, there was no evidence of binding to hemoglobin. Thus, HtaB is not the protein that initially binds to hemoglobin for heme extraction.

HtaB can accept heme from HtaA, as shown in Figure 3.2 (Allen and Schmitt, 2011). In panel A, HtaB is analyzed before and after incubation with excess holo HtaA. In panel B, holo HtaA is analyzed before and after incubation with HtaB. From panel A, it can be seen that after HtaB is incubated with holo HtaA, there is a significant increase in absorbance at the Soret band. This shows that HtaB can accept heme from the holo HtaA. In panel B, it can also be seen after

holo HtaA is incubated with HtaB, there is a clear reduction of the Soret band for HtaA. This also provides evidence that holo HtaA can donate its heme with HtaB acting as the acceptor.

The goal of this study was to complement the previous microbiological studies with biophysical characterization of this protein. Herein we describe the optical and CD spectra, Raman characterization of eh ferric, ferrous, and ferrous-CO states, and unfolding induced by both heating and addition of GdnHCl.

3.2 Materials and Methods

3.2.1 *General*

UV-visible spectra were taken on a CaryBio UV-Visible spectrophotometer. Fast protein liquid chromatography (FPLC) was performed on a GE Healthcare ÄKTApurifier. Water from a Barnstead water purifier had 18.2 mΩ resistance. Buffer A was a solution of 100 mM Tris-Cl and 150 mM NaCl at pH 8.0. Buffer B was a solution of 100 mM Tris-Cl, 150 mM NaCl, and 2.5 mM *d*-desthiobiotin at pH 8.0. Buffer R was a solution of 100 mM Tris-Cl, 150 mM NaCl, and 1 mM 2-(4-hydroxypenylazo)benzoic acid. The His-column binding buffer was a solution of 20 mM sodium phosphate, 0.5 M NaCl, and 20 mM imidazole at pH 7.4. His-column elution buffer was a solution of 20 mM sodium phosphate, 0.5 M NaCl, and 500 mM imidazole at pH 7.4.

3.2.2 *Expression and Purification*

Large-scale lysogeny broth (LB) media was prepared by adding 10 g of tryptone, 10 g of sodium chloride (NaCl), and 5 g of yeast extract to a 2-L flask and filling it up to 1000 mL with water. Small-scale solutions were prepared by adjusting the above ratios to 100 mL. Glucose was added to a final concentration of 0.3%. The broth media was autoclaved and cooled to room temperature. Kanamycin (80 μM final) was added to the room-temperature broth media. The

small-scale flasks were inoculated with the *E. coli* cells containing the HtaB sequence (Figure 3.3) with an N-terminal strep tag cloned into the pET-24a(+) expression vector (supplied by Dr. Michael Schmitt) using the sterile flame loop technique. The flasks were incubated at 37 °C at 220 rpm overnight. The contents of the flask in 5 mL portions were returned to the 2-L flask containing the 1000 mL LB and kanamycin to allow for large-scale growth. The cells were grown until the OD_{600} was between 0.5 and 0.7. The media were induced with isopropyl β-D-1-thiogalactopyranoside (IPTG) with a final concentration of 100 μM, and the temperature was decreased to 28 °C. The media were allowed to shake overnight. The cells were harvested using a Beckman centrifuge with a JLA 8.100 rotor at 3100 rpm for 30 min at 4 ºC. The cells were lysed using a buffer consisting of 0.1 mM phenylmethanesulfonyl fluoride (PMSF), 0.2 mg/mL lysosome, 10 mM $MgCl_2$, 1 μg of DNAase, 1 μg of RNAase, and buffer A. The lysed cell solution was exposed to sonication on a Branson Ultrasonics Sonifier for 30 min at 15% amplitude with 10 sec on and off pulses. The solution was centrifuged at 7000 rpm for 40 min at 4ºC. The supernatant was collected and stored at -80ºC.

The protein was purified using FPLC. A 5 mL Step-Tactin Superflow column from GE Healthcare was equilibrated with buffer A. Approximately 50 mL of the cell solution was loaded onto the column. Unbound material was washed out with buffer A. HtaB was eluted by the addition of buffer B via a linear gradient of 0-100%. Fractions (2 mL) were collected. The fractions containing HtaB were centrifuged at 6500 rpm for 20 min at 4ºC. The tubes were again filled with buffer A, and this process repeated three times. The purity of the proteins was tested by sodium dodecyl sulfate polyacrylamide gel electrophoresis (SDS-PAGE). Figure 3.4 shows the protein yield for HtaB expression. The protein was stored at -20ºC.

The plasmid containing His-tagged HtaB-WT (sequence in Figure 2.5) previously constructed in a pET24a(+) expression vector was a gift from Dr. Michael Schmitt (Allen and Schmitt, 2009). The His-tagged HtaB-WT-containing cells were grown in the same manner as described above. His-tag binding buffer (20 mM sodium phosphate, 0.5 M NaCl, 20 mM imidazole, pH 7.4) was used in the place of buffer A in the lysis buffer. A 5 mL HisTrap HP column from GE Healthcare prepped in the same manner as above with binding buffer. The protein was loaded onto the column and eluted with His-tag elution buffer (20 mM sodium phosphate, 0.5 M NaCl, 500 mM imidazole, pH 7.4). Fractions were collected and centrifuged. Protein purity was tested by SDS-PAGE. The protein was stored at -20 °C.

3.2.3 *HtaB-WT Sire Directed Mutagenesis*

E. coli cells containing the pET24a(+) plasmid with the strep-tagged HtaB-WT gene were grown overnight in 10 mL of Luria-Bertani (LB) broth. The DNA from the *E. coli* was extracted using the QIAprep Spin Miniprep Kit according to the directions from the manufacturer. The extracted DNA was analyzed via nanodrop spectroscopy to determine its concentration. The primers were designed from Sigma Aldrich for the Y56A and H121A mutations and are shown in Table 3.1. The extracted plasmids were transformed using the polymerase chain reaction. The parameters used for the PCR reaction are shown in Table 3.2. The results of the PCR were analyzed using gel electrophoresis with a 2% agarose gel. The running buffer used was Tris-acetate-EDTA (10x TAE) buffer. The samples were loaded and run at 70 V for 70 min. The gel was stained with SYBR safe dye for 30-45 min. Figure 3.5 shows the image of the gel using a UVP BioDoc-It^{TM} Imaging System from the Y56A mutation after PCR.

After determining which plasmids had been successfully mutated, DpnI digestion was performed on the selected plasmids by combining 38.5 μL PCR reaction mixture with 5 μL DpnI

buffer (from Sigma-Aldrich) and water to a final volume of 49 μL. To the mixture, 1 μL of DpnI was added. The mixture was incubated at 37°C for 1 h; 1 μL of DpnI was added again and the solution incubated for 1 h.

The plasmids were transformed into competent BL21 (DE3) cells by adding 1 μL of plasmid to 50 μL competent cells. The cells were incubated on ice for 20 min, heat shocked in a 42°C water bath for 45 s, and incubated again on ice for 2 min. To the cell solution, 250 μL warm LB broth without kanamycin was added and incubated at 37°C for 1 h. The cell solution was inoculated onto agar plates and incubated at 37°C overnight. One colony was selected from the plate. Half of the colony was inoculated in 5 mL LB with kanamycin. The other half of the colony was streaked onto a new agar-kanamycin plate and grown overnight at 37°C to preserve the cell line. The DNA from the newly grown *E. coli* cells was extracted using the QIAprep Spin Miniprep Kit. The concentration of the DNA was determined using nanodrop spectroscopy. The DNA was then sent for sequencing at GENEWIZ to confirm that the mutation was successful. The WT and mutant gene sequences were aligned using the Clustal Omega program. The results of the sequence alignment of WT and H121A are shown in Figure 3.6.

After confirming the mutation, cells from the agar-kanamycin plate were grown in 10 mL of LB broth containing kanamycin overnight. The stock mutant-containing cells were made by adding 20% glycerol to the cell solution to a final volume of 1 mL. The stock solutions were placed in cryogenic tubes, flash frozen with liquid nitrogen for 2 min, then stored at -80°C.

The HtaB mutants were expressed in the same manner as described in section 3.3.2.

3.2.4 *UV-visible Absorption Spectroscopy*

The absorbance spectra of HtaB and the mutants were taken with a Cary 50 Bio UV-visible spectrophotometer. The spectra were taken at room temperature in buffer A.

3.2.5 *Determination of Percent Heme-loaded and Soret Extinction Coefficients*

A stock solution of (5.5×10^{-5} M, $\varepsilon_{280} = 43824\ M^{-1}\ cm^{-1}$, Fischer Scientific) bovine serum albumin (BSA) was dissolved in H_2O and used as a standard for the Bradford assay. The BSA absorbance was taken at 280 nm and diluted to have a final concentration of approximately 200 μg/mL. The solutions were prepared by adding the indicated amount of water to an Eppendorf tube. The BSA solution and Coomassie Brilliant Blue G-250 solution were added at 2 min intervals to cuvettes. Each sample was allowed to stand for 10 min before the spectrum was recorded. The reaction was run in duplicate.

HtaB-WT (800 μL of diluted stock solution, $Abs_{280} \sim 0.3$) was combined with 200 μL of dye. The HtaB-dye solution was allowed to sit for 10 min. The spectrum was taken of the solution. The absorbance at 595 nm was used with the calibration curve from the Bradford assay to determine the stock concentration of HtaB-WT.

For the pyridine-hemochrome assay (Berry and Trumpower, 1987), a basic pyridine solution was prepared by mixing 4 mL of pyridine with 6 mL of 400 mM NaOH. A 500 μL saturated sodium dithionate solution was prepared in a capped glass vial. Into a cuvette with a septum, 740 μL of pyridine solution were added using a 500 μL glass syringe. The spectrum was blanked with the pyridine solution. To the cuvette, 250 μL of the HtaB-WT solution used for the Bradford assay was added. The cuvette was inverted to ensure mixing. The spectrum was taken. The sodium dithionite solution (10 μL) was added via glass syringe. The spectrum was taken. The concentration of heme was calculated using the extinction coefficient of the bispyridine ferrous heme complex at 556 nm ($\varepsilon_{556} = 34640\ M^{-1}\ cm^{-1}$ at 556 nm) (Berry and Trumpower, 1987).

3.2.6 *CD Spectroscopy of HtaB-WT and Mutants*

Circular dichroism spectra were recorded using a Jasso J-810 spectropolarimeter using quartz Suprasil cuvettes with a 1 mm path length. The spectra were taken from 190 to 260 nm. The scanning speed was set to 100 nm/min in the continuous scanning mode. The data pitch was set to 0.5. As-isolated samples of HtaB-WT (~25% heme loaded), HtaB-Y56A (~5%), HtaB-H121A (~5%) were recorded in 100 mM Tris-Cl and 150 mM NaCl at pH 7.0. The final spectra each represent an average of 20 scans.

3.2.7 *Heme Transfer Between Y56A and Hemoglobin*

A five mL StrepTactin column was equilibrated with five column volumes of buffer A. One mL of 39 μM as-isolated HtaB-Y56A was loaded onto the column. Fractions were checked via UV-visible spectroscopy while loading to ensure no protein had eluted from the column. Two mL of 100 μM equine hemoglobin (ε_{280} = 12.91 mM^{-1} cm^{-1}, Sigma-Aldrich) were slowly loaded onto the column while checking fractions to ensure no protein had eluted from the column. The column was capped and incubated overnight at 4 °C. Excess hemoglobin was eluted with buffer A. The protein was eluted with buffer B. The buffer was exchanged with buffer A by centrifugation at 6500 rpm and 4°C for 40 min.

3.2.8 *Heme Titration of HtaB and Mutants*

A sample of approximately 24% heme-loaded 7.7 μM HtaB-WT (concentration calculated from ε_{280} from ExPASY) was used for the single cuvette heme titration. A solution of 2.0 mM hemin was prepared in DMSO (ε_{624} = 6.23 mM^{-1} cm^{-1}, Sigma-Aldrich). Single 1 μL aliquots of hemin were added to the solution and allowed to stir on ice for 10 min. The volume of DMSO in the cuvette was not allowed to exceed 2%. The UV-visible spectrum was recorded after each hemin addition and incubation until a hemin:protein ratio of 0.75 was reached.

A sample of approximately 5% heme loaded 18 μM HtaB-Y56A (concentration calculated from calculated ε_{280} from ExPASY) was used for the two cuvette heme titration technique. A 3.7 mM hemin solution was prepared in DMSO (ε_{624} = 6.23 mM^{-1} cm^{-1}, Sigma-Aldrich). Two quartz cuvettes were used for the titration: one containing the protein in buffer and the other containing only buffer. Hemin was added in 1 μL aliquots, without the volume of DMSO exceeding 2% in the protein solution, to both cuvettes. The cuvettes were allowed to stir on ice for 10 min. The spectrophotometer was blanked with the cuvette containing only buffer with hemin additions. The spectrum of HtaB-Y56A after the hemin addition and incubation was recorded. This was repeated up to a hemin:protein ratio of 0.74.The experiment was repeated for HtaB-H121A and His-tagged HtaB in the same manner.

3.2.9 *Resonance Raman Spectroscopy*

Resonance Raman Spectroscopy analysis was performed at North Dakota State University by Dr. Kenton Rodgers and Dr. Gudrun Lukat-Rodgers.

Resonance Raman (rR) spectra were recorded from ferric samples using the 413.1-nm emission line from a Kr^+ laser and ferrous samples with 441.6-nm excitation from a HeCd laser. The Raman shifts for toluene, dimethyl sulfoxide, and methylene bromide were used as external standards for spectral calibration. Spectra were recorded at ambient temperature using the 135° backscattering geometry with the laser beam focused to a line on a spinning 5 mm NMR tube. UV−visible spectra were recorded before and after rR experiments to verify that the samples were not altered by their exposure to the laser beam. The final protein concentration was 30 μM for the HtaB-WT. The buffers used were 100 mM glycine (9.6), Tris-HCl (pH 8.8 or 8.0), and sodium phosphate buffer (pH 5.8). Ferrous samples were prepared under anaerobic conditions by adding buffered dithionite in 300-fold molar excess over heme. The Fe^{II}-CO samples were

prepared with a 300-fold molar excess of dithionite under an atmosphere of natural abundance CO or ^{13}CO at pH 8.8.

3.2.10 *Thermal Unfolding in the Presence of GdnHCl*

Thermal unfolding was performed on the UV-visible spectrophotometer equipped with a TC125 Quantum Northwest temperature controller. A screw-top quartz cuvette with a 1 cm path length was used. As-isolated HtaB was prepared in 50 mM NaH_2PO_4 at pH 7.0 containing 1 M GdnHCl. The thermal unfolding was carried out over a temperature range of 34 to 82 ˚C. Spectra were recorded every two ˚C after a 1 min incubation period at each temperature.

Kaleidagraph (version 4.01, Synergy Software) was used to fit the data using a two-state protein unfolding model (Swint and Robertson, 1993):

$$A = \frac{(A_f + m_f T) + (A_U + m_U T)\exp[\frac{\Delta H_m}{R(Tm^{-1} - T^{-1})}]}{1 + \exp[\frac{\Delta H_m}{R(T_m^{-1} - T^{-1})}]}$$

where A is the absorbance at any temperature along the unfolding curve, A_f is the absorbance of the folded state, m_f is the slope of A vs. T for the folded state, A_U is the absorbance of the unfolded state, m_U is the slope of A vs. T for the unfolded state, T_m is the temperature at which the protein is half unfolded, ΔH_m is the enthalpy of unfolding, R is the ideal gas constant, and T is the temperature (Kelvin).

3.2.11 *Time Scale Unfolding of HtaB in the Presence of 4.0 M GdnHCl*

Solutions of ChtB and GdnHCl were each prepared in buffer A. The GdnHCl stock concentration was determined to be 7.5 M by the refractive index method (Pace and Scholtz, 1997). The stock GdnHCl solution was added to the ChtB solution to give a final concentration

of 4 M. The absorbance was recorded every 5 min for 12 h. The absorbance at 407 nm (Soret) vs. time was fit to a single-term exponential function:

$$A_t = (A_0 - A_\infty)\exp(-k_U t) + A_\infty$$

where A_t is the absorbance at any time during the unfolding reaction, A_0 is the initial absorbance, A_∞ is the absorbance of the completely unfolded protein, (A_0 - A_∞) is the total change in absorbance for complete unfolding, and k_U is the unfolding rate constant. The sample was dialyzed after unfolding to evaluate the reversibility of the unfolding process.

3.3 Results and Discussion

3.3.1 *HtaB and Mutants Growth and Expression*

In the absence of glucose, the competent cells containing the HtaB gene did not grow well, as shown in Figure 3.7. After one h of shaking in the large-scale broth, the cells reached an average OD_{600} maximum of approximately 0.2. Beyond one h of incubation, the OD_{600} dropped below 0.1 and remained unchanged even after seven h. As described above, the pET vector may be experiencing early expression of HtaB before the inducing agent is added. It may also be the case that the glucose levels of the cell are being depleted, causing the levels of cAMP to rise in the cell. This may lead to early expression of HtaB. Because HtaB is a foreign protein to *E. coli*, an early protein expression may have a toxic effect on the growth of the competent cells before the proper OD_{600} can be reached.

The addition of glucose to the large-scale broth showed a positive effect on the growth of the competent cells, as shown in Figure 3.8. An OD_{600} of 0.6 was reached after four h of shaking. All growth and expressions for HtaB and mutants were performed with the addition of 0.3% glucose to help maximize the expression of protein. The FPLC spectra from the

purification of HtaB-WT, HtaB-Y56A, and HtaB-H121A are shown in Figure 3.9, Figure 3.10, and Figure 3.11, respectively. Each spectra shows a single protein peak on the onset of linear gradient of buffer B. The single-peak fractions were collected and analyzed by SDS-PAGE to assess protein purity. The SDS gel for HtaB-WT is shown in Figure 3.12. The protein was confirmed to be pure HtaB-WT with a molecular weight of approximately 32 kDa.

3.3.2 *UV-visible Spectroscopy of HtaB-WT and Mutants*

The UV-visible spectra of HtaB-WT and mutants are shown in Figure 3.13. HtaB-WT shows a Soret peak at 409 nm and four α/β bands at 505, 546, 567, and 626 nm. The charge-transfer band at 626 nm is indicative of a high-spin heme iron interacting with an oxygen species, which is often through a Tyr ligand (Tiedemann and Stillman, 2011; Rodgers and Lukat-Rodgers, 2014). The H121A mutant showed a UV-visible spectrum similar to that of HtaB-WT, having a hypsochromic-shifted Soret peak at 405 nm. The Soret peak of Y56A showed a bathochromic shift to 414 nm with a single-large band in the α/β region between 545 and 600 nm. The disappearance of the charge-transfer band at 626 nm is consistent with the loss of an oxygen-bound ligand, which indicates that Y56 may be the acting axial ligand.

3.3.3 *Determination of Percent Heme Loading and Soret Extinction Coefficient*

The results for the determination of percent heme-loaded for HtaB-WT and mutants are shown in Figure 3.14.

The Bradford assay was run on a BSA stock solution of approximately 5.5×10^{-5} M. The solution of HtaB used four μL of HtaB, 200 μL dye, and 790 μL water. The absorbance of this solution at 595 nm was 0.22 nm. Using the equation from the Bradford assay, the concentration of the protein was found to be 0.60 μg/μL (21.6 μM).

An aliquot of the same solution of HtaB was subjected to the pyridine hemochrome assay. The absorbance of the bispyridine ferrous heme complex was 0.086 at 556 nm. Given the literature extinction coefficient of 34640 M^{-1} cm^{-1} at this wavelength (Berry and Trumpower, 1987), the concentration of pyridine hemochrome was 9.93 μM (which is also the concentration of holo protein). From the Bradford assay, the total concentration of HtaB, containing both holo and apo protein, was 21.6 μM, indicating that the HtaB solution was 45% heme loaded. Using the absorbance at the Soret of 0.63 (the solution was diluted by 2x, so the absorbance of the stock solution was 1.26) and given the holo protein concentration of 9.93 μM, the extinction coefficient for HtaB-WT at 409 nm is 1.26×10^5 M^{-1} cm^1.

The Soret:280 nm ratio is an indication of the heme loading of a protein. The Soret:280 nm ratio for the HtaB-WT sample used in the above experiment was 1.13. If a Soret:280 nm ratio of 1.13 corresponds to 45% heme loading, a Soret:280 nm ratio of 2.44 would be expected for the fully heme loaded species. From the results of HtaB-WT, the Soret:280 nm ratios of HtaB-Y56A and HtaB-H121A were calculated to be approximately 0.14 (6% heme loaded) and 0.09 (4% heme loaded), respectively. The results indicate that the Tyr and His conserved residues are important for heme binding of HtaB. This is consistent with previous microbiological results that mutations in the respective Tyr and His residues in HtaA decreases the heme binding of the protein (Allen and Schmitt, 2011).

3.3.4 *CD Spectroscopy of HtaB-WT and Mutants*

The CD spectra of HtaB-WT, Y56A, and H121A are overlaid in Figure 3.15. HtaB-WT appears to contain mostly β-sheets, as apparent by the single minimum at 215 nm. Both of the HtaB mutants are very similar to that of HtaB-WT. There appears to be no change in the protein

secondary structure with the mutations of the conserved Tyr and His residues. In addition there appears to be no significant change in secondary structure as the percent heme loading decreases.

3.3.5 *Hemoglobin Heme Transfer to HtaB-Y56A*

Previous studies showed that HtaB-WT has the ability to accept heme when hemoglobin is the sole iron source (R. Uluisik, unpublished data). Our experiments show that HtaB-Y56A can also accept heme from hemoglobin. Figure 3.16 shows the spectrum of a sample HtaB-Y56A before and after incubation with hemoglobin. Before incubation, the Soret:280 ratio was 0.06:1, indicating predominately apo protein. After incubation, the Soret:280 changed from 0.06 (~2% heme-loaded) to 0.7 (~24% heme-loaded), which indicates a significant increase in heme-bound protein. After the uptake of heme from Hb, the Soret showed a hypsochromic shift from 415 nm to 409 nm. In addition to the change at the Soret, the bands at 546 nm and 567 nm disappeared, and new bands appeared at 505 nm and 624 nm. This spectrum is similar to that of HtaB-WT. As described above, a band at approximately 625 nm is consistent with a 6-coordinate, high-spin heme complex in which one of the axial ligands is coordinated through an oxygen atom. Since the presumed Y56 axial ligand is no longer present, the spectrum may indicate that the protein has undergone a conformational change to provide another oxygen-coordinated axial ligand, presumably a tyrosine or water molecule.

3.3.1 *HtaB Hemin Titration*

The results of the one-cuvette hemin titration for a sample of HtaB-WT (~24% heme-loaded) are shown in Figure 3.17. The Soret:280 nm ratio increased from 0.6 to 1.4. As the ratio of hemin to HtaB-WT increased the λ_{max} Soret stayed almost constant (changing from only 410 to 408 nm over the range of ratios of 0.00-0.58). This indicates that most of the hemin is being taken up at the hemin binding site of the protein. A shoulder starts to appear at approximately

365 nm, as the amount of added heme increases. This might be due to free hemin in solution or heme on the surface of the protein. A plot of Abs_{365}/Abs_{406} vs. the ratio of hemin to HtaB-WT (Figure 3.18) shows an increase as the concentration of hemin increases, indicating that the additional hemin is not binding to the canonical binding site. This titration resulted in a sample that was approximately 60% heme-loaded.

The result for the two-cuvette heme titration of HtaB-Y56A is shown in Figure 3.19. HtaB-Y56A as-isolated was approximately 5% heme-loaded. As described above, the fully heme-loaded Soret:280 nm ratio for HtaB-Y56A was expected to be 2.52. HtaB-Y56A reached a Soret:280 nm ratio of 1.41, indicating that the sample ended as only ~50% heme-loaded. Figure 3.20 shows the plot of the absorbance at the Soret versus the heme:protein ratio. Once the heme:protein ratio of 0.4 was reached, the slope of the line changed little, again indicating little or no further binding. The reason for the inability of this protein to fully bind hemin is not known.

The results for the two-cuvette heme titration for a sample of HtaB-H121A is shown in Figure 3.21. HtaB-H121A as-isolated was approximately 4% heme loaded. A shoulder around 365 nm began to form once the heme:protein ratio reached 0.65. The formation of a shoulder could indicate that the heme is binding in another position. A plot of the Abs_{365}:Abs_{Soret} ratio versus the heme:HtaB-H121A ratio (Figure 3.22) was constructed to assess whether or not the spectra were changing. There may be some numerical evidence of heme binding outside the conical pocket. The protein was not fully heme-loaded by the end of the titration (~45%).

Figure 3.23 shows the results of the two cuvette heme titration of the His-tagged HtaB. The as-isolated spectrum of His-tagged HtaB-WT is similar to that of strep-tagged HtaB-WT. Both spectra show a Soret peak at 409 nm and similar α/β regions. Upon heme additions, the

protein spectrum of His-tagged HtaB changes. A shoulder peak at approximately 435 nm beings to appear. The α/β regions begin to change with two dominant bands at 545 nm and 570 nm becoming more prevalent as the heme:protein ratio increases. The region around 350 nm decreases, which is different from what is seen in the Strep-tagged HtaB. It may be that the His tag itself is binding the heme. This is not surprising as His is a known heme axial ligand of various proteins (Arnoux et al., 1999; Alontaga et al., 2009; Kumar et al., 2013). It has been shown that the His-tag can interfere with proper heme binding to the protein (Owens et al., 2012).

3.3.2 *Resonance Raman of Ferric HtaB-WT*

The Resonance Raman (rR) spectra were taken by Dr. Kenton Rodgers and his group at North Dakota State University.

The rR spectrum of ferric HtaB is pH independent, as evidenced by the unchanging high-frequency spectrum over the pH range from 5.8 to 9.6 (Figure 3.24). The ν_3, ν_{38}, and ν_2 core stretching frequencies of 1483, 1520 and 1561 cm^{-1}, respectively, reveal the heme to be in a 6-coordinate high spin (6cHS) state (Hu et al., 1996). Another protein in a heme uptake pathway, *Yersinia pseudotuberculosis* (*Yp*) HasA, has been shown to exist as an equilibrium mixture of 6cHS and 5-coordinate high-spin (5cHS) states (Ozaki et al., 2014), the former presumably having a water molecule as the sixth ligand. *Yp*HasA also does not show a pH dependence over the pH range from 5 to 10. *Serratia marcescens* (*Sm*) HasA (Lukat-Rodgers et al., 2008) and *Cd*HmuT are mixtures of 6cHS and six-coordinate low-spin (6cLS) states (Draganova et al., 2015). Even though the CR domain of HtaB shares approximately 27% sequence identity and 38% similarity with the CR2 domain of HtaA, the hemin binding motifs are distinct because *Cd*HtaA is 5cHS in the ferric form (Uluisik et al., 2017). HtaA exhibits a rR spectrum typical of

5cHS hemin that is bound to the protein through a proximal tyrosine ligand. The ν_3 (1490 cm^{-1}) and ν_2 (1568 cm^{-1}) rival the intensity of the ν_4 which is unusual for other hemin proteins but has been observed in bovine liver catalase (Chuang et al., 1988) and *Shigella dysenteriae* ShuT (Eakanunkul et al., 2005), both of which share the proximal Tyr binding motif.

3.3.3 *Resonance Raman of Ferrous Carbonyl HtaB-WT*

Through the sensitivity of Raman-active Fe-CO group frequencies to π-back bonding and donor strength of the *trans* (proximal) ligand, resonance Raman spectra of heme protein carbonyls are useful probes of both the bonding and non-bonding properties of the heme pocket. The extent of π-back bonding is evidenced by the ν_{Fe-C}, ν_{C-O} frequencies which, when placed on a plot of ν_{Fe-CO} versus ν_{C-O} frequencies, yield insight into the electrostatic and steric properties of the distal heme pocket and the nature of the *trans* axial ligand (Vogel et al., 2000; Spiro and Wasbotten, 2005; Streit et al., 2010; Spiro et al., 2013). The Fe−^{13}CO isotopolog of HtaB was used to verify the identity of rR bands corresponding to the Fe−C stretching (ν_{Fe-CO}), Fe-CO bending (δ_{Fe-CO}) and C−O stretching (ν_{C-O}) modes, as shown in Figure 3.25.

Under an atmosphere of carbon monoxide, the UV-visible spectrum of ferrous HtaB exhibits a shift of the Soret band maxima to 417, along with sharpening and shifting of the Q bands (Figure 3.25). These absorbance changes are consistent with the formation of the HtaB carbonyl.

The Soret-excited rR spectrum of HtaB−CO reveals two ν_{Fe-CO} bands at 503 and 532 cm^{-1}, which shift to 501 and 527 cm^{-1}, respectively, upon ^{13}CO substitution. Despite having two ν_{Fe-CO} stretches, the spectrum reveals only one ν_{C-O} band and a single δ_{Fe-CO} band at 1949 and 562 cm^{-1}, respectively, which shift to 1902 and 554 cm^{-1} in the ^{13}CO isotopolog (Figure 3.25). Placement of the ν_{C-O} and ν_{Fe-CO} frequencies on the π-back bonding correlation plot is consistent

with two heme carbonyls having different proximal ligands (Figure 3.26). One form falls near the line correlating ν_{C-O} and ν_{Fe-CO} of carbonyls having neutral imidazole ligands. The other falls on the correlation line neutral proximal ligands coordinated through an O atom. This position is consistent with a proximal Tyr ligand whose coordinated O atom interacts with a single hydrogen bond donor (*vide infra*).

The CO ligand in the *trans* ImH form is in a weak hydrogen bond interaction with the distal pocket as evidenced by its low position along the neutral imidazole line (Smulevich et al., 1988). This interaction likely involves the native, conserved Tyr56 axial ligand interacting with the exogenous CO ligand like that reported for *Cd*HmuT mutants R237A and M292A (Draganova et al., 2016). The position of the form having an O-bound proximal ligand, which is likely the conserved Tyr56, is indicative of stabilization of the oxygen by a single neutral hydrogen-bonding partner. The position is close to both *Yp*HasA (Ozaki et al., 2014) and *Sm*HasA (Caillet-Saguy et al., 2008) which have been shown to have a *trans* neutral His that is hydrogen bonded to the axial Tyr (Arnoux et al., 1999; Ozaki et al., 2014). The *trans* ligand environment of HtaB differs from that of *Cd*HmuT, which has been shown to have a pair of hydrogen bonds from the guanidinium side chain of a nearby Arg residue (Draganova et al., 2015; Akbas et al., 2016). The positioning of the Arg hydrogen-bonding partner of the Tyr ligand in the crystal structure of *Cg*HmuT has been shown (Muraki and Aono, 2015). A possible neutral hydrogen-bonding partner could be Tyr53 which could stabilize the Tyr56 heme ligand in HtaB, similar to what is seen with IsdB (Gaudin et al., 2011).

3.3.4 *Thermal Unfolding in the Presence of GdnHCl*

It was previously shown that heating HtaB to 70°C did not show any significant change in the Soret (R. Uluisik, unpublished data). Therefore, the thermal denaturation was monitored in

the presence of a 1.0 M GdnHCl. Figure 3.27 shows the unfolding curve for HtaB. The apparent T_m in the presence of 1.0 M GdnHCl was 61 °C. There is an isosbestic point at 375 nm for the unfolding spectra up to the T_m point (data not shown). After the T_m, the spectra deviated from the isosbestic point.

The HtaB solution was allowed to cool back to the starting temperature to test for reversibility of the unfolding. Approximately 50% of the Soret was recovered after refolding.

3.3.5 *Time Scale Unfolding of HtaB in the Presence of 4.0 M GdnHCl*

The unfolding curve of HtaB in the presence of 4 M GdnHCl is shown in Figure 3.28. As HtaB unfolded, the Soret band decreased, and a shoulder band around 350 nm increased. The data at 409 nm were fit to a single-term exponential decay function, which suggested a single first-order unfolding process. Unfolding was taken to 95% completion. The rate constant was 0.018 ± 0.001 min^{-1} (half-life of 39 min). In contrast, HtaA-CR2 was shown to have a half-life of 330 min in the presence of 6.6 M GdnHCl (Uluisik et al., 2017). After dialysis, the Soret band decreased by 50%, indicating that HtaB was less heme loaded after dialysis. Considering the loss of some protein from dialysis, the refolding of HtaB is at least 50% reversible.

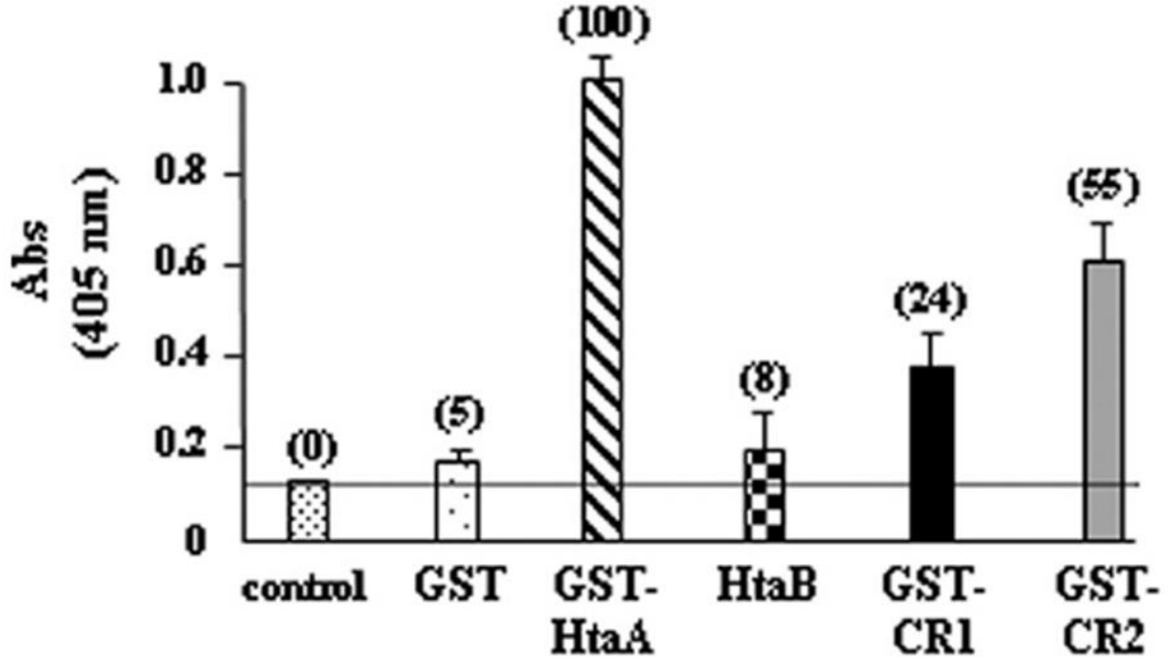

Figure 3.1 Hemoglobin binding to various hmu gene proteins. Taken from (Allen and Schmitt, 2011).

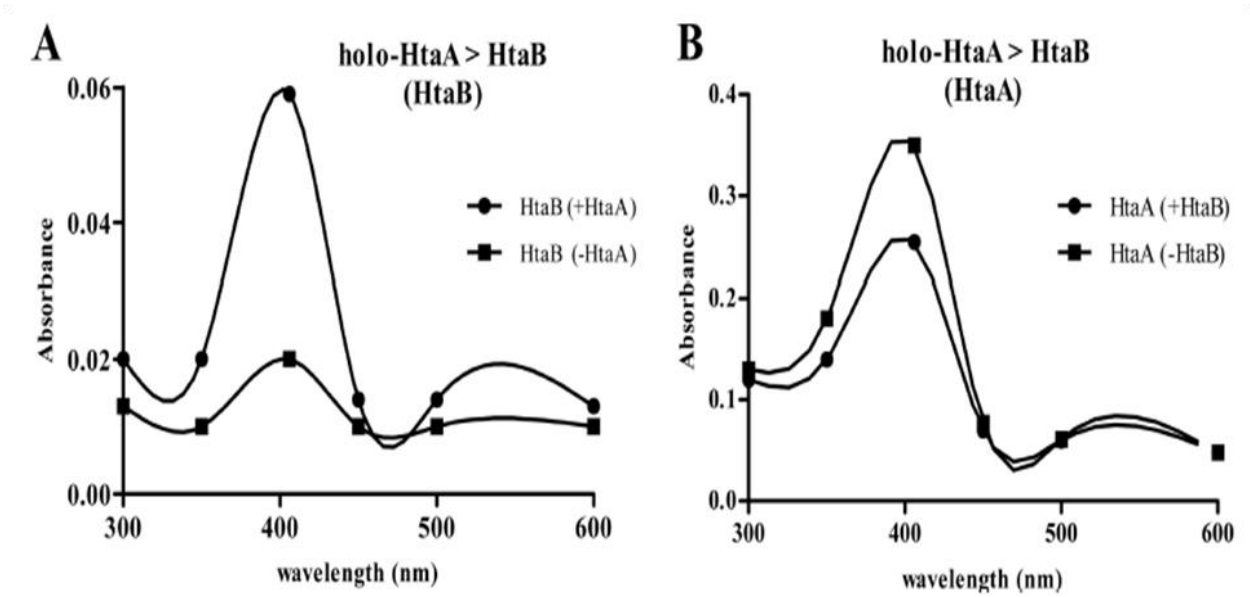

Figure 3.2 Heme transfer between HtaA and HtaB. Taken from (Allen and Schmitt, 2011).

MAS**<u>WSHPQFEK</u>**SGGGGGGENLYFQGAEEPAAASQCEMVQVIESGTLKWGVKHSYRQYI
LNNKLANGNWKVAGDIKEVGEKRGKDFYFEVPVDPQISNLEIKDNKIVEAEINTKDSSIV
FEGHHGSLYSELHNPYVTTKDNVVKAGVSYVGYYVPGKNMTEYKEADRTEANKRSGR
DTFGNGTTAGWTLNETDATLSGSNMRYVPQPKTKDNVIDGVDVIFMGQYDGDYNSDL
DDVKVDLKLKKVCKDEAEKLKAEYKKNVELASQKAAHSQSGSRTGGESTSTAPTSSTS
GFN

Figure 3.3 The sequence of the conserved domain of HtaB as supplied by Dr. Michael Schmitt. The strep tag sequence is underlined and bolded.

	HtaB-WT	HtaB-Y56A[a]	HtaB-H121A[a]
mL Isolated	8.0	8.0	10.0
Abs_{280}	0.56 (4x dilute)	1.25	1.70
$[protein]_{final}$ (μM)	53	~ 30	~ 40
Vol of broth used (L)	3	3	3
mg/L	4.5	2.6	4.3

[a]The values calculated for the mutants were based on comparing the calculated area under the curve for HtaB-WT with the mutants. The values for the mutants are approximate.

Figure 3.4 Comparing the protein yield of HtaB-WT, HtaB-Y56A, and HtaB-H121A.

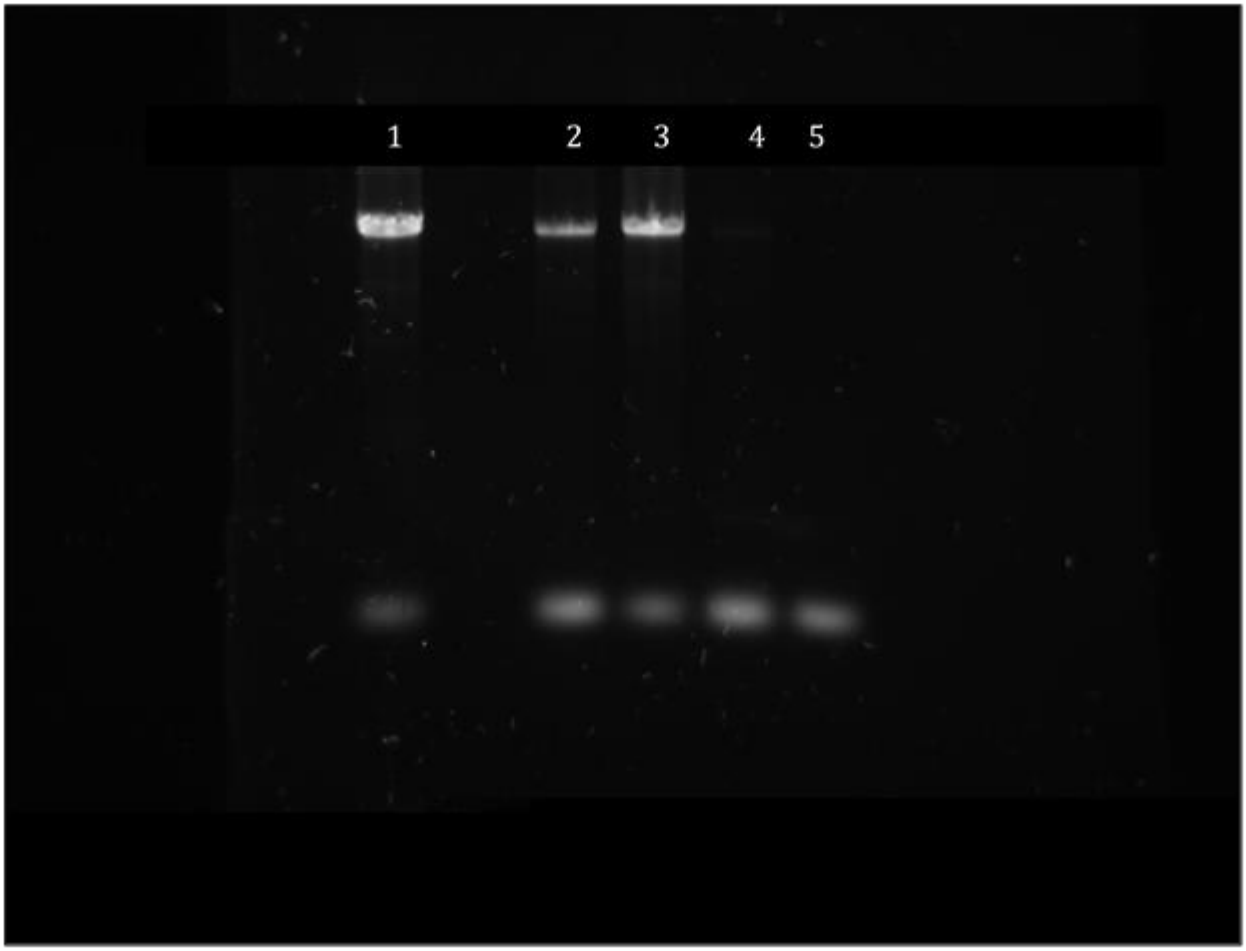

Figure 3.5 Agarose gel of the PCR reaction of HtaB Y56A. Lanes corresponding to the five reactions in Table A are shown.

```
HtaB-CR     TATGGCCAGCTGGAGCCACCCGCAGTTCGAAAAGAGCGGTGGTGGTGGTGGTGAAAATCT  62
H121A-F     TATGGCCAGCTGGAGCCACCCGCAGTTCGAAAAGAGCGGTGGTGGTGGTGGTGAAAATCT  120
            ************************************************************

HtaB-CR     GTATTTCCAGGGTGCTGAAGAACCGGCAGCCGCATCTCAGTGTGAGATGGTGCAGGTGAT  122
H121A-F     GTATTTCCAGGGTGCTGAAGAACCGGCAGCCGCATCTCAGTGTGAGATGGTGCAGGTGAT  180
            ************************************************************

HtaB-CR     CGAAAGTGGCACGCTGAAGTGGGGTGTGAAACACTCCTATCGTCAGTATATTCTTAATAA  182
H121A-F     CGAAAGTGGCACGCTGAAGTGGGGTGTGAAACACTCCTATCGTCAGTATATTCTTAATAA  240
            ************************************************************

HtaB-CR     CAAGCTAGCTAACGGTAATTGGAAAGTTGCCGGAGATATTAAAGAAGTCGGAGAAAAGAG  242
H121A-F     CAAGCTAGCTAACGGTAATTGGAAAGTTGCCGGAGATATTAAAGAAGTCGGAGAAAAGAG  300
            ************************************************************

HtaB-CR     GGGGAAAGACTTCTACTTTGAGGTTCCCGTTGATCCGCAGATATCGAACCTTGAGATAAA  302
H121A-F     GGGGAAAGACTTCTACTTTGAGGTTCCCGTTGATCCGCAGATATCGAACCTTGAGATAAA  360
            ************************************************************

HtaB-CR     AGACAATAAAATCGTAGAGGCCGAAATCAATACTAAGGATTCAAGCATTGTTTTTGAAGG  362
H121A-F     AGACAATAAAATCGTAGAGGCCGAAATCAATACTAAGGATTCAAGCATTGTTTTTGAAGG  420
            ************************************************************

HtaB-CR     GCATCACGGTTCCCTTTATTCGGAATTGCATAACCCCTACGTCACGACCAAAGATAATGT  422
H121A-F     GGCGCACGGTTCCCTTTATTCGGAATTGCATAACCCCTACGTCACGACCAAAGATAATGT  480
            *   ************************************************************

HtaB-CR     GGTTAAAGCAGGTGTAAGTTACGTTGGATATTATGTTCCCGGCAAGAATATGACTGAATA  482
H121A-F     GGTTAAAGCAGGTGTAAGTTACGTTGGATATTATGTTCCCGGCAAGAATATGACTGAATA  540
            ************************************************************

HtaB-CR     CAAGGAAGCTGACCGAACTGAAGCCAACAAGCGTTCAGGGCGTGACACCTTTGGTAATGG  542
H121A-F     CAAGGAAGCTGACCGAACTGAAGCCAACAAGCGTTCAGGGCGTGACACCTTTGGTAATGG  600
            ************************************************************

HtaB-CR     AACAACTGCTGGTTGGACTCTAAACGAGACTGACGCCACACTTAGCGGATCTAATATGCG  602
H121A-F     AACAACTGCTGGTTGGACTCTAAACGAGACTGACGCCACACTTAGCGGATCTAATATGCG  660
            ************************************************************

HtaB-CR     CTATGTTCCTCAGCCTAAGACTAAAGATAACGTGATTGACGGCGTCGATGTCATCTTTAT  662
H121A-F     CTATGTTCCTCAGCCTAAGACTAAAGATAACGTGATTGACGGCGTCGATGTCATCTTTAT  720
            ************************************************************

HtaB-CR     GGGTCAGTACGATGGCGACTACAACTCTGACCTCGACGATGTAAAAGTTGACCTCAAGCT  722
H121A-F     GGGTCAGTACGATGGCGACTACAACTCTGACCTCGACGATGTAAAAGTTGACCTCAAGCT  780
            ************************************************************

HtaB-CR     CAAGAAAGTCTGTAAGGACGAAGCAGAAAAGCTCAAGGCTGAATATAAGAAAAATGTAGA  782
H121A-F     CAAGAAAGTCTGTAAGGACGAAGCAGAAAAGCTCAAGGCTGAATATAAGAAAAATGTAGA  840
            ************************************************************

HtaB-CR     GCTTGCTAGCCAGAAGGCTGCGCACAGTCAGTCAGGGAGCCGCACGGGTGGGGAGTCCAC  842
H121A-F     GCTTGCTAGCCAGAAGGCTGCGCACAGTCAGTCNGG-NGCCGCACGGGTGGGGAGTCCAC  899
            ********************************** **  **********************

HtaB-CR     TTCGACTGCACCGACAAGTTCTACTTCTGGTTTTAACTAAAAG----------------  885
H121A-F     TTCGACTGCACCGACAAGTTCTACTTCTGGTTTTAACTAAAAGCTTGCGGCCGCACTCGA  959
            ****************************************
```

Figure 3.6 DNA sequence alignment of wild type HtaB-CR and the HtaB-CR H121A mutant in the forward direction. The missing stars represent the mutation in the seventh row (CAT = His, GCG = Ala). Clustal Omega was used for the alignment (Sievers et al., 2011; Li et al., 2015).

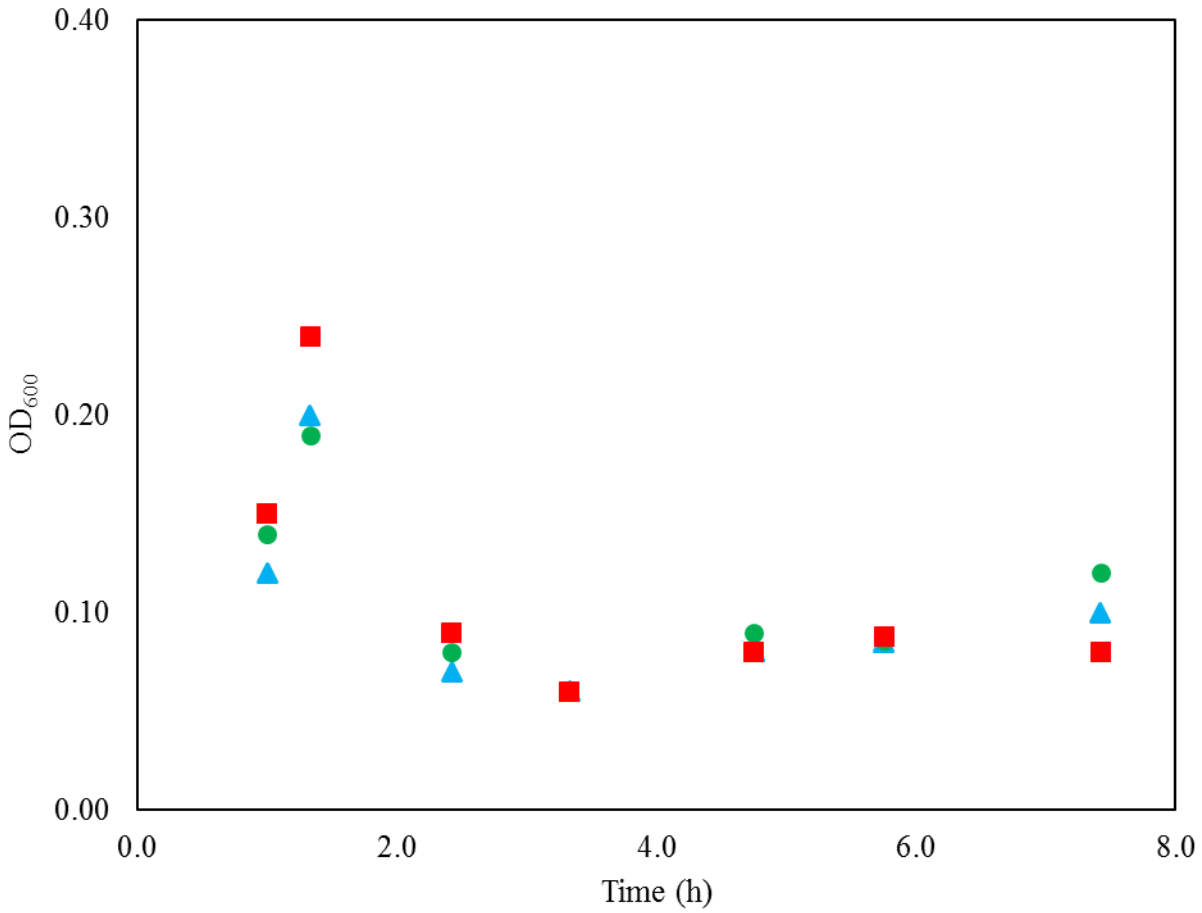

Figure 3.7 The optical densities at 600 nm for the growth of HtaB-containing cells with no glucose are plotted as a function of time. The three data points represent triplicate runs.

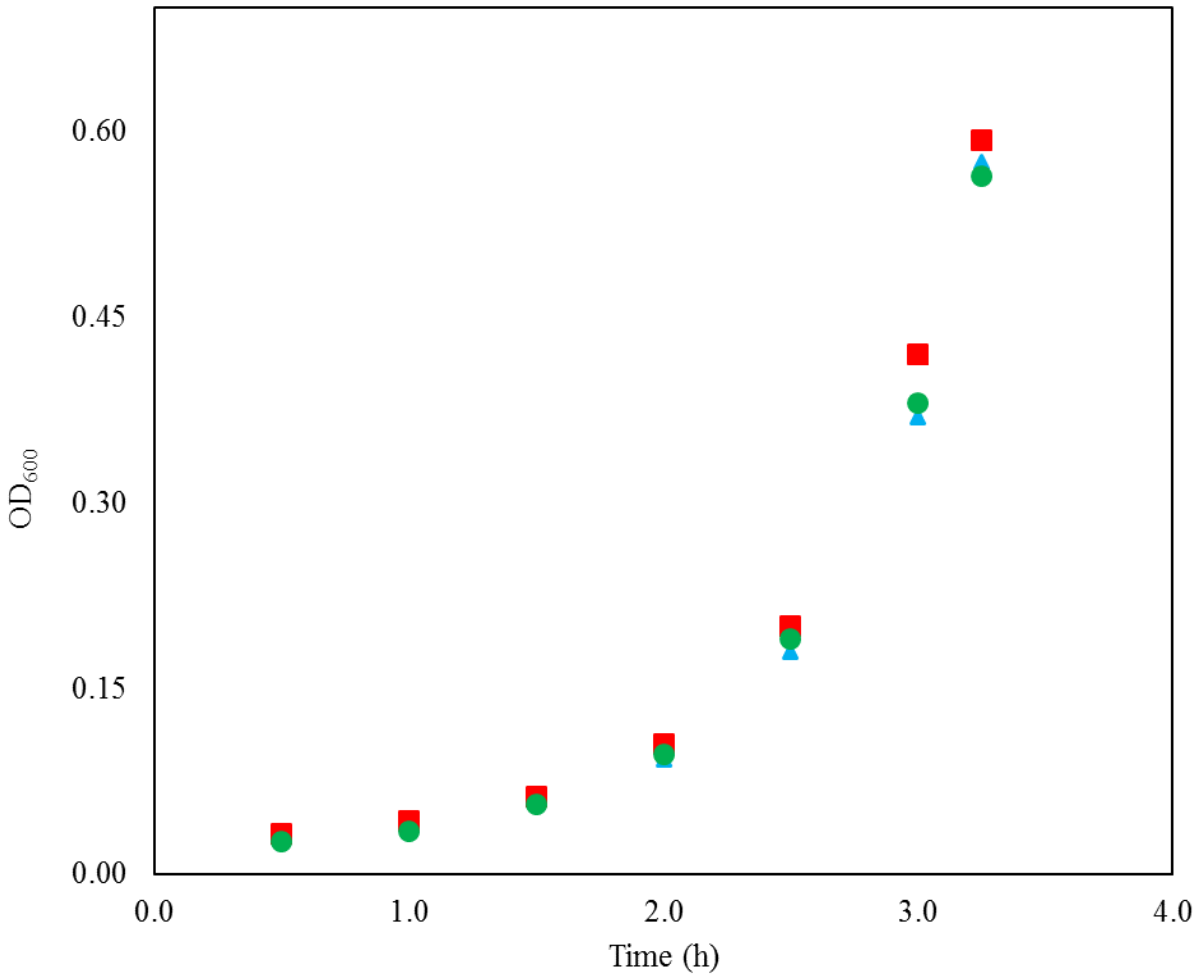

Figure 3.8 The optical densities at 600 nm for the growth of HtaB-containing cells with 0.3% glucose are plotted as a function of time. The three data points represent triplicate runs.

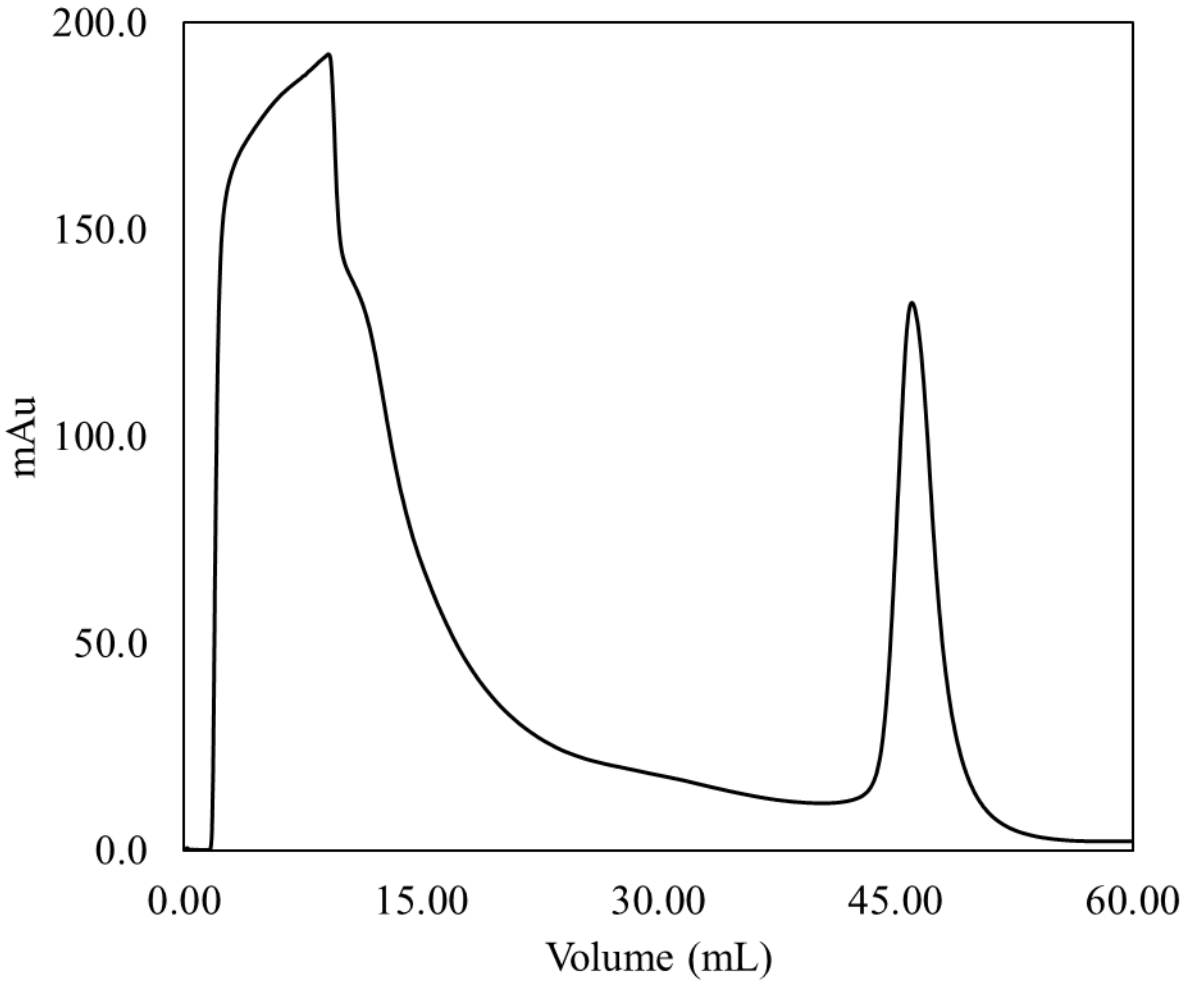

Figure 3.9 Absorbance as fraction collected of strep-tagged HtaB-WT purified on a StrepTactin column. HtaB-WT is seen as a peak between 42-50 mL. The FPLC was run at 4 °C with a linear gradient of buffer B (0-100%).

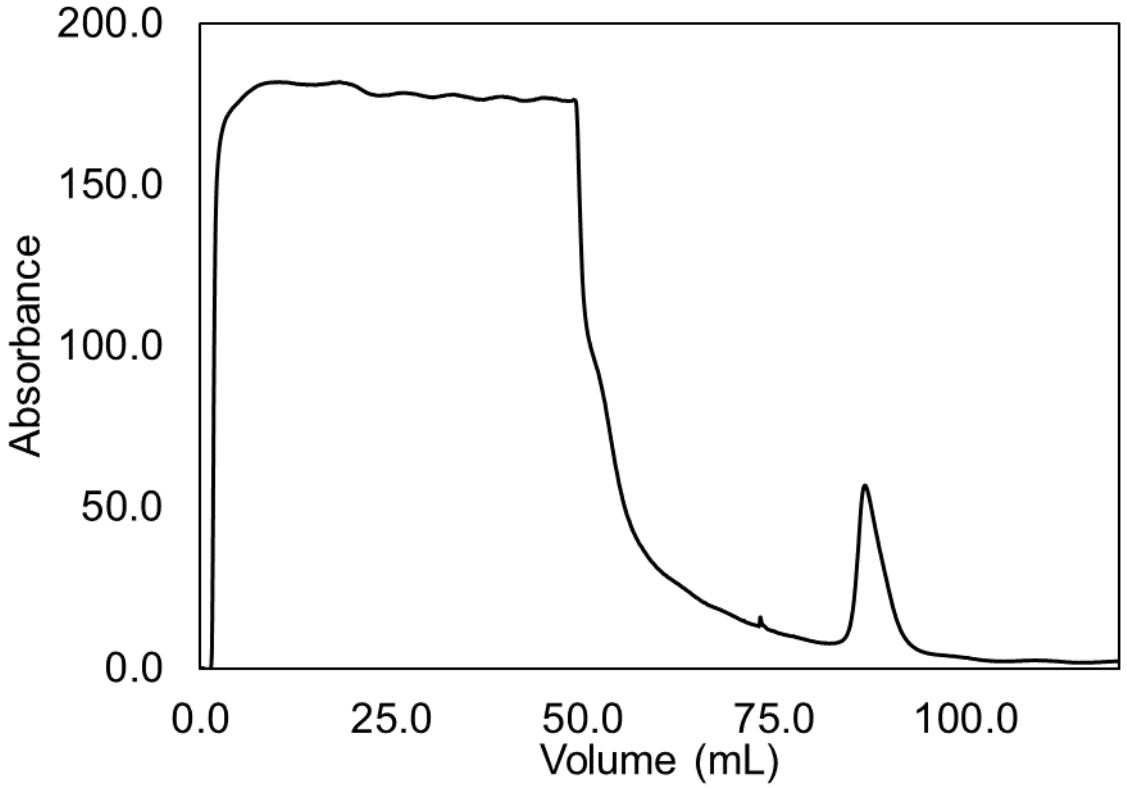

Figure 3.10 Absorbance as fraction collected of strep-tagged HtaB Y56A purified on a StrepTactin column. HtaB Y56A is seen as a peak between 84-92 mL. The FPLC was run at 4 °C with a linear gradient of buffer B (0-100%).

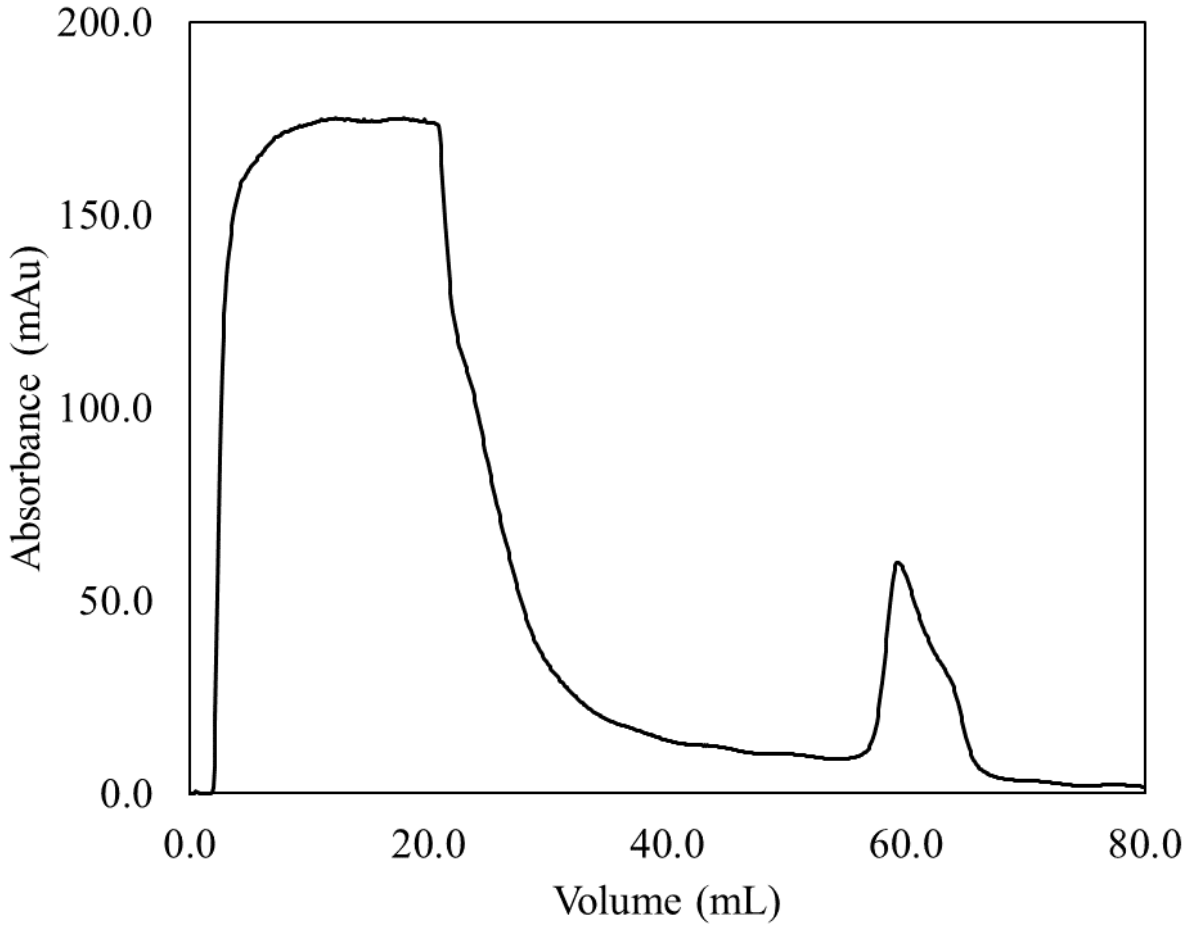

Figure 3.11 Absorbance as fraction collected of strep-tagged HtaB H121A purified on a StrepTactin column. HtaB H121A is seen as a peak between 56-66 mL. The FPLC was run at 4 °C with a linear gradient of buffer B (0-100%).

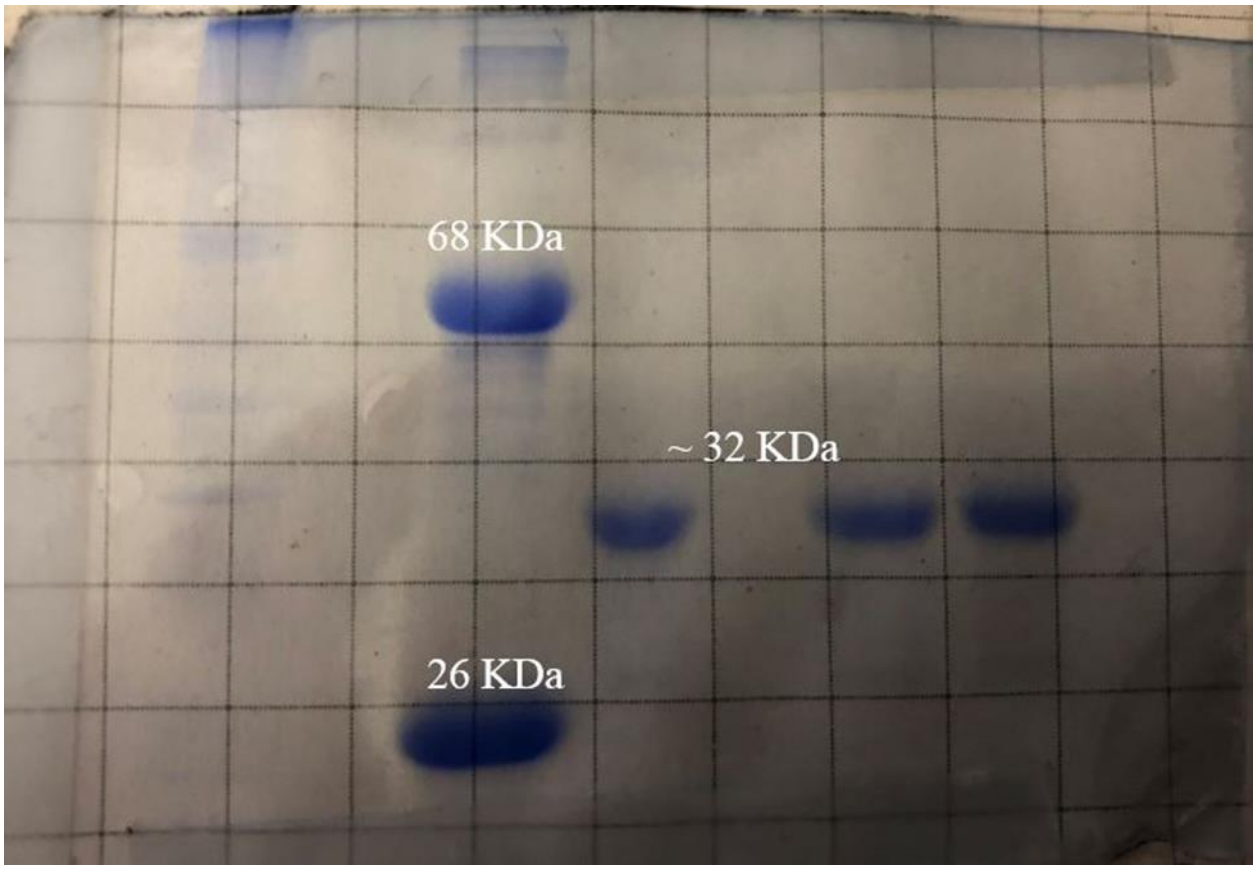

Figure 3.12 SDS PAGE gel of WT HtaB-CR confirms a molecular weight of ~ 32 kDa. The first two lanes consist of protein ladders, and lanes 3-5 consist of purified strep-tagged HtaB. The big bands in the second lane represent proteins with masses of 68 kDa and 26 kDa.

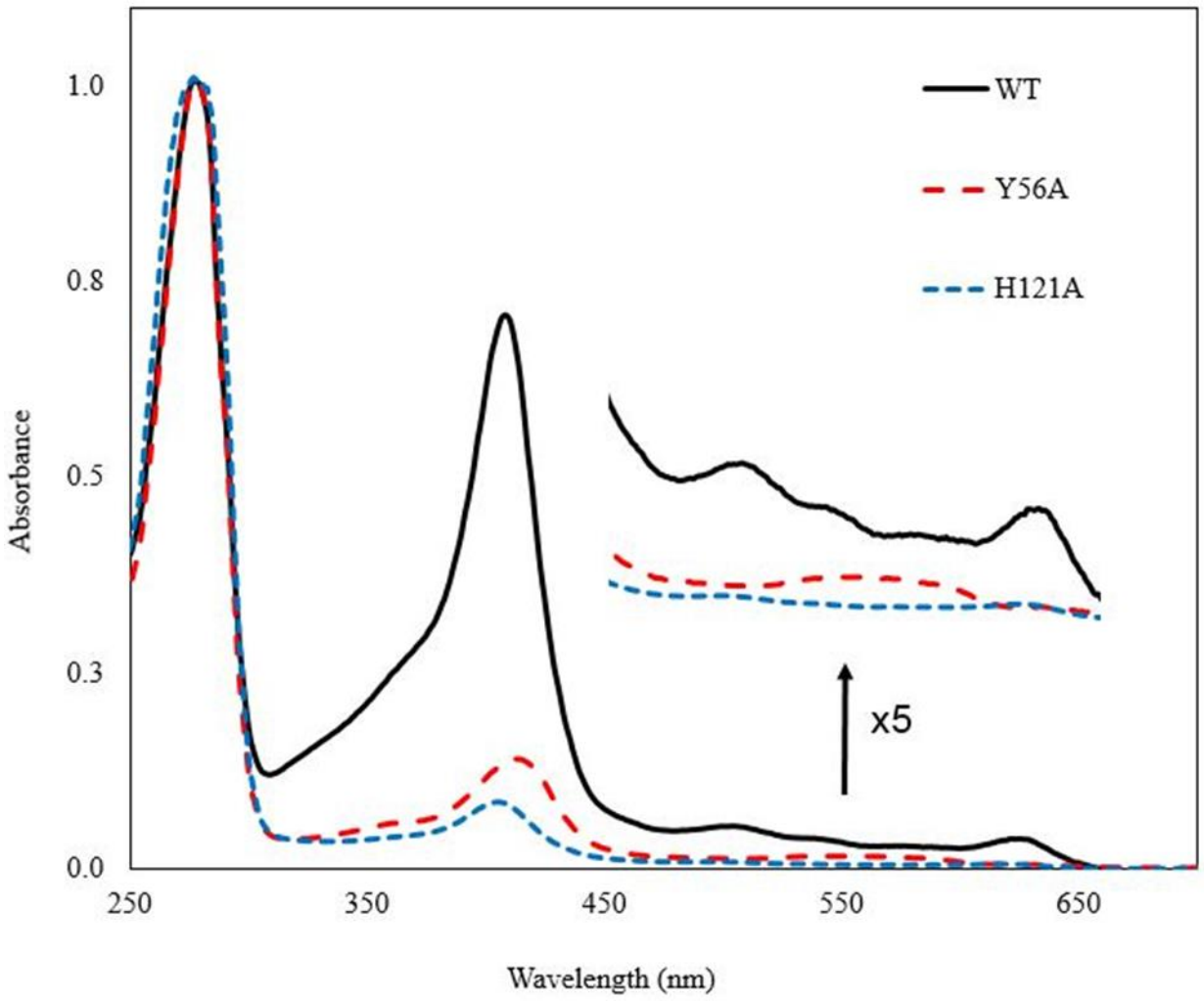

Figure 3.13 The UV-visible spectra of HtaB-WT, Y56A, and H121A. The absorbances at 280 nm have been normalized to 1.0. All spectra were taken in buffer A.

	HtaB-WT	HtaB-Y56A[a]	HtaB-H121A[a]
Bradford Concentration (μM)	21.6	-	-
Abs_{556} Pyridine hemochrome	0.34 (4x dilute)	-	-
Holoprotein (μM)	9.93	-	-
As-isolated Heme Loading	45%	6%	4%
Ratio Soret:280 nm	1.13	0.14	0.09
Theoretical Fully Heme-loaded Soret:280 nm ratio	2.44	2.52	2.25

[a]The values calculated for the HtaB mutants are based on the experimental results for HtaB-WT.

Figure 3.14 Comparing the heme-loading of HtaB-WT, HtaB-Y56A, and HtaB-H121A.

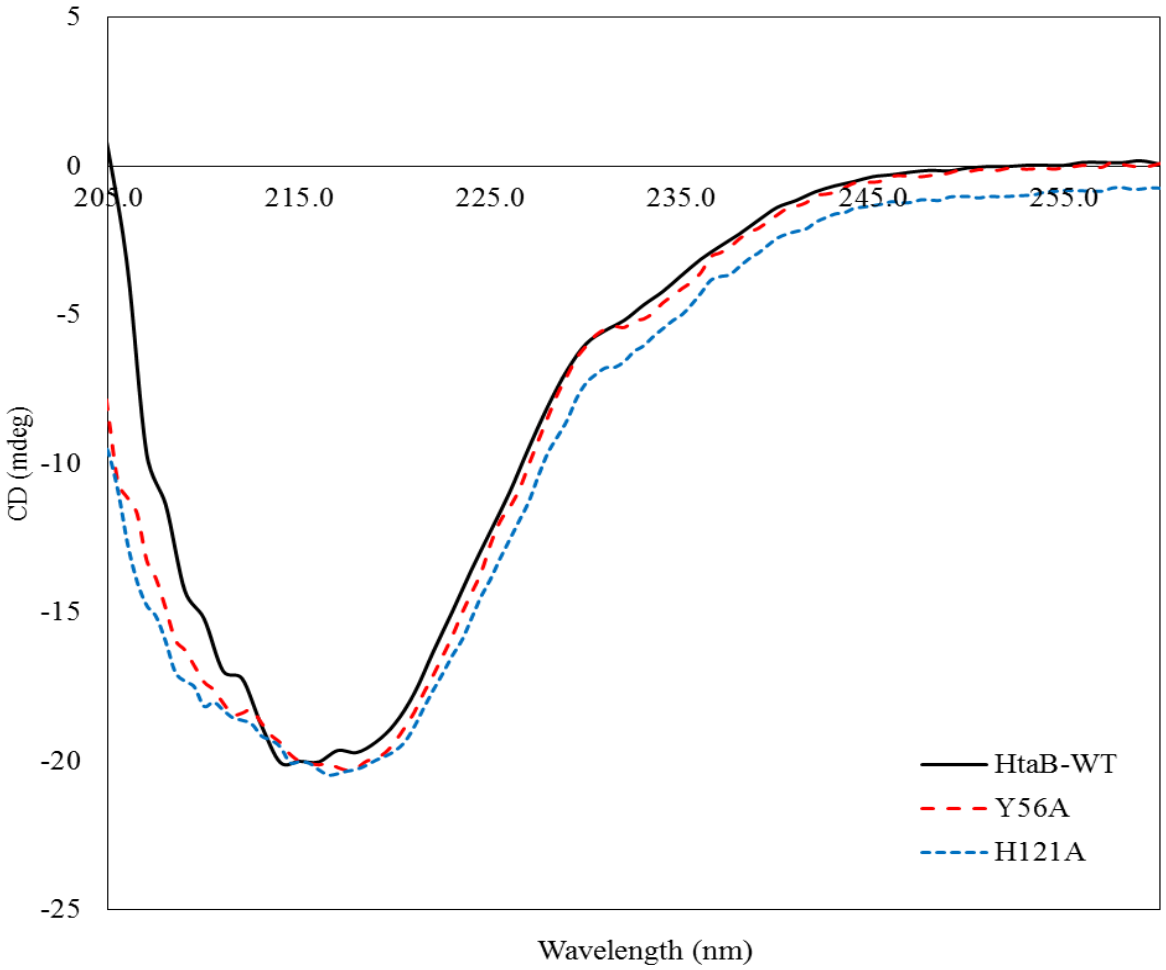

Figure 3.15 Circular dichroism spectra of HtaB-WT, Y56A, and H121A. All spectra were an average of 20 scans in buffer A.

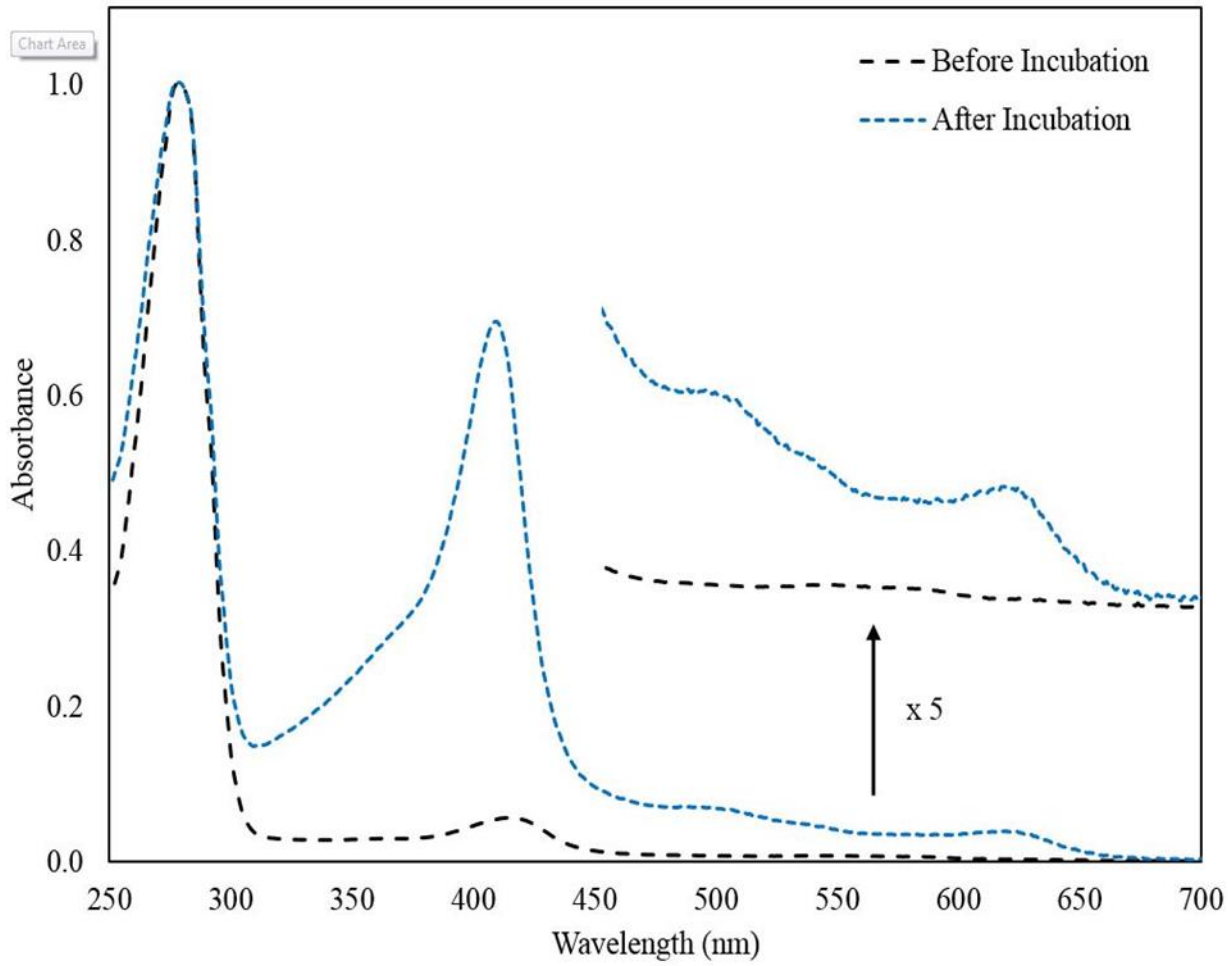

Figure 3.16 The UV-visible spectra of 40 μM HtaB Y56A are shown before and after incubation overnight at 4 °C with 100 μM hemoglobin. The spectra were normalized to 1.0 at 280 nm.

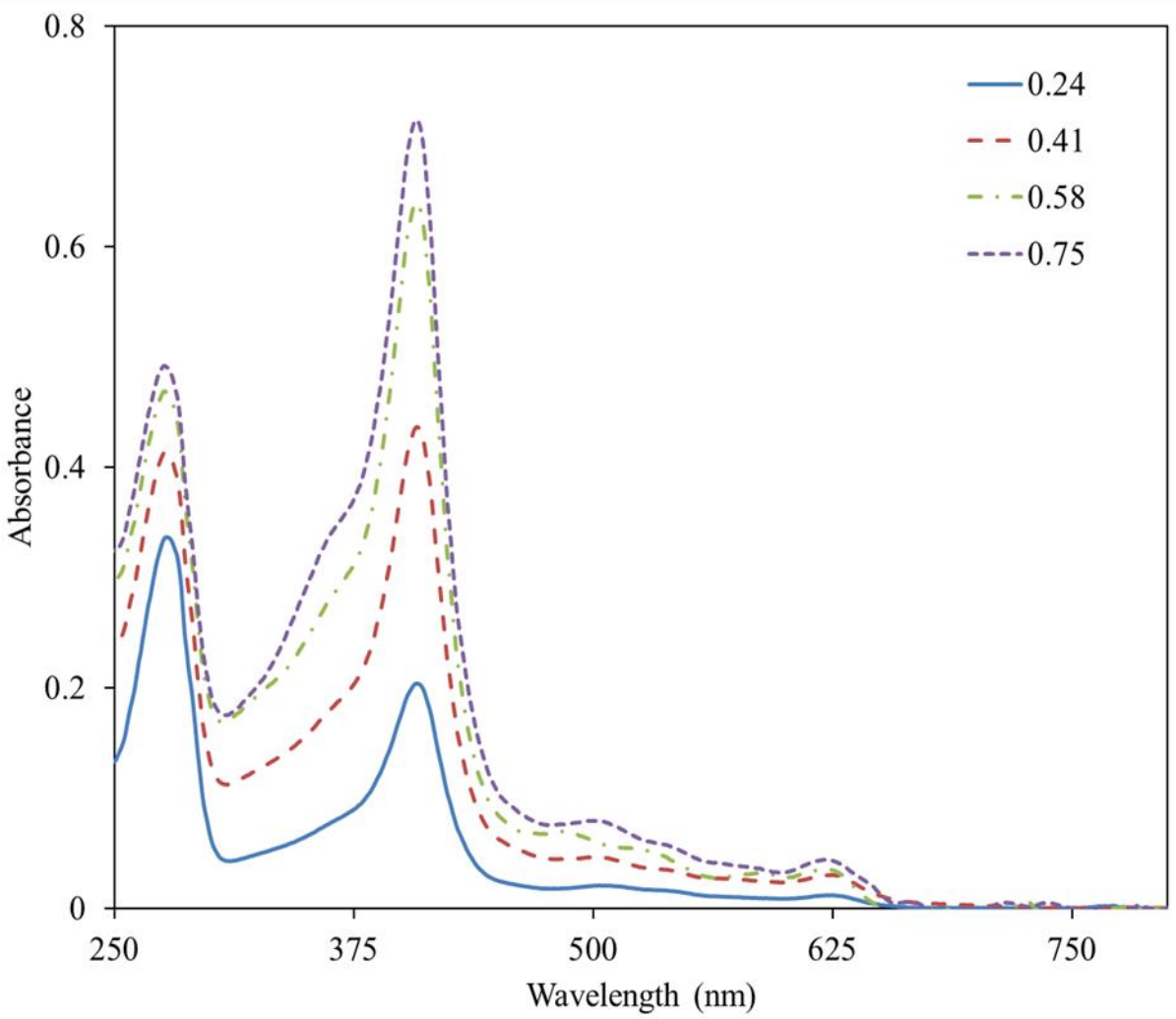

Figure 3.17 Absorbance versus wavelength of a solution of HtaB-WT with the indicated ratio of hemin added. The spectra were taken in buffer A.

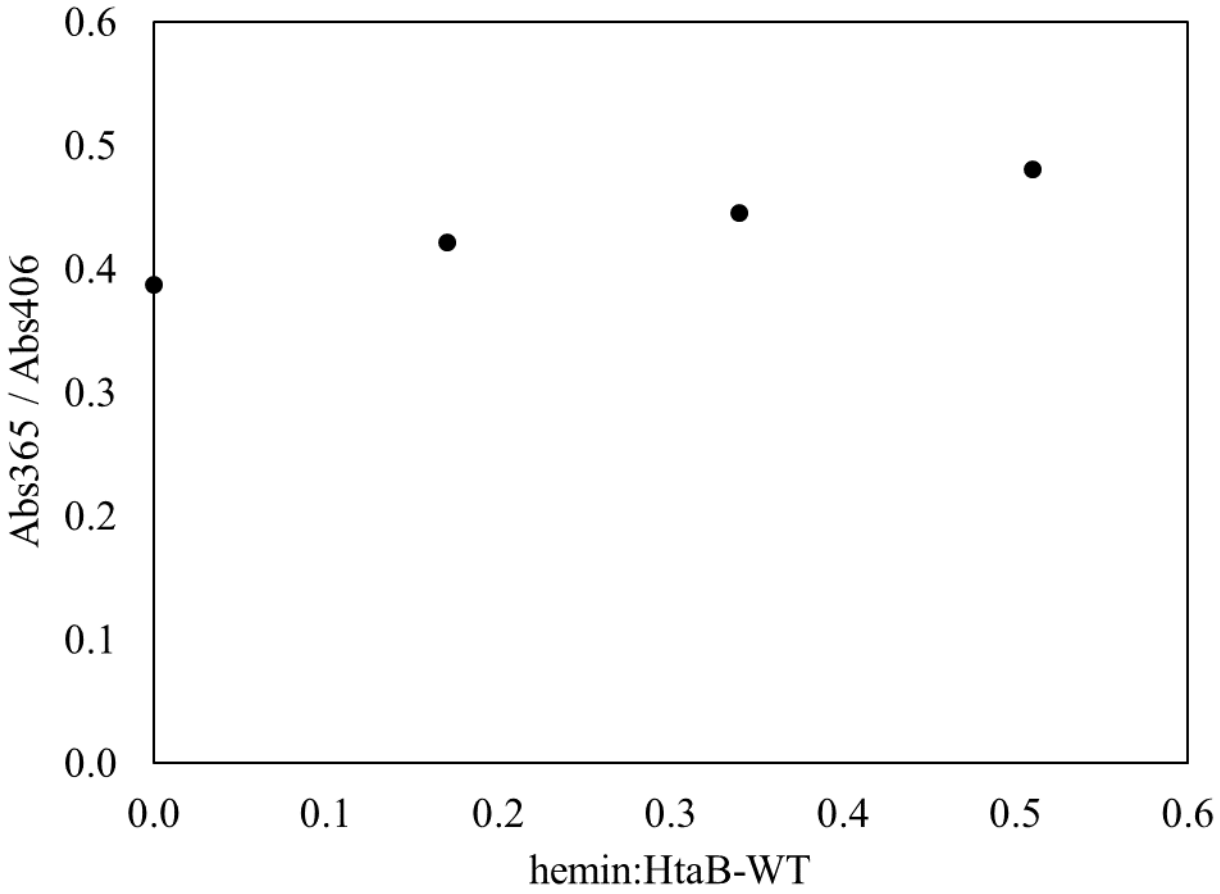

Figure 3.18 The ratio of the absorbances at 365 nm and 406 nm of WT HtaB as a function of the ratio of hemin to WT HtaB.

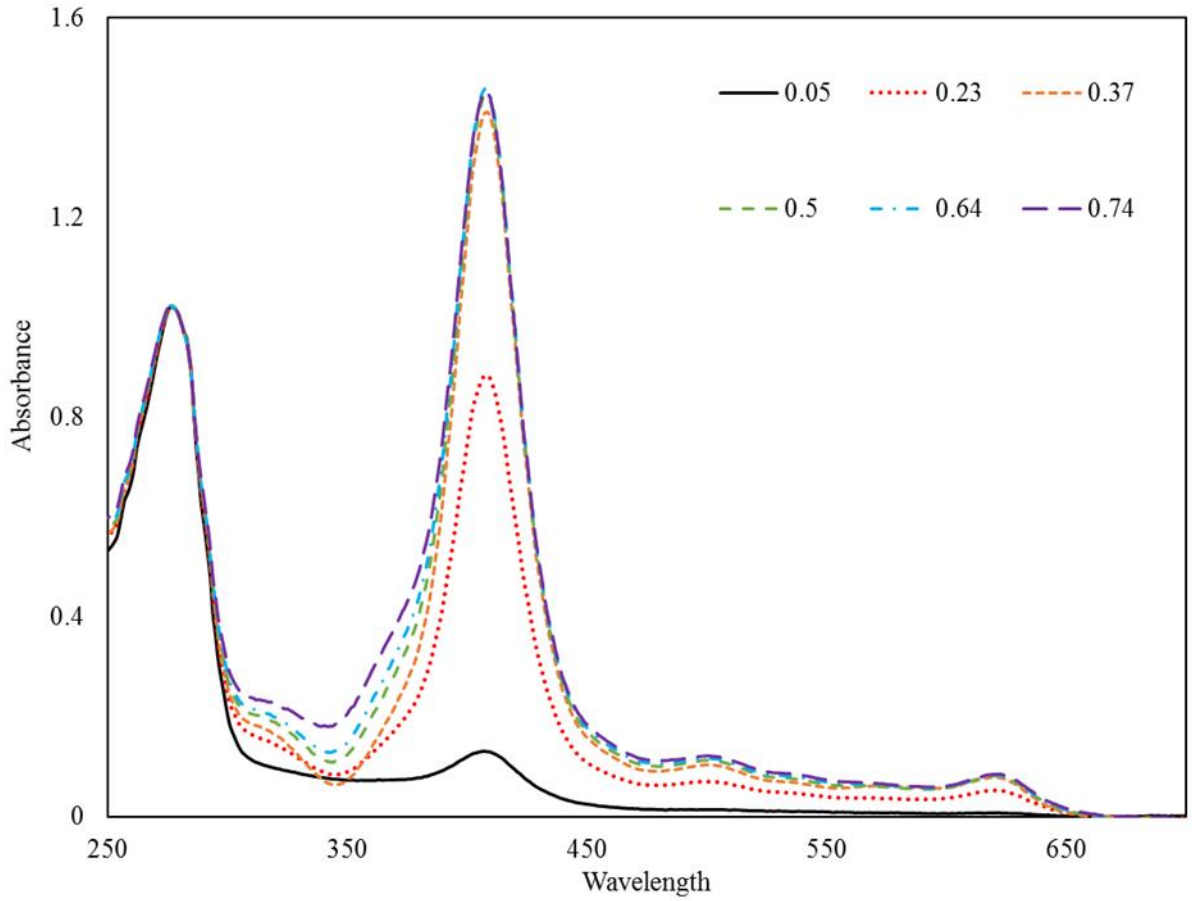

Figure 3.19 Absorbance versus wavelength for the two cuvette heme titration of HtaB Y56A up to a heme:protein of 0.74. The spectra are normalized to 1.0 at 280 nm. All spectra were taken in buffer A.

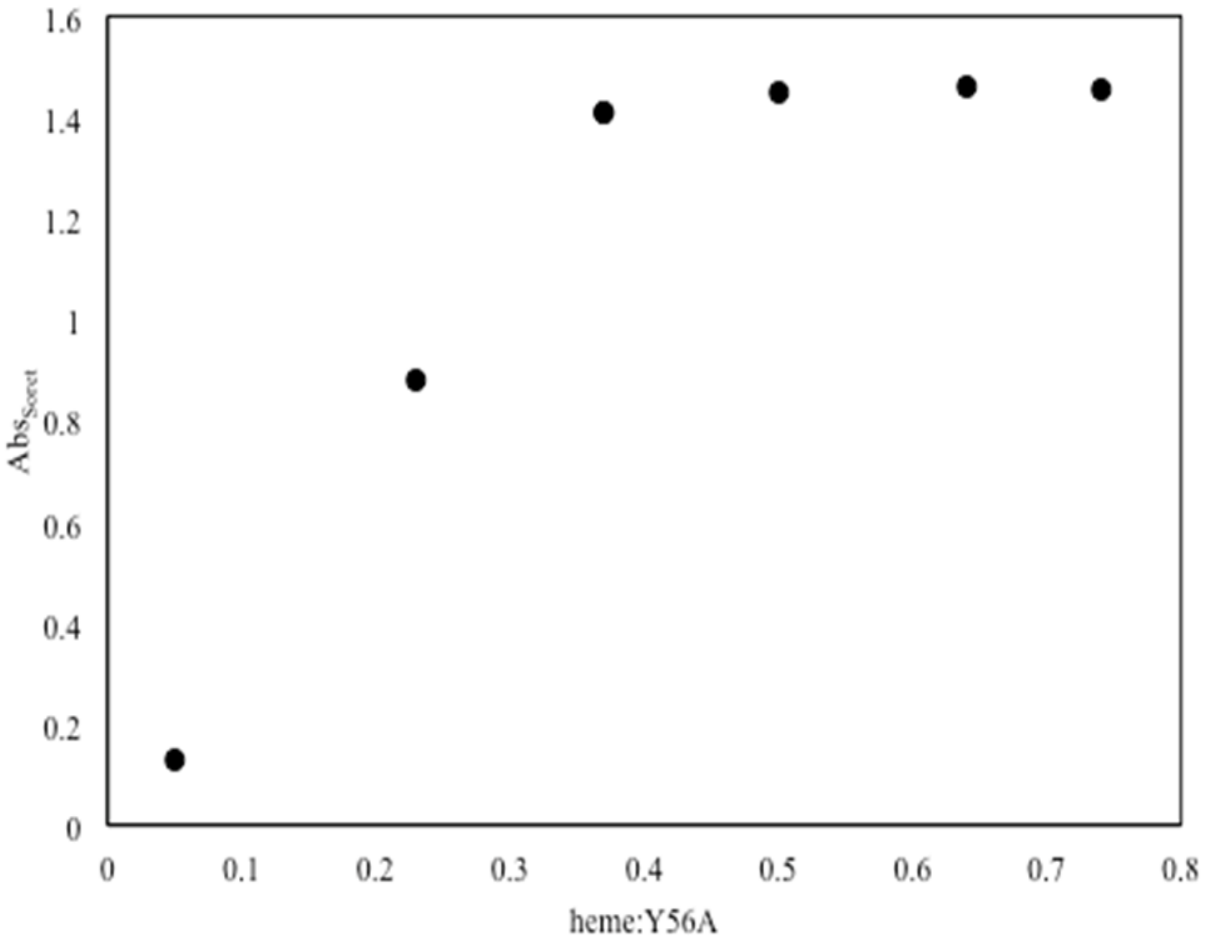

Figure 3.20 The absorbance at the Soret is plotted as a function of the ratio of the concentration of heme to the concentration of HtaB-Y56A. The titration is performed until a heme:protein of 0.74.

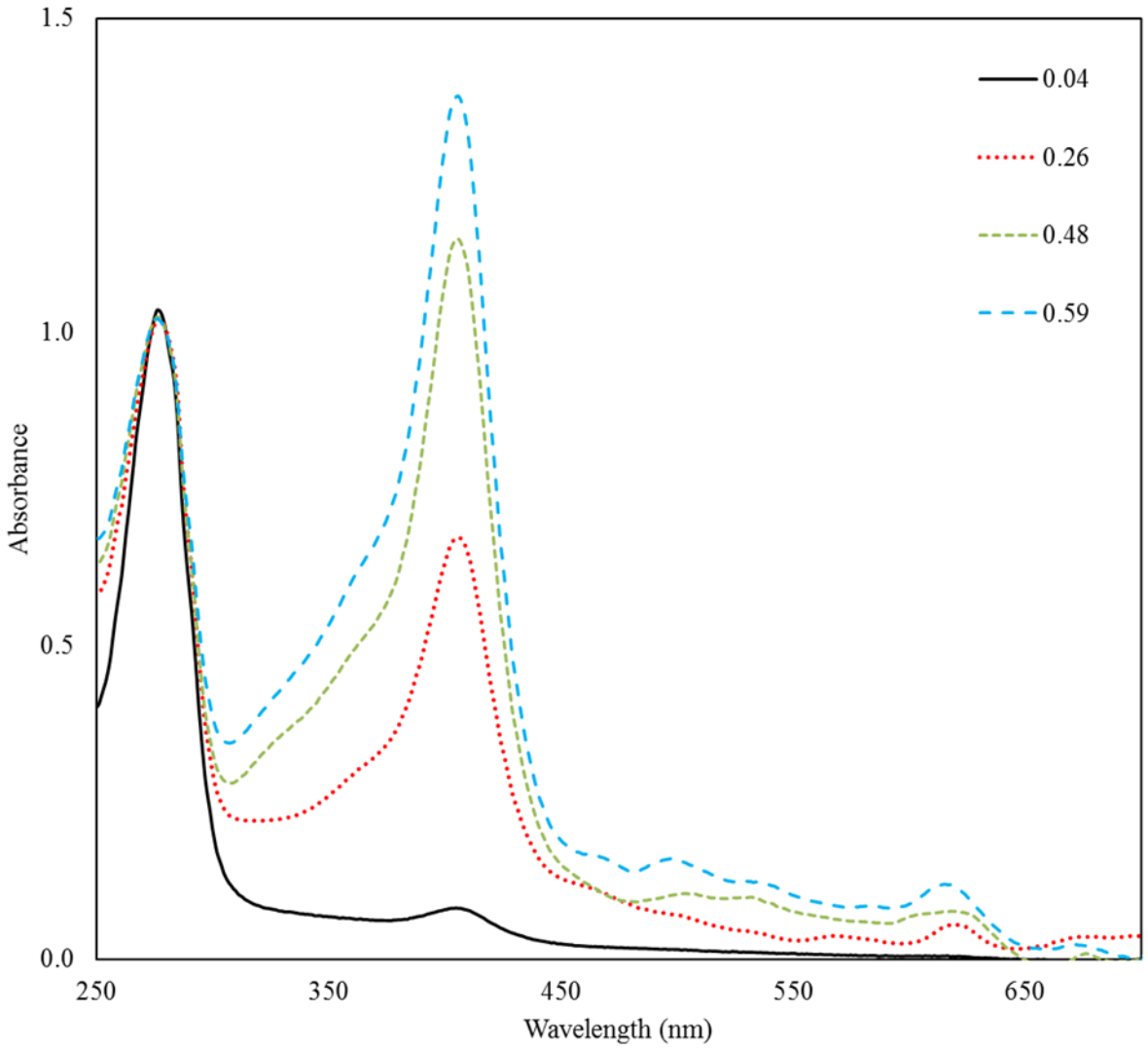

Figure 3.21 Absorbance versus wavelength of the two cuvette heme titration of HtaB-H121A with the indicated ratio of hemin added. The spectra were normalized to 1.0 at 280 nm. The spectra were taken in buffer A.

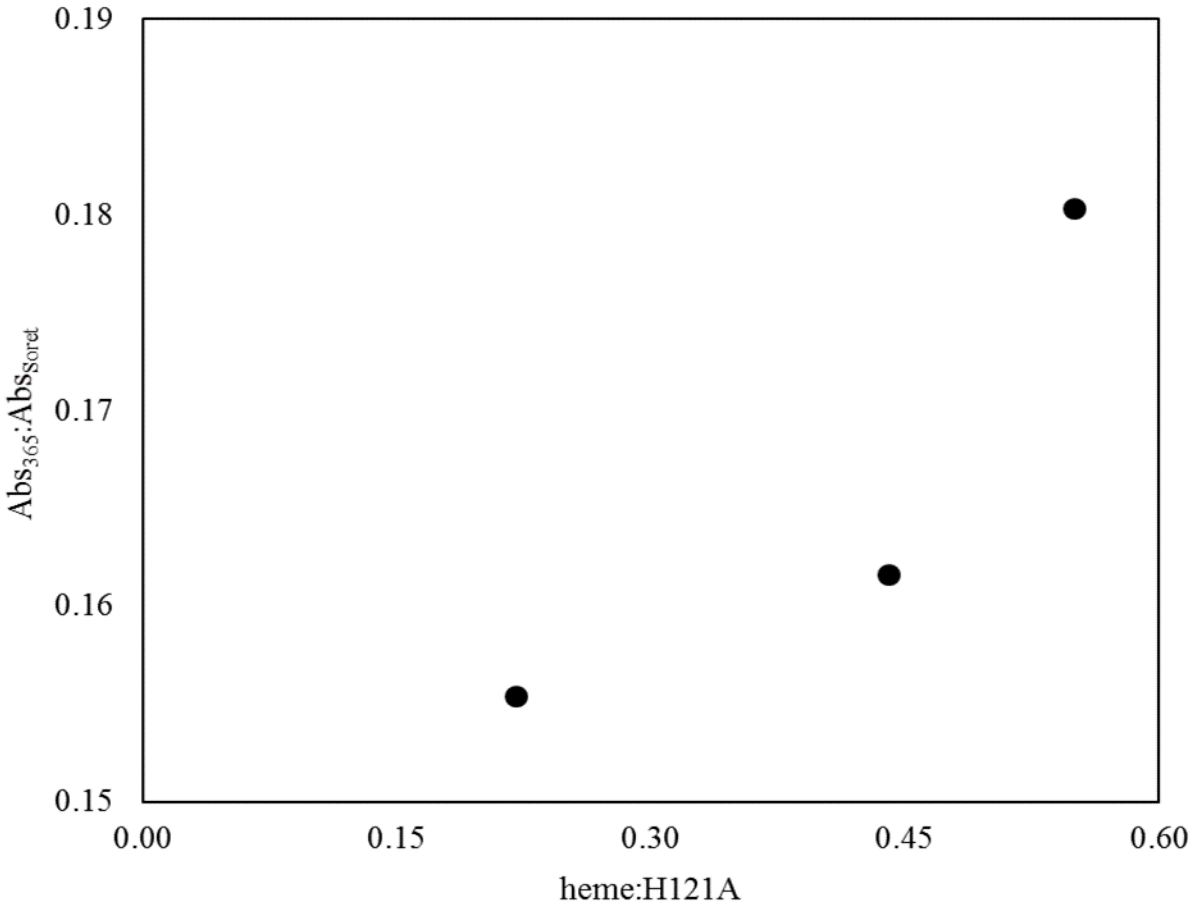

Figure 3.22 The Abs_{365}:Abs_{Soret} is plotted as a function of the ratio of the concentration of heme to the concentration of HtaB-H121A. The titration is performed until a heme:protein of 0.65.

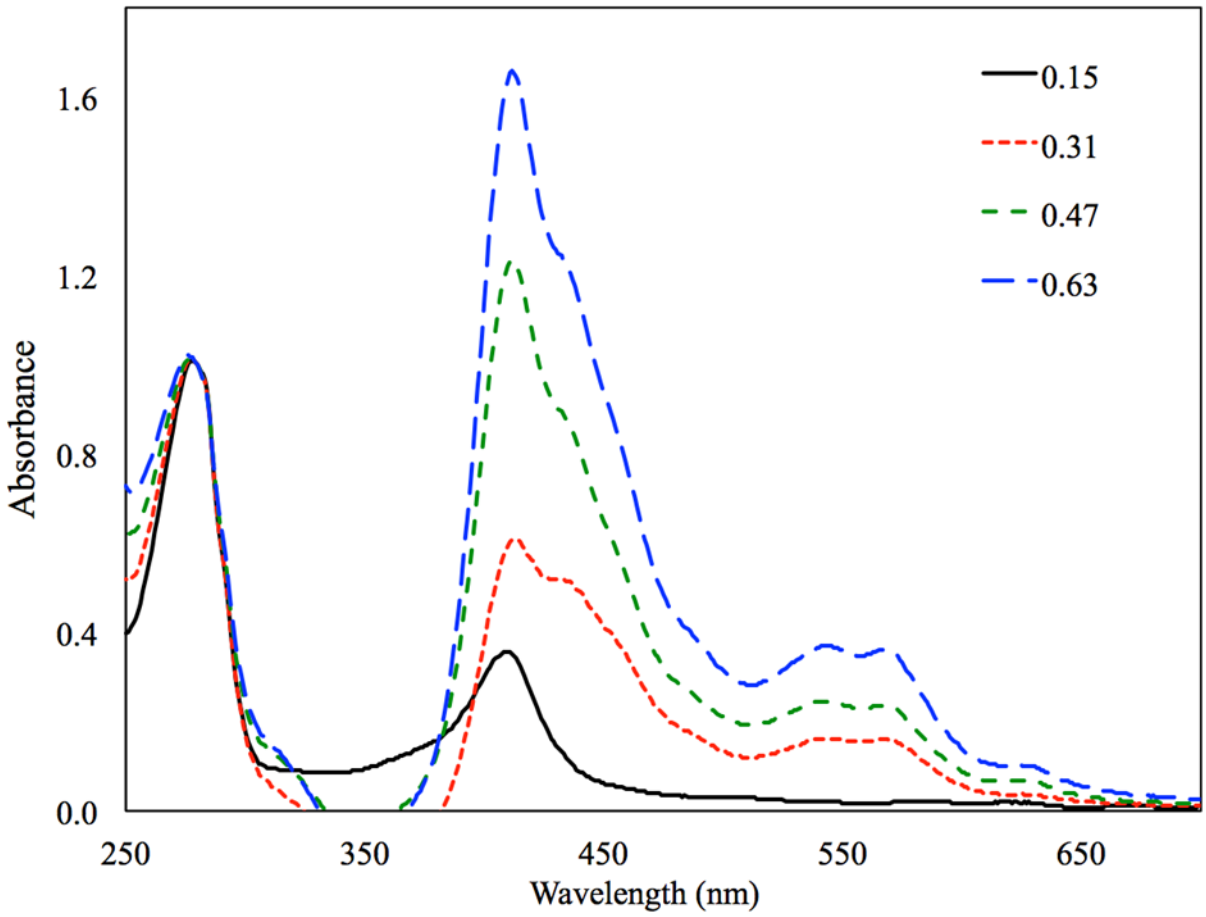

Figure 3.23 UV-visible spectra of as-isolated His-tagged HtaB overlaid with increasing titrations of hemin. The spectra represent the different equivalents of heme. All spectra are normalized to 1.0 at 280 nm and taken in buffer A.

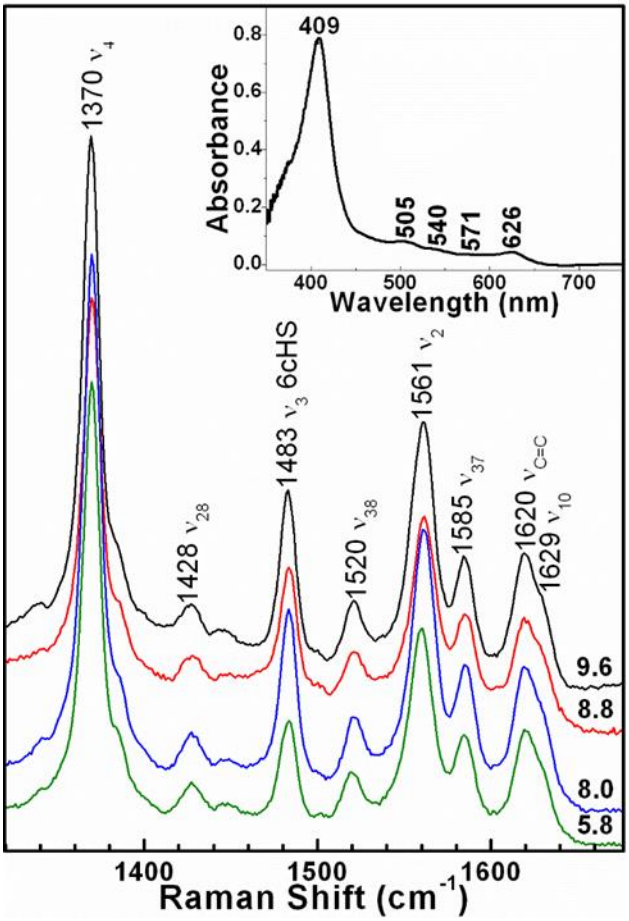

Figure 3.24 Ferric high-frequency rR of HtaB as a function of pH. Glycine (pH 9.6, black), Tris-HCl (pH 8.8, red and 8.0, blue), and phosphate (pH 5.8, green) buffers at 100 mM were used. Resonance Raman scattering was excited with 413.1-nm emission from a Kr^+ laser using ten mW of power. The assignments are made by analogy with other heme proteins.

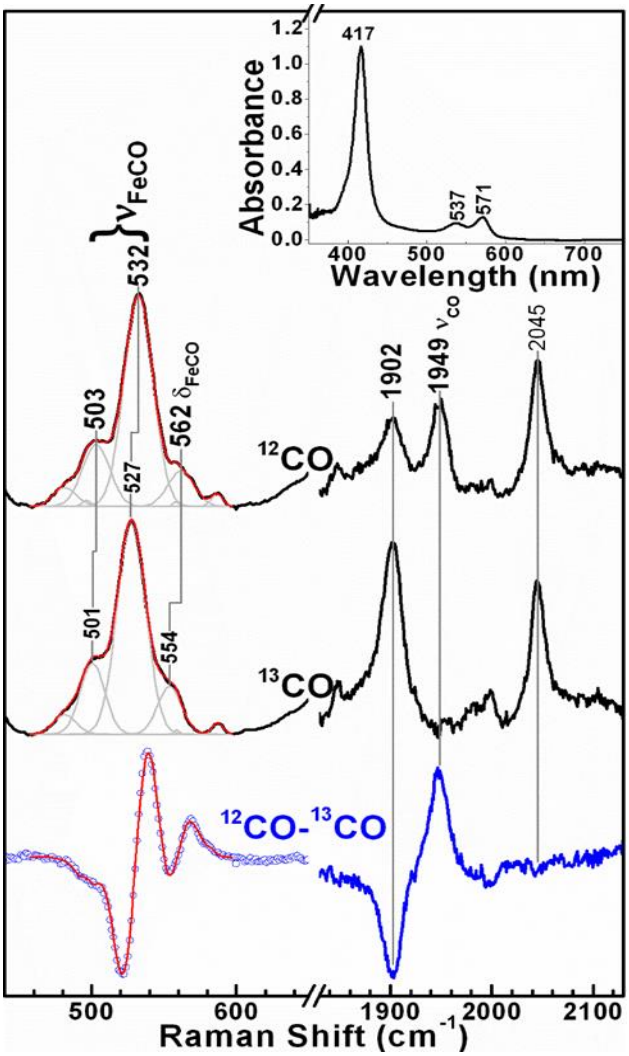

Figure 3.25 Resonance Raman spectra of the heme carbonyls of HtaB-WT. Raman scattering was excited using 413.1-nm emission from a Kr+ laser; 5.7 mW. Natural-abundance HtaB−CO (top), HtaB−13CO (middle) and 12CO−13CO difference (blue, bottom) spectra are shown in the vFe−CO, δFeCO, and vC−O regions. Bands in the low-frequency region were fit using Gaussian peak functions (gray). These bands were used to calculate the red difference spectrum superimposed on the blue points in the bottom left spectrum. The bands sensitive to 13CO substitution are labeled with their respective mode designations. Spectra were recorded at pH 8.8. Inset: UV-visible absorbance spectrum of HtaB−CO.

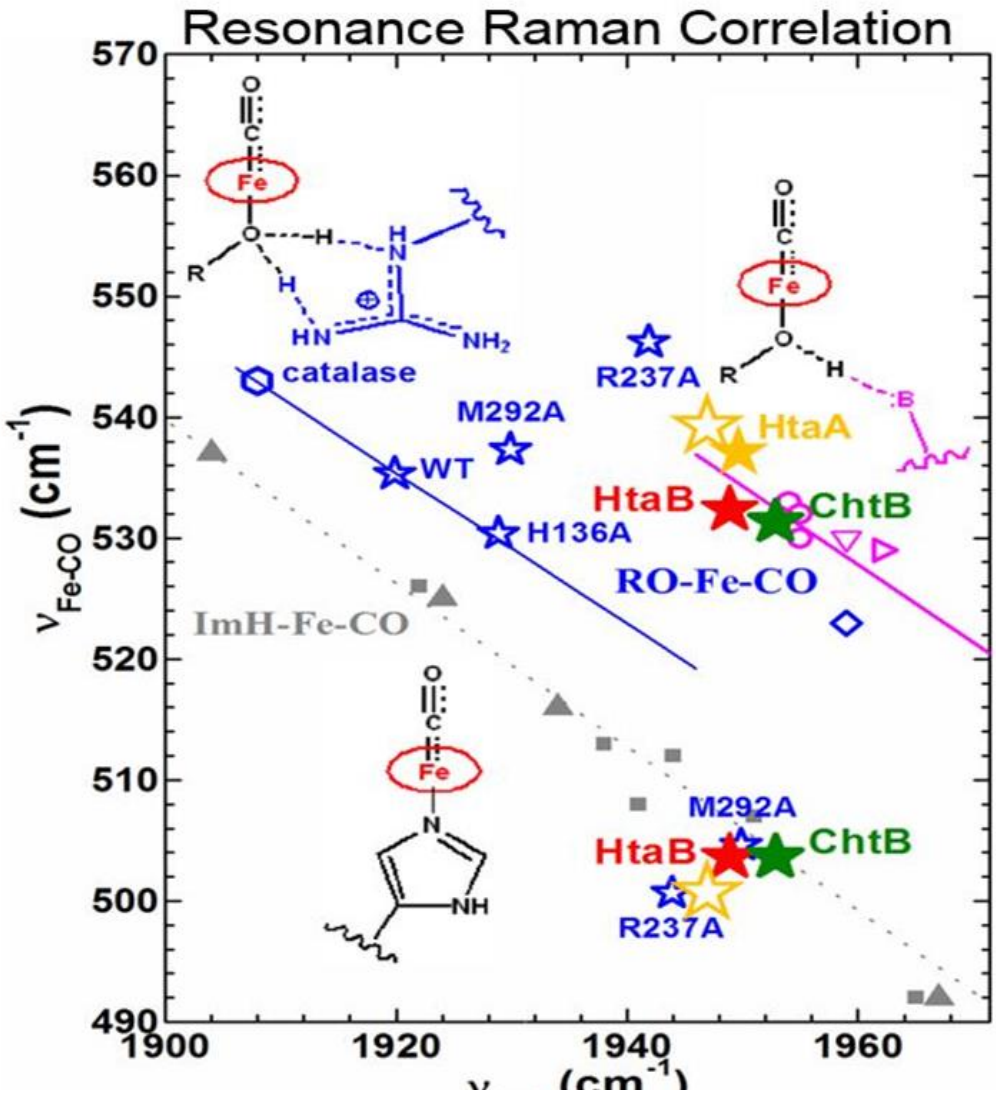

Figure 3.26 Resonance Raman correlation plot showing the frequency of the iron-carbon bond stretching as a function of the frequency of the carbon-oxygen bond stretching. Data courtesy of Dr. Kenton Rodgers and Dr. Gudrun Lukat-Rodgers. The two forms of HtaB-CO are shown as filled red stars while the two forms of ChtB-CO are shown as filled green stars. HmuT and mutants of HmuT are shown as unfilled blue stars (Draganova et al., 2015; Draganova et al., 2016); catalase as a blue hexagon (Hu and Kincaid, 1992); SmHasA(WT), SmHasA(H83A), SmHasA(H32A) as magenta circles (Lukat-Rodgers et al., 2008). The data for HRP (grey triangle) and globins (grey squares) have been previously compiled (Lukat-Rodgers et al., 2008). The dotted line is the least squares fit for six-coordinate heme carbonyls in which the proximal ligands is a neutral imidazole from a histidine residue (Smulevich et al., 1988; Lukat-Rodgers et al., 2008; Streit et al., 2010). The solid blue line represents a compilation of heme proteins in which the ligand trans to CO is coordinated through an oxygen atom that is hydrogen bonded to an arginine residue via two hydrogen bonds (Hu and Kincaid, 1992; Draganova et al., 2015). The solid magenta line is the least squares fit for six-coordinate Fe-CO adducts which are coordinated through an O atom having a single hydrogen bond to histidine or tyrosine (Lukat-Rodgers et al., 2008).

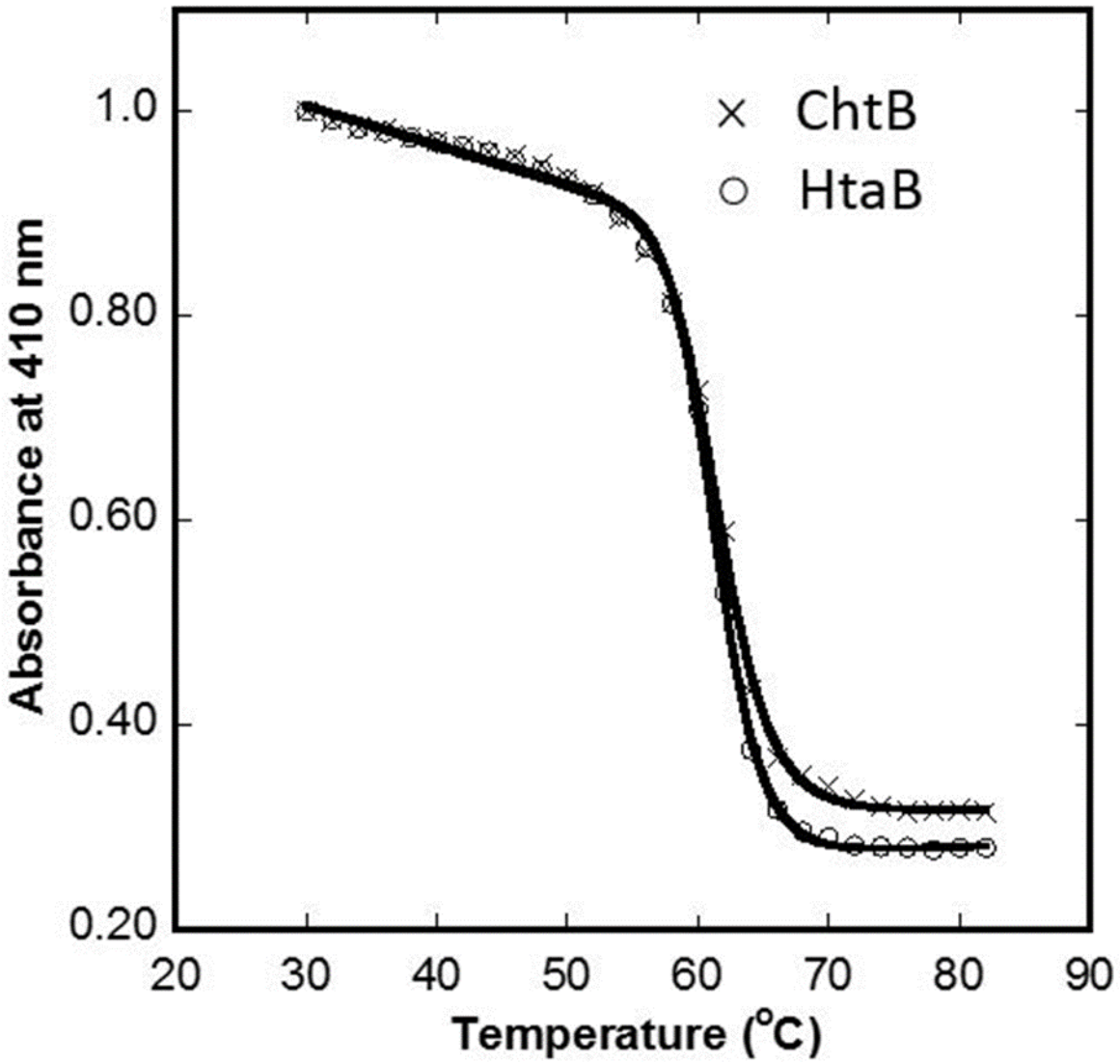

Figure 3.27 Absorbance at 410 nm as a function of temperature for the ChtB and HtaB conserved regions (CR). Experiments were performed in 1 M GdnHCl in buffer A. The line is a fit to the equation described in Section 3.2.10.

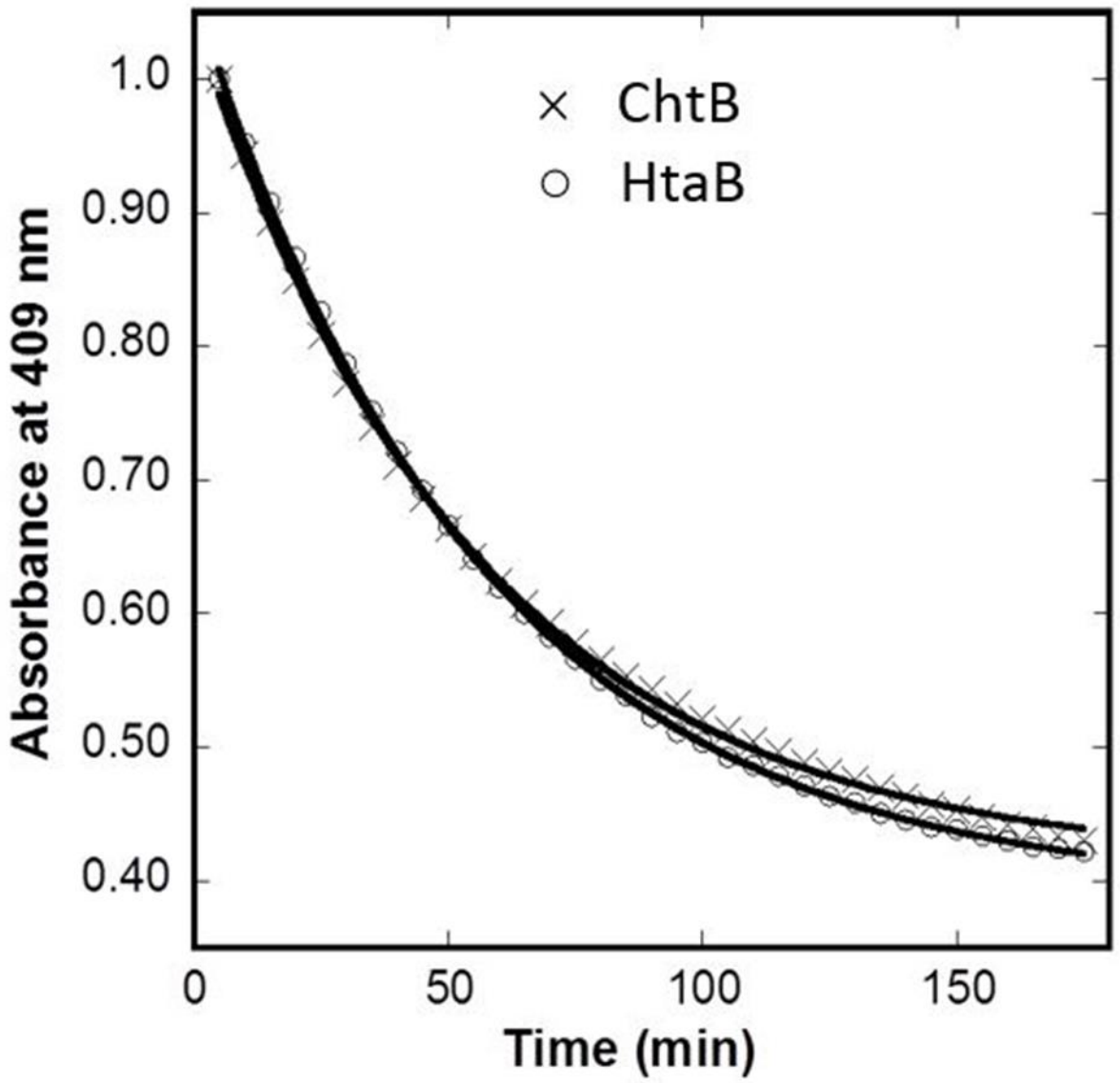

Figure 3.28 Absorbance at 409 nm versus time of the ChtB and HtaB conserved regions (CR) at 25 °C. Experiments were performed in 4 M GdnHCl in buffer A pH 8.0. The line is a fit to the equation described in Section 3.2.11.

Table 3.1 HtaB Mutant Primers

Primer Name	Primer sequence (5'-3')
H121A-Forward	CGTTTTAGTGGTG**CGC**ACGGCATCTTG
H121A-Reverse	CAAGATGCCGTG**CGC**ACCACTAAAACG
Y56A-Forward	CGCTGGCTTC**GCG**GAAGCTGGCTCTG
Y56A-Reverse	CAGAGCCAGCTTCC**GCG**AAGCCAGCG

Table 3.2 PCR reaction mixtures of lanes 1-5 from HtaB-Y56A agarose gel.

Y56A PCR Reaction					
	1	**2**	**3**	**4**	**5**
Plasmid	2 µL (45 ng/µL)	2 µL	2 µL	2 µL	2 µL
Forward Primer	4 µL (10 µM)	8 µL	4 µL	8 µL	8 µL
Reverse Primer	4 µL (10 µM)	8 µL	4 µL	8 µL	8 µL
dNTP	1 µL (0.2 mM)	1 µL (0.2 mM)	1 µL (0.2 mM)	1 µL (0.2 mM)	1 µL (0.2 mM)
DMSO	2.5 µL (5%)	2.5 µL (5%)	1 µL (2%)	1 µL (2%)	1 µL (2%)
10x Buffer	5 µL	5 µL	5 µL	5 µL	5 µL
H_2O	30.5 µL	22.5 µL	32.0 µL	24.0 µL	24.0 µL
pfu Polymerase	1 µL	1 µL	1 µL	1 µL	0 µL

4 CHAPTER 4: EXPERIMENTAL CHARACTERIZATION OF THE CHTB HEME UPTAKE PROTEIN IN *CORYNEBACTERIUM DIPHTHERIAE*

The Raman spectroscopy sections are intended for publication verbatim in Rizvan C. Uluisik, Brandon L. Ferrell, Gudrun S. Lukat-Rodgers, Courtni E. Allen, Michael P. Schmitt, Kenton R. Rodgers, and Dabney W. Dixon.

4.1 *ChtB in Corynebacterium diphtheriae*

ChtB is a 32.6 kDa hemin-binding protein encoded in the *chtA-chtB* operon (Allen et al., 2013). Transcription from a promoter region upstream of *chtA* is repressed under high-iron conditions, similar to the strategy observed for the *hmu* gene cluster. A putative DtxR-binding site overlaps the *chtA* promoter region. The *chtAB* operon is surrounded by inverted repeats composed of identical putative IS elements. The configuration of the *chtAB* region suggests that the gene may be present on a composite transposon in certain *C. diphtheriae* strains. Further analysis shows that only six out of 13 *C. diphtheriae* strains studied contain the *chtAB* genes.

Sequence analysis predicts that ChtB has an N-terminal leader peptide, which suggests that it is secreted; it also has a predicted C-terminal transmembrane region that anchors the protein to the cytoplasmic membrane (Allen et al., 2013). ChtB contains a single conserved domain (CR) similar to that associated with hemin and hemoglobin binding in HtaA and HtaB (Allen and Schmitt, 2009). Due to the high sequence similarity between HtaB and ChtB over the full length of the protein, it is possible that the two proteins may have similar functions (Allen et al., 2013).

Previous western blotting studies show that ChtB is expressed more in low-iron media than in high-iron media, providing evidence that ChtB expression is iron-regulated (Allen et al., 2013). Localization studies show that ChtB is predominately associated with the cytoplasmic

membrane, which is consistent with a C-terminal transmembrane region on the protein. These results are similar to those seen for HtaA and HtaB (Allen and Schmitt, 2009).

ELISA analysis shows that ChtB binds hemoglobin with a K_d ~5.1 x 10^{-7} M (Allen et al., 2013), a binding constant about half that of CR1 and CR2 of HtaA. The deletion of the *chtB* gene had no effect on growth with hemoglobin as the sole iron source; this was similar to the observation for *htaB*. However, an *htaB-chtB* double mutation shows a significant reduction in bacterial growth when compared to the WT. This suggests that HtaB and ChtB have similar functions in iron utilization and may also be able to substitute for one another.

4.2 Materials and Methods

4.2.1 *Expression and Purification*

The ChtB construct, which includes an N-terminal Strep tag, was a gift of Dr. Michael Schmitt (Figure 4.1). ChtB was expressed and purified from BL21(DE3) (pET*chtB*) cells. Protein expression was performed as described above.

Purification was performed manually using a five mL Strep Trap HP column (GE Healthcare). The column was equilibrated by washing with five column volumes of buffer A. The supernatant from the procedure described above was loaded onto the column, and the column was washed with buffer A to remove any unbound material. The eluted fractions were checked via UV-visible spectroscopy to ensure all unbound material had eluted off the column. Solutions of various concentrations of buffer B, ranging in 10% increments from 10% to 100% (one column volume each), were used to elute the protein off the column. The fractions were checked with UV-visible spectroscopy to confirm the elution of the protein. A buffer exchange by centrifugation (4600 x g, 15 min, and three times) was performed on the fractions using an

Amicon Ultra centrifugal filter with a 10 kDa molecular weight cut off to remove *d*-desthiobiotin from solution. The purity of the fractions was confirmed by using SDS-PAGE.

4.2.2 *Spectroscopy: UV-visible and Circular Dichroism*

UV-visible spectra were taken as described in Section 3.3.4.

Circular dichroism spectra were recorded using a Jasso J-810 spectropolarimeter using quartz Suprasil cuvettes with a 1 mm path length. The spectra were taken from 190 to 260 nm. The scanning speed was set to 100 nm/min in the continuous scanning mode. The data pitch was set to 0.5. As-isolated ChtB (~40% heme loaded) was recorded in 100 mM Tris-Cl and 150 mM NaCl at pH 7.0. The final spectrum represents an average of 15 scans.

The same ChtB sample was heme-loaded to 100% using the two cuvette method previously described. A CD spectrum of heme-loaded ChtB was obtained as described above. The final spectrum was an average of 15 scans.

4.2.3 *Determining Percent Heme Loading*

Bovine serum albumin (BSA) was used as the standard for the assay. The concentration of BSA was calculated using UV-visible spectroscopy with an extinction coefficient of 43,824 M^{-1} cm^{-1} at 280 nm (Fisher). A stock solution of 458 μg/mL BSA was made by dissolving a small amount of BSA in 1 mL of buffer A. Coomassie Brilliant Blue G-250 was from Thermo Scientific. A solution containing 200 μL dye and 800 μL buffer and allowed to stand for 10 min before being used to blank the UV-visible spectrophotometer. BSA standards were made by adding 2 to 10 μL of BSA stock to Eppendorf tubes containing volumes of buffer ranging from 798 to 790 μL, making a total protein and buffer volume of 800 μL. To each Eppendorf tube, 200 μL of dye were added to make a final volume of 1000 μL. The solution allowed to incubate for 10 min. The absorbance at 595 nm was recorded for each sample. Each standard was repeated in

duplicate and averaged. A plot of [BSA] in μg/mL vs. Abs_{595} was constructed. The plot was fit to a linear equation. The ChtB sample was prepared in the same manner as the 6 μL BSA standard. The sample was allowed to incubate for 10 min, and the spectrum was taken. The absorbance at 595 nm was used to calculate the concentration of ChtB from the standard curve.

The same ChtB sample from the Bradford assay was used to determine the percent heme-loaded of as-isolated ChtB using the pyridine hemochrome assay (Berry and Trumpower, 1987). A pyridine solution was prepared under the fume hood in a 15 mL conical centrifuge tube (Thermo) by adding 4 mL of pyridine and 6 mL of 400 mM NaOH, and the solution was inverted to ensure mixing. The UV-visible spectrophotometer was blanked by adding 750 μL of the pyridine solution into a black-capped quartz cuvette using a 500 μL glass syringe. The ChtB sample was prepared by adding 250 μL of ChtB into the cuvette and shaken to ensure mixing. A saturated sodium dithionite solution was prepared by adding excess sodium dithionite into 500 μL of buffer A. The solution was quickly mixed, and 10 μL of the dithionite solution was added to the cuvette containing ChtB using a ten μL glass syringe. The solution was shaken to ensure mixing, and a spectrum was taken. The heme concentration was calculated using an extinction coefficient of 34640 M^{-1} cm^{-1} at 556 nm (Berry and Trumpower, 1987).

4.2.4 *Resonance Raman Spectroscopy*

Resonance Raman studies were performed by Dr. Kenton Rodgers as described in Section 3.3.8.

4.2.5 *ChtB pH Titration*

A 1 mL solution of as-isolated ChtB in a buffer consisting of 20 mM Tris-Cl (7.0-9.0, Sigma), 20 mM CHES (pH range 8.6-10.0, Sigma), and 20 mM CAPS (pH range 9.7-11.1, Sigma) was prepared with a starting absorbance of 0.369 at the Soret. Aliquots of 1 M NaOH (2

μL each) were added to the solution while stirring. The solution was allowed to stir for 5 min before the next NaOH addition. As-isolated ChtB was titrated with NaOH from pH 6.7 to 10.96.

4.2.6 *Heme Transfer between ChtB and HtaB*

Hemin transfer from fully heme-loaded ChtB to HtaB was assessed using as-isolated His-tagged HtaB (heme loading ~ 15%). A 1 mL sample of strep-tagged ChtB was fully heme loaded by the two cuvette described for the heme titration. The protein solution was run down a desalting column to ensure that no free heme was in solution. The ChtB solution was loaded onto a five mL streptavidin column. The column was washed with 4 CV of buffer A. A volume of 1 mL of His-tagged HtaB was added to the column. The column was capped and allowed to sit at 4 °C for one h. HtaB was washed off with buffer A in 2 mL fractions. The fractions were checked via UV-visible spectroscopy to track the elution of HtaB from the column. ChtB was eluted with a linear gradient of buffer B in 2 mL fractions. The fractions were checked with UV-visible spectroscopy. The fractions were collected and concentrated using the centrifuge at 6000 rpm for 15 min. An SDS PAGE was used to test for the purity of the samples.

4.2.7 *Thermal Unfolding in the Presence of GdnHCl*

Thermal unfolding was performed on the UV-visible spectrophotometer equipped with a TC125 Quantum Northwest temperature controller. A screw-top quartz cuvette with a 1 cm path length was used. As-isolated ChtB was prepared in 50 mM NaH_2PO_4 at pH 7.0 containing 1 M GdnHCl. The thermal unfolding was carried out over a temperature range of 34 to 82 ˚C. Spectra were recorded every two ˚C after a 1 min incubation period.

Kaleidagraph (version 4.01, Synergy Software) was used to fit the data using a two-state protein unfolding model (Swint and Robertson, 1993):

$$A = \frac{(A_f + m_f T) + (A_U + m_U T)\exp[\frac{\Delta H_m}{R(Tm^{-1} - T^{-1})}]}{1 + \exp[\frac{\Delta H_m}{R(T_m^{-1} - T^{-1})}]}$$

where A is the absorbance at any temperature along the unfolding curve, A_f is the absorbance of the folded state, m_f is the slope of A vs. T for the folded state, A_U is the absorbance of the unfolded state, m_U is the slope of A vs. T for the unfolded state, T_m is the temperature at which the protein is half unfolded, ΔH_m is the enthalpy of unfolding, R is the ideal gas constant, and T is the temperature (Kelvin).

4.2.8 *Time Scale Unfolding in the Presence of 4.0 M GdnHCl*

Solutions of ChtB and GdnHCl were each prepared in buffer A. The GdnHCl concentration was determined to be 7.5 M by the refractive index method (Pace and Scholtz, 1997). The stock GdnHCl solution was added to the ChtB solution to give a final concentration of 4 M. The absorbance was recorded every 5 min for 12 h. The absorbance at 407 nm (Soret) vs. time was fit to a single-term exponential function:

$$A_t = (A_0 - A_\infty)\exp(-k_U t) + A_\infty$$

where A_t is the absorbance at any time during the unfolding reaction, A_0 is the initial absorbance, A_∞ is the absorbance of the completely unfolded protein, (A_0 - A_∞) is the total change in absorbance for complete unfolding, and k_U is the unfolding rate constant. The sample was dialyzed after unfolding to evaluate the reversibility of the unfolding process.

4.2.9 *Fluorescence of GdnHCl-induced Unfolding of ChtB*

The GdnHCl-induced unfolding of as-isolated ChtB (~30% heme loaded) and heme loaded (~80%) was investigated by observing the tryptophan emission spectrum at 340 nm on a Perkin Elmer LS fluorescence spectrophotometer. The unfolding was followed using a double

cuvette technique in which one cuvette contained buffer A and the other contained ChtB in buffer A. A GdnHCl titration was performed on both cuvettes in the same manner up to a GdnHCl concentration of 2.1 M. The protein was excited with 285 nm light, and the emission spectrum was observed between 300 to 500 nm. The same was performed on fully heme-loaded ChtB to investigate the effect of heme loading on unfolding.

The unfolding curves were analyzed using the following equation (Pace and Scholtz, 1997):

$$I = \frac{(I_F + m_F[D]) + (I_U + m_U[D])\exp[\frac{m([D] - [D]_{\frac{1}{2}})}{RT}}{1 + \exp[\frac{m\left([D] - [D]_{\frac{1}{2}}\right)}{RT}]}$$

where I is the fluorescence intensity at any point along the curve, I_F is the intensity of the folded state, m_F is the slope of the folded state, [D] is the concentration of GdnHCl, I_U is the intensity of the unfolded state, m_U is the slope of the unfolded state, $[D]_{1/2}$ is the concentration of GdnHCl at the midpoint of the unfolding curve, R is the ideal gas constant, and T is the temperature in Kelvin.

4.3 Results and Discussion

4.3.1 *ChtB Expression and Purification*

The FPLC chromatogram of the purification of ChtB is shown in Figure 4.2. The SDS gel used to assess protein purity is shown in Figure 4.3. ChtB appears to be pure and shows a molecular weight of approximately 27 KDa. This matches the expected molecular weight calculated from the protein sequence (26.6 KDa).

4.3.2 *UV-Visible Spectroscopy of ChtB*

Figure 4.4 shows the UV-visible spectrum of ChtB overlaid with that of HtaA-CR2 and HtaB. ChtB has a Soret peak of 407 nm and three α/β-peaks at 501, 542, and 625 nm. A charge transfer band appears at 625 nm in all three spectra. This band is consistent with a high-spin heme coordinated through an oxygen-containing ligand, often a tyrosine (Du et al., 2011; Tiedemann and Stillman, 2011). The UV-visible spectrum of ChtB is very similar to that of HtaB, which is proposed to have a Tyr axial ligation; the Soret peak of ChtB has only a one nm hypsochromic shift in comparison to HtaB. As-isolated ChtB has a higher Soret:280 ratio, indicating that as-isolated ChtB is more heme-loaded than as-isolated HtaB.

4.3.3 *Determination of Percent Heme Loading*

The as-isolated ChtB sample was determined to have a concentration of 1.71 μg/mL by the Bradford Assay. The sample was diluted by a factor of 167 in comparison to the stock solution. Therefore, the stock solution was found to be 285 μg/mL. The molecular weight of this construct of ChtB is 26.6 KDa. Using these values, the concentration of as-isolated ChtB was found to be 10.2 μM.

The spectrum after the addition of sodium dithionite and pyridine contains the signature β peak at 525 nm and α peak at 556 nm (Berry and Trumpower, 1987). The absorbance of at 556

nm was 0.055. This peak corresponds to the presence of the bispyridine ferrous heme complex (Berry and Trumpower, 1987). Using the extinction coefficient of this complex and the absorbance, the concentration was calculated to be 1.59 μM. The original ChtB solution was diluted by a factor of 4, so the concentration of heme in the original solution was 6.35 μM and hence the concentration of holo protein. Using the total protein concentration obtained from the Bradford assay and the heme concentration, the amount of holo protein was determined to be approximately 60%.

The ChtB stock solution showed an absorbance at the Soret (407 nm) of 0.715. The Soret peak corresponds to the heme-bound protein. Since the concentration of holo protein in the stock solution was determined, the extinction coefficient at the Soret can be determined using Beer's Law. The extinction coefficient at the Soret (407 nm) was calculated to be $1.13 \times 10^5\ M^{-1}\ cm^{-1}$.

4.3.4 *Resonance Raman of ferric ChtB*

ChtB forms a 6cHS hemin complex with spectral characteristics consistent with a proximal Tyr binding motif (Figure 4.5). The ν_3, ν_{38}, and ν_2 core stretching frequencies of 1486, 1522 and 1560 cm^{-1}, respectively, indicate 6cHS hemin (Hu et al., 1996). Unlike ferric HtaB, peripheral substituent modes in ChtB exhibit slight pH dependences, as seen in the shifts of the in-plane vinyl stretch from 1613 to 1627 cm^{-1}, the in-plane $C_\beta C_\beta$ stretch from 1560 to 1558 cm^{-1}, the in-plane pyrrole breathing mode from 761 to 754 cm^{-1}, out-of-plane pyrrole fold from 739 to 735 cm^{-1} and an increase at 666 cm^{-1}, and out-of-plane wags from 329 to 327 cm^{-1} and from 311 to 308 cm^{-1}. None of these vibrations are particularly sensitive to the coordination number or spin state of the heme, as evidenced by the constancy in the ν_4 and ν_3 frequencies among these proteins. This indicates that the structural determinants for coordination number and

spin state in the hemin binding pockets of HtaB and ChtB are similar, with the environments that impact conformations of the peripheral substituents being slightly variable.

4.3.5 *Resonance Raman of ferrous ChtB*

Ferrous ChtB was solely 5cHS as evidenced by its ν_3 at 1468 cm^{-1} and Soret maximum of 425 nm. The ν_{11}, ν_2, and ν_{10} core stretching frequencies of 1556 cm^{-1}, 1584 cm^{-1}, and 1623 cm^{-1}, respectively, indicate a 5cHS heme environment, similar to the 5cHS contribution to the ferrous HtaB spectrum. The absence of bands attributable to a 6cLS form indicates that reduction destabilizes its 6cLS heme to an even greater extent than in HtaB.

4.3.6 *Resonance Raman of ferrous carbonyl ChtB*

Through the sensitivity of Raman-active Fe-CO group frequencies to π back bonding and donor strength of the *trans* (proximal) ligand, resonance Raman spectra of heme protein carbonyls are useful probes of both the bonding and non-bonding properties of the heme pocket. The extent of π-back bonding is evidenced by the ν_{Fe-C}, ν_{C-O} frequencies which, when placed on a plot of ν_{Fe-CO} versus ν_{C-O} frequencies, yield insight into the electrostatic and steric properties of the distal heme pocket and the nature of the *trans* axial ligand (Vogel et al., 2000; Spiro and Wasbotten, 2005; Streit et al., 2010; Spiro et al., 2013). The Fe−^{13}CO isotopolog of ChtB was used to verify the identity of rR bands corresponding to the Fe−C stretching (ν_{Fe-CO}), Fe-CO bending (δ_{Fe-CO}) and C−O stretching (ν_{C-O}) modes, as shown in Figure 4.6.

Under an atmosphere of carbon monoxide, the UV-visible spectrum of ferrous ChtB exhibits a shift of the Soret band maxima to 415 nm, along with sharpening and shifting of the Q bands (Figure 4.6). These absorbance changes are consistent with the formation of the ChtB carbonyl.

ChtB−CO exhibits two ν_{Fe-CO} bands [503(−3) and 531(−5) cm^{-1}], one δ_{FeCO} band at 563(−13) cm^{-1} and one ν_{C-O} band at 1953(−47) cm^{-1}, similar to what was observed for HtaB−CO (Figure 4.6). Placement of these pairs of ν_{C-O} and ν_{Fe-CO} frequencies on the π-back bonding correlation plot is consistent with two heme carbonyls having different proximal ligands (Figure 3.26). One form falls near the line correlating ν_{C-O} and ν_{Fe-CO} of carbonyls having neutral imidazole ligands. The other falls on the correlation line neutral proximal ligands coordinated through an O atom. This position is consistent with a proximal Tyr ligand whose coordinated O atom interacts with a single hydrogen bond donor. These results are similar to what was seen in HtaB-WT.

4.3.7 *pH Titration of ChtB*

The pH titration showed no significant spectral changes over the 6.7 – 10.9 pH range (data not shown). There was only a 3% change at the Soret and a 7% change in the charge transfer band at 625 nm.

4.3.8 *Heme Transfer between ChtB and HtaB*

Previous studies showed that holo HtaA can transfer a heme to HtaB (Allen and Schmitt, 2011). This has been the only transfer shown thus far in the *hmu-cht* heme uptake pathway. As discussed in Chapter 2, HtaB and ChtB both have significant sequence similarities, suggesting that the proteins may have similar functions as intermediate transport proteins. Previous studies have also shown that single deletions of *htaB* or *chtB* showed no effect on cell growth with hemoglobin as the sole iron source, while a double deletion significantly reduced cell growth (Allen et al., 2013). Based on these results it was proposed that HtaB and ChtB may be able to substitute for one another. Because these two proteins may have the same function and may be able to substitute for one another, the possibility of heme transfer between the two was studied.

To assess heme transfer between HtaB and ChtB, heme-loaded strep-tagged ChtB was bound to a StrepTactin column and incubated with as-isolated His-tagged HtaB. The proteins were separated by washing the column with buffer A to elute all His-tagged HtaB followed by the elution of strep-tagged ChtB with a linear gradient of buffer B. The fractions were collected, concentrated, and assessed for purity by SDS-PAGE, as shown in Figure 4.7. The gel clearly shows that there is only one protein per fraction. The UV-visible spectra of as-isolated ChtB before and after the transfer are shown overlaid in Figure 4.8. The spectra show clear indications that heme loading of ChtB decreased after incubation. This is evident a decrease in the Soret:280 nm ratio from 1.50 to 0.68, indicating a decrease in the amount of heme-loaded strep-tagged ChtB. Figure 4.9 shows the shows the UV-visible spectra of His-tagged HtaB before and after the transfer. The Soret:280 nm ratio increased from 0.41 to 0.86, indicating an increase in the amount of heme-loaded His-tagged HtaB. The results show that HtaB and ChtB readily transfer heme to one another. This indicates that there may be an extent of crossover of heme transfer between the *hmu* and *cht* heme uptake pathways *in vitro*.

4.3.9 *CD Spectroscopy*

The CD spectra of as-isolated ChtB is shown in Figure 4.10. Like HtaB (Figure 3.15), ChtB appears to consist mostly of β-sheets as indicated by a single local minimum at approximately 215 nm. The CD shows little difference between as-isolated ChtB (~30% heme-loaded) and holo ChtB (~70% heme-loaded), as shown in Figure 4.11. The transition from apo- to holo-ChtB does not have any effect on the secondary structure of the protein.

4.3.10 *Time Scale Unfolding in the Presence of GdnHCl*

The unfolding curve of ChtB in the presence of 4 M GdnHCl is shown in Figure 3.28. The kinetics were assessed in GdnHCl for comparison with an earlier study on HtaA (Uluisik et

al., 2017). The curve was fit to a single-term exponential decay function, which suggested a single first-order unfolding process. Unfolding was taken to 95% completion. The rate constant was 0.018 ± 0.001 min-1 (half-life of 39 min). The kinetics for HtaB were identical. In contrast, HtaA-CR2 was shown to have a half-life of 330 min in the presence of higher (6.6 M) GdnHCl (Uluisik et al., 2017). Thus, both HtaB and ChtB are significantly less stable that HtaA-CR2 with respect to unfolding. After dialysis to remove GdnHCl, the Soret band of ChtB decreased by 40%. Considering the loss of some protein from dialysis, the refolding of ChtB is at least 60% reversible. The reversibility of ChtB is similar to that of HtaB.

4.3.11 *Thermal Unfolding in the Presence of GdnHCl*

Figure 3.27 shows the thermal unfolding curves for HtaB and ChtB in 1 M GdnHCl. Previous studies showed that HtaB without the presence of denaturant did not readily unfold, so 1 M GdnHCl was added to facilitate protein unfolding (R. Uluisik, data not shown). The apparent T_m was 61 °C for ChtB. ChtB had an isosbestic point at approximately 390 nm up to the T_m, similar to what was observed for in HtaB (data not shown). The ChtB solution was allowed to cool back to the starting temperature and incubate for 30 min. Approximately 60% of the original absorbance at the Soret was recovered, indicating that ChtB was able to bind heme upon refolding. HtaB showed similar properties with approximately 50% of the Soret was recovered upon refolding.

The thermal unfolding curves of HtaB and ChtB in 1 M GdnHCl are almost identical, with lower T_m values (61 °C) compared to HtaA 84 °C (Uluisik et al., 2017). The unfolding is also more readily reversed, with HtaB, ChtB and HtaA recovering 50%, 60% and 30%, respectively of the original spectrum upon cooling. It was previously shown that a deletion of *htaA* reduces cell growth, but a single deletion of *htaB or chtB* showed no effect on cell growth

(Allen et al., 2013). A double deletion, however, slightly decreased cell growth in comparison to WT. The results from the thermal unfolding help to strengthen the proposal that HtaB and ChtB are very similar and can substitute for one another in the heme uptake pathway.

4.3.12 *GdnHCl-induced Unfolding of ChtB*

Fluorescence spectroscopy was used to observe the effect of heme loading on the stability of WT ChtB with respect to increasing concentrations of GdnHCl. The tryptophan emission at 340 nm was monitored as a function of the concentration of GdnHCl. Figure 4.12 and Figure 4.13 show the unfolding curves for as-isolated (~30% heme-loaded) and holo (~80%) protein, respectively. The midpoint denaturation concentrations were 0.75 ± 0.03 for as-isolated and 0.63 ± 0.03 for heme-loaded. The $D_{1/2}$ values for the as-isolated and holo proteins were not substantially different. The experiment implies that heme loading does not substantially affect the stability of the protein with respect of the concentration of GdnHCl.

MAS**<u>WSHPQFEK</u>**ENVAATGKECAITVESGTVKWGIKQSWRSYILGNIAHGTWKTSGHV
KDNNREKSGNDFQFSFDVDPAKTKITVKDGKVISSEIRTQDSSIVFTGHNDALHSEFKSPII
STSGSTLNAGSGYAVYYIPGKAMGQYTKDDHTEKNKKTGEGYFAQGQVSEWKTSGED
GAKLTLKGSNLQYTPQRGTDGHRGTIEGVDLLFMGQYDANYKPSVDDVEVELQVKNT
CGAIDGTADPDTSPFGGLPKIWGI

Figure 4.1 The sequence of the conserved domain of ChtB as supplied by Dr. Michael Schmitt. The strep tag sequence is underlined and bolded.

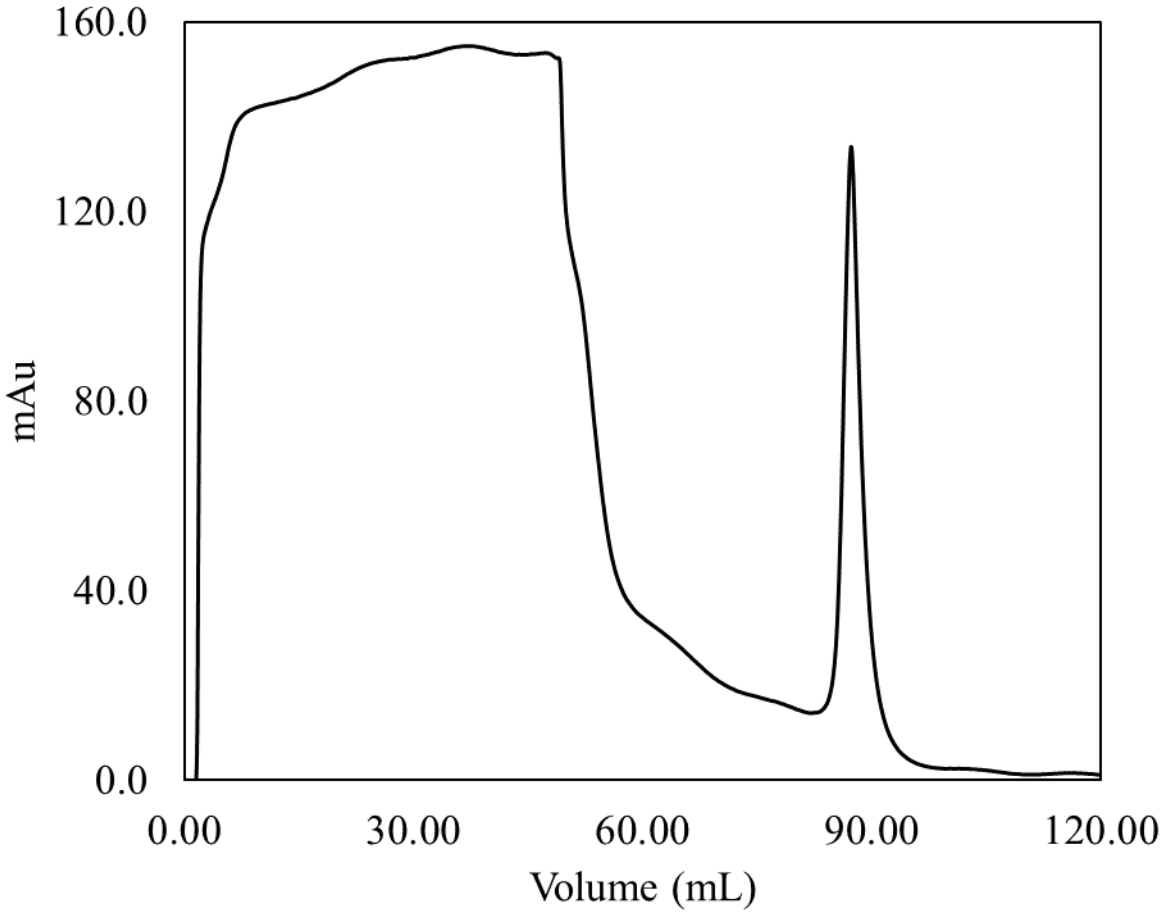

Figure 4.2 Absorbance as fraction collected of strep-tagged ChtB-WT purified on a StrepTactin column. ChtB-WT is seen as a peak between 85-95 mL. The FPLC was run at 4 °C with a linear gradient of buffer B (0-100%).

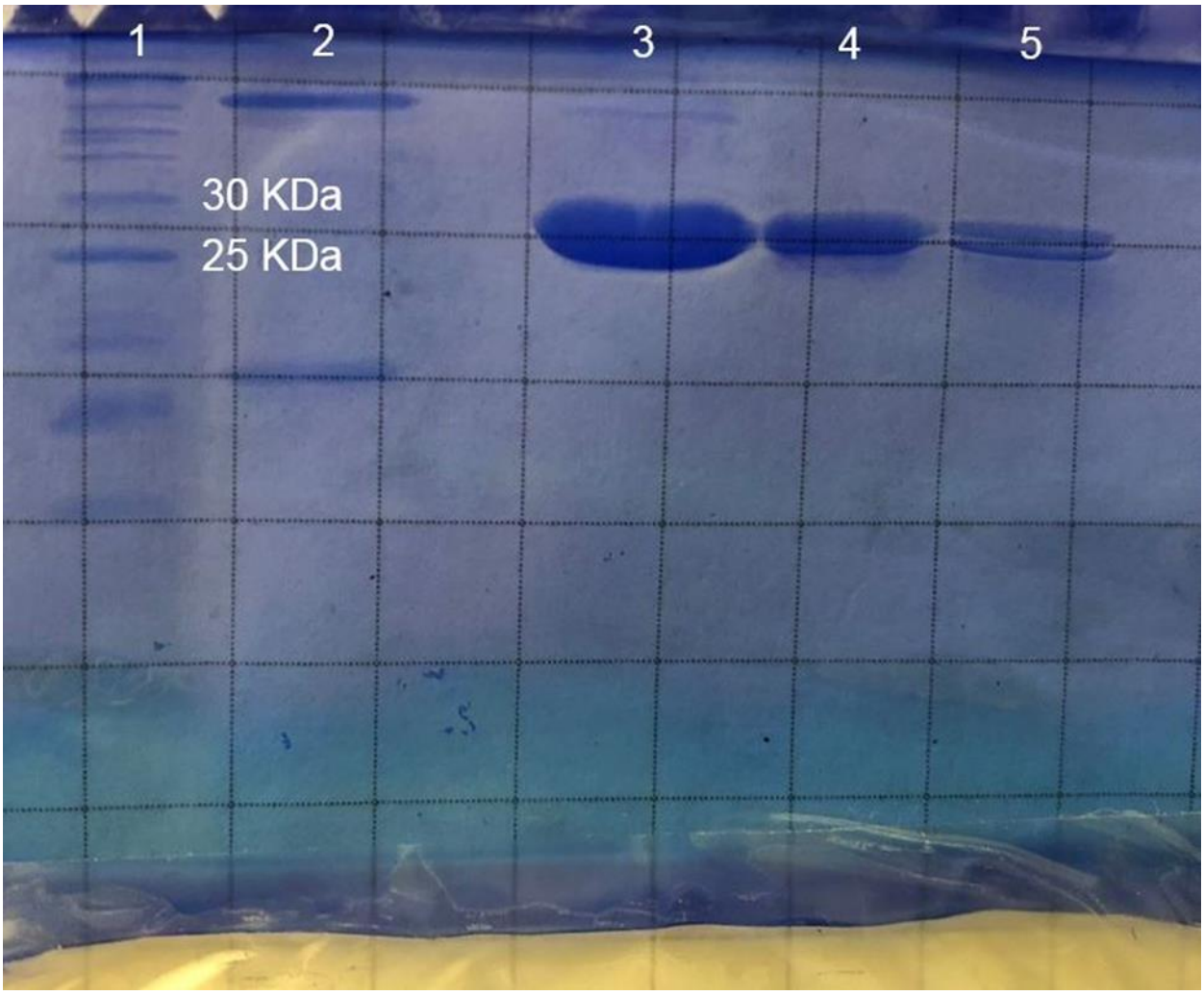

Figure 4.3 SDS PAGE of ChtB-WT after purification. Lane 1 consists of the protein ladder. Lane 2 contains both BSA (67 kDa) and myoglobin (17 KDa). Lanes 3-4 consist of varying concentrations of ChtB after purification.

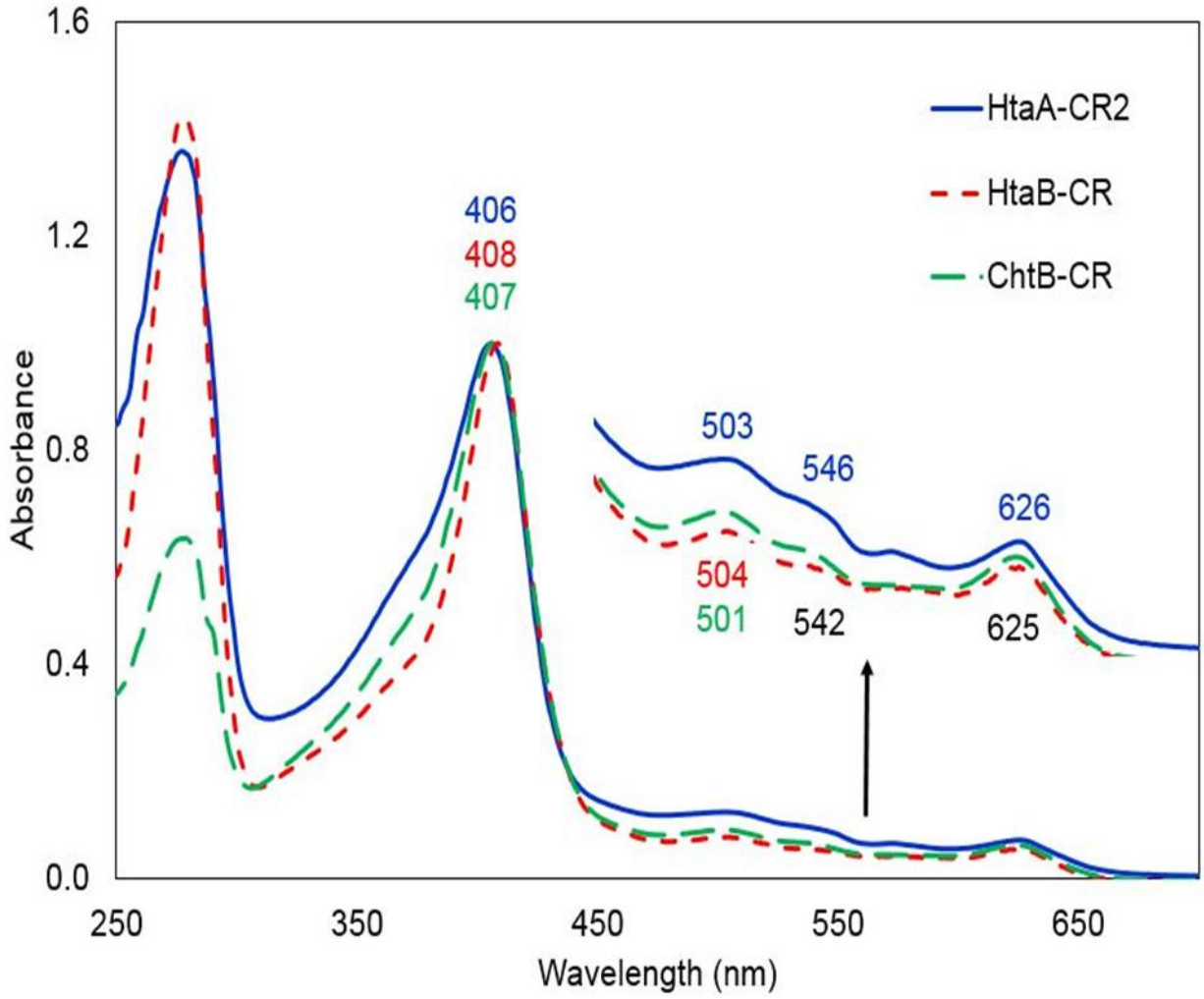

Figure 4.4 The spectra of as-isolated HtaA-CR2, HtaB-CR, and ChtB-CR overlaid. These spectra are normalized to 1.0 at the Soret. The spectra were taken buffer A at room temperature.

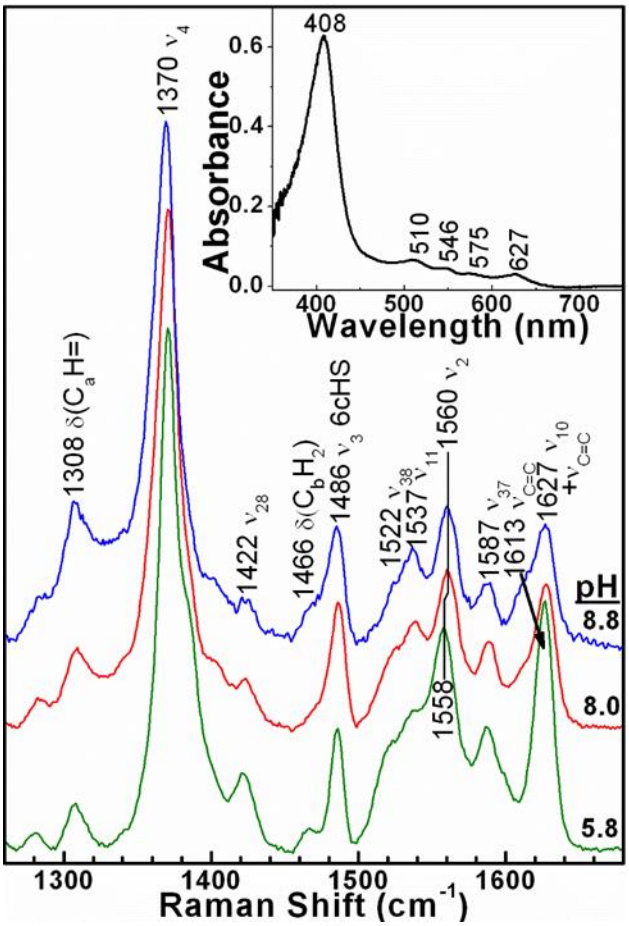

Figure 4.5 Ferric high-frequency rR of ChtB as a function of pH. Tris-HCl (pH 8.8, blue and 8.0, red) and phosphate (pH 5.8, green) buffers at 100 mM were used. The excitation wavelength from 413.1 nm from Kr ion laser with 11.4 mW of power. The $\nu_{C=C}$ band shifts under the ten band as the pH is decreased indicating a change in the interactions between the vinyl groups and the heme pocket.

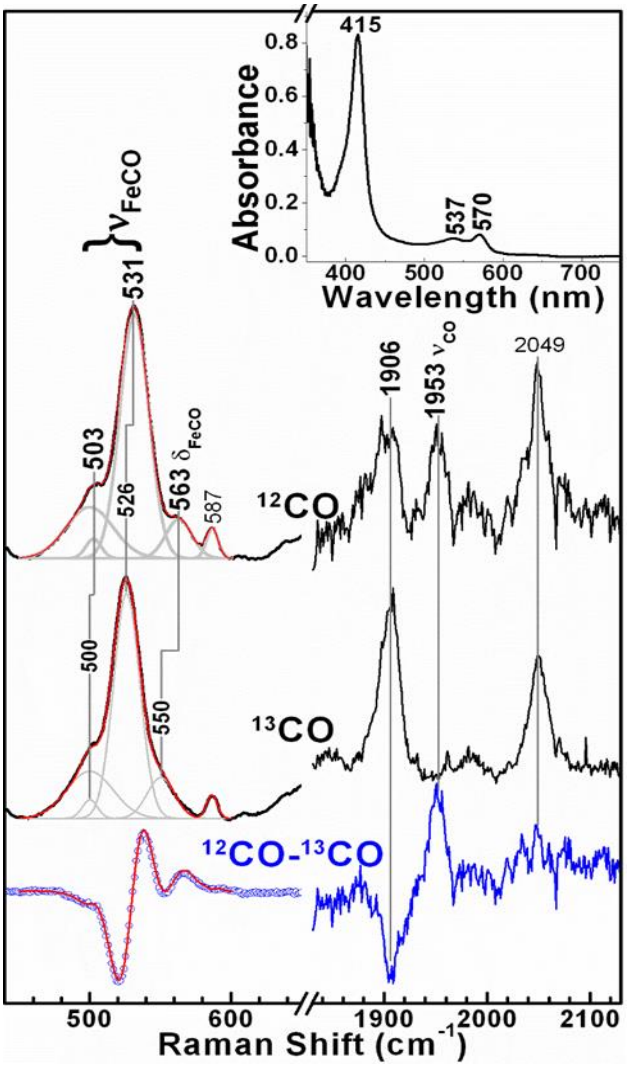

Figure 4.6 Resonance Raman spectra of the ferrous carbonyls of WT ChtB with conditions and interpretation as described in the legend of Figure 3.25.

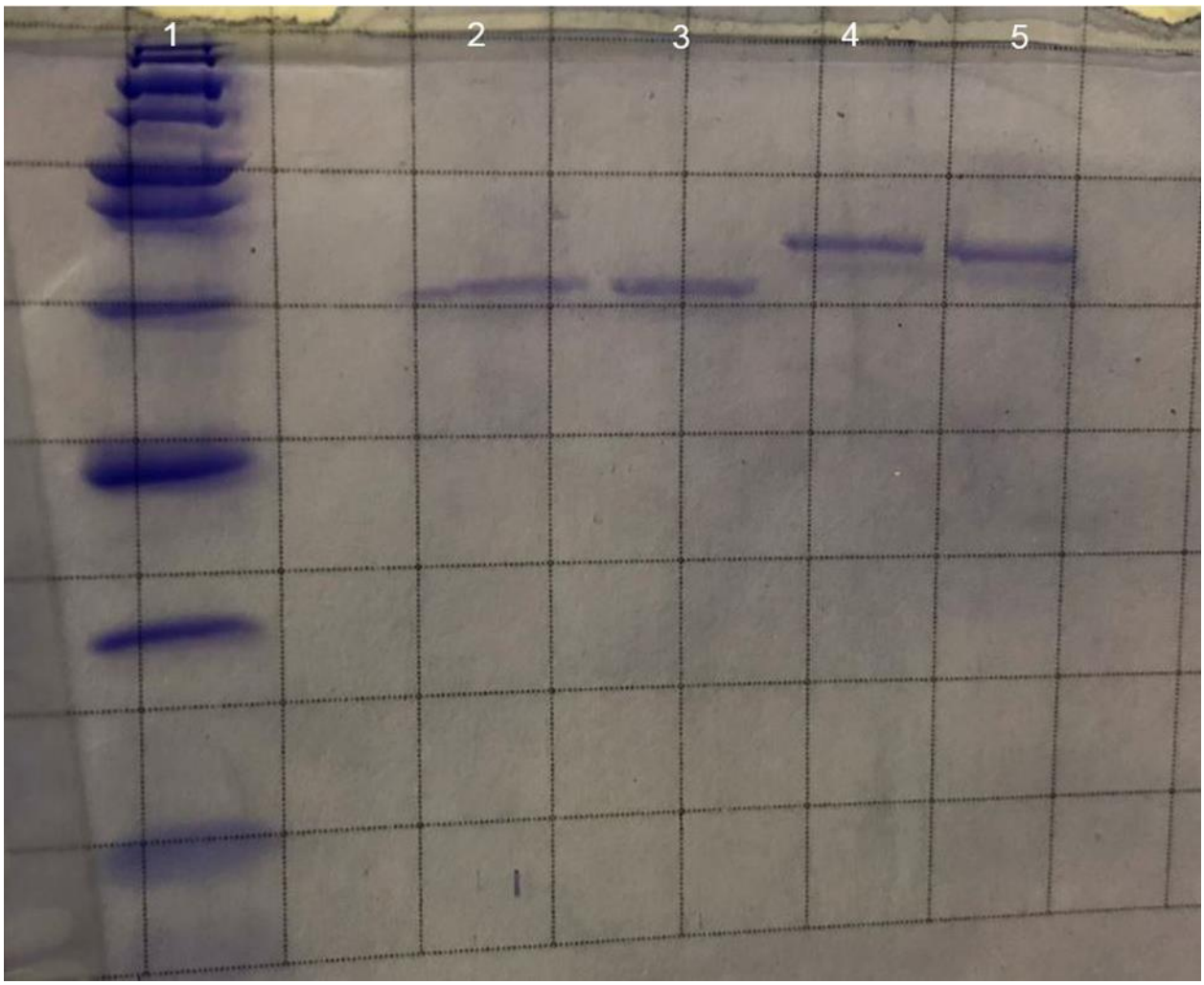

Figure 4.7 SDS PAGE of HtaB-WT and ChtB-WT after the heme transfer experiment. ChtB-WT is in lanes 2-3, and HtaB is in lanes 4-5.

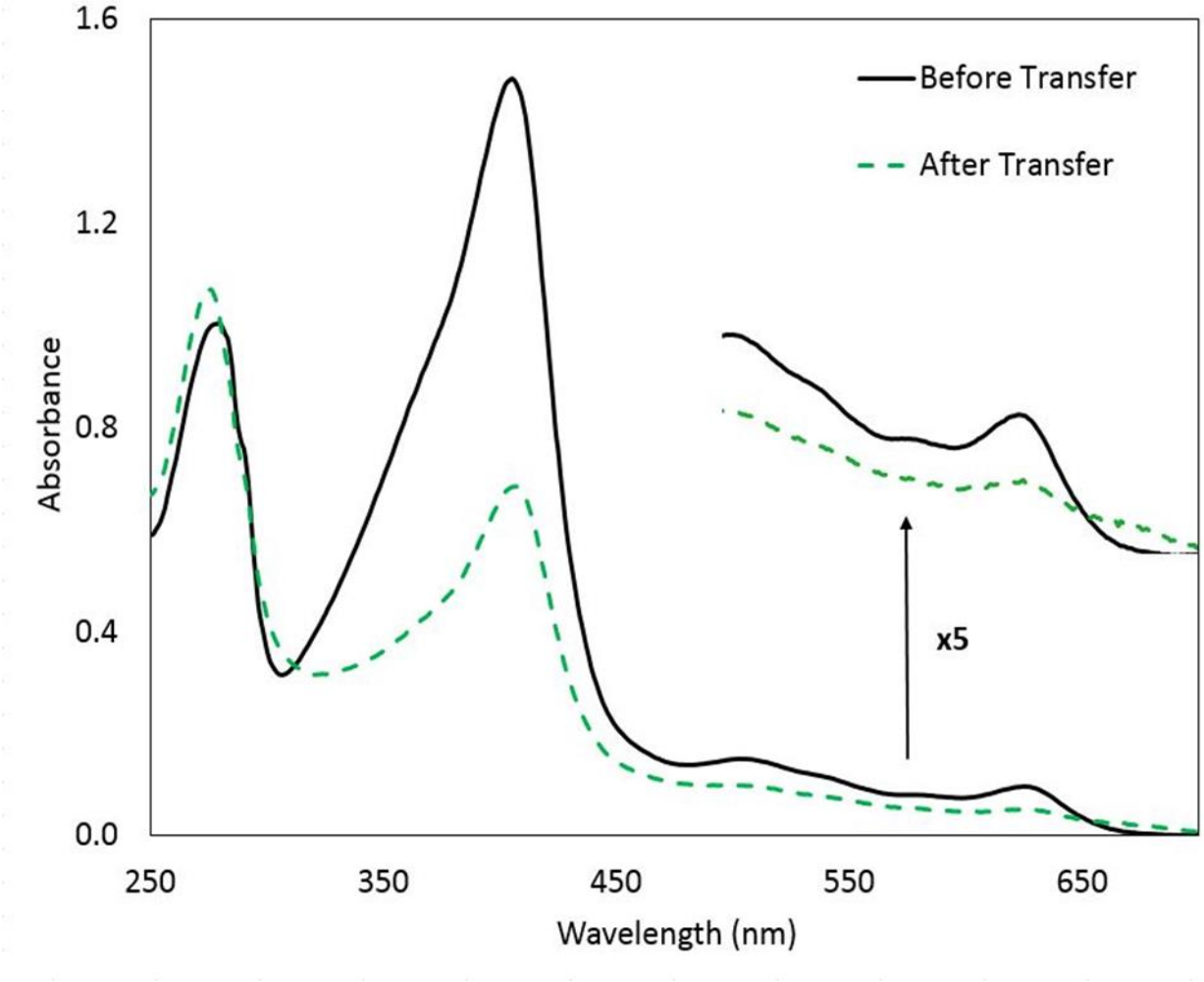

Figure 4.8 Absorbance versus wavelength of a solution of heme-loaded ChtB-WT before and after incubation with as-isolated HtaB-WT. The spectra were taken in buffer A.

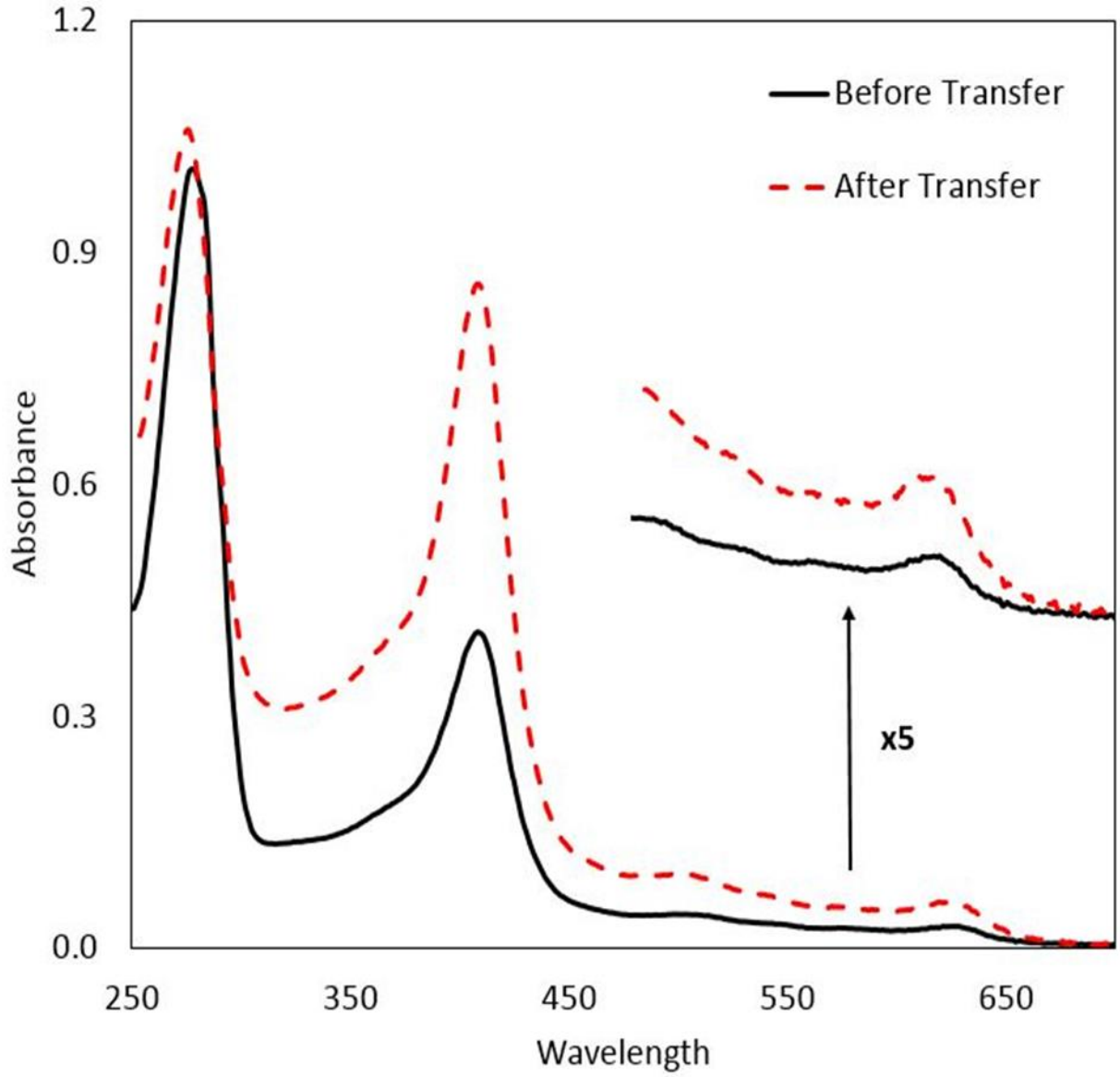

Figure 4.9 Absorbance versus wavelength of a solution of as-isolated HtaB-WT before and after incubation with heme-loaded ChtB-WT. The spectra were taken in buffer A.

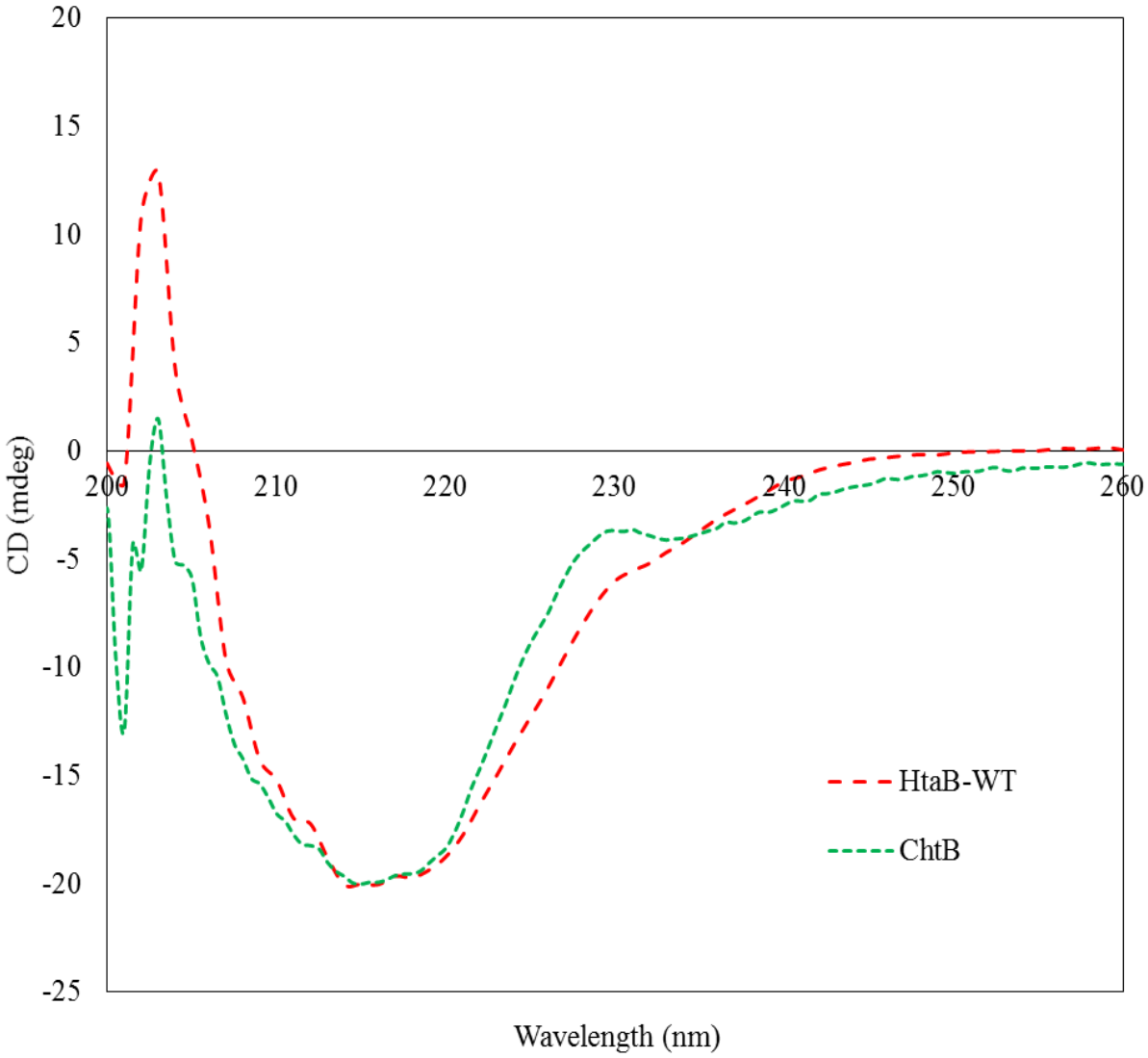

Figure 4.10 Circular dichroism spectra of as-isolated ChtB-WT and HtaB-WT normalized to -20 mdeg at 215 nm. The spectra are an average of 20 scans taken in buffer A.

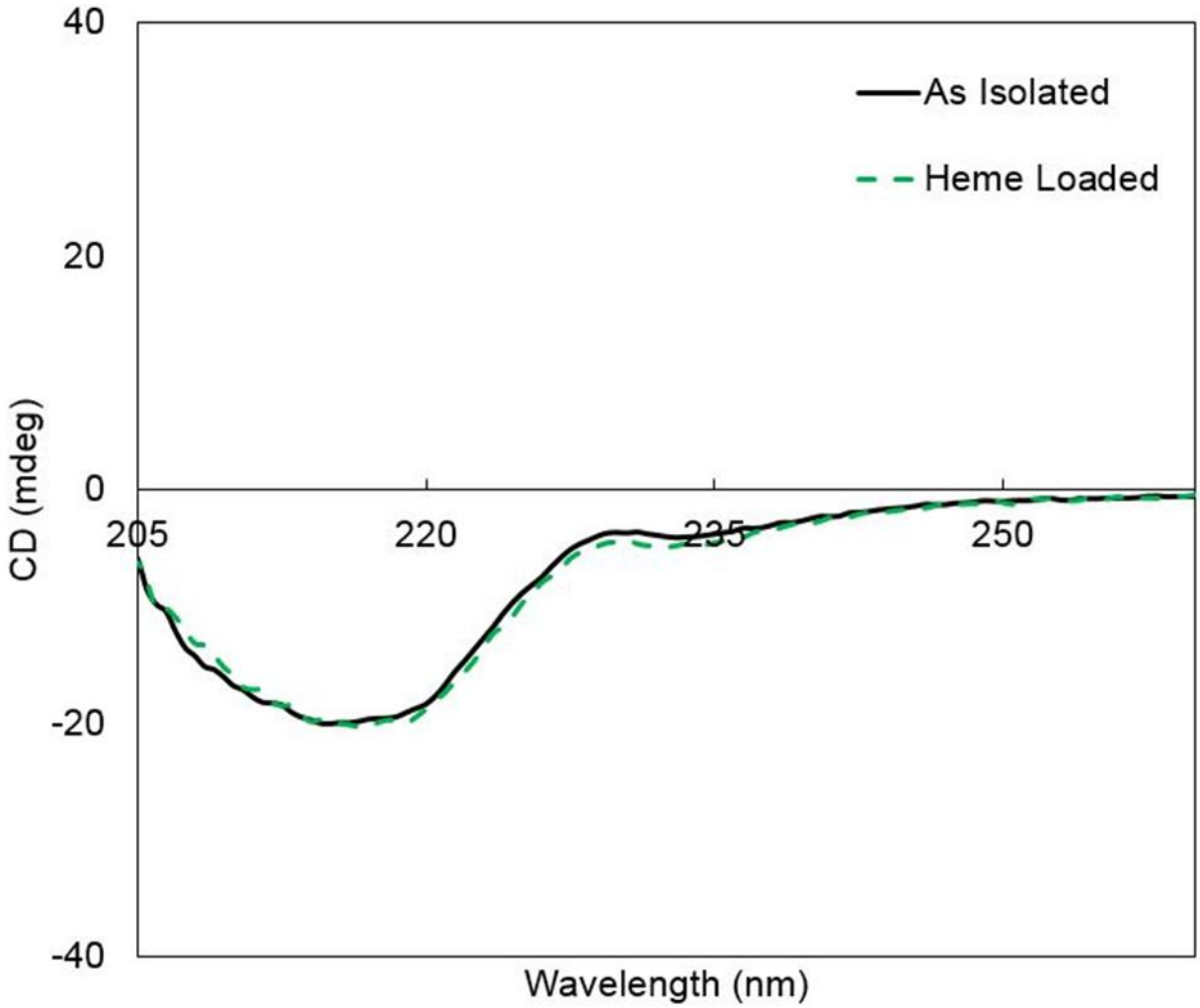

Figure 4.11 CD spectra of ChtB-WT before and after heme loading. The spectra are an average of 20 scans taken in buffer A.

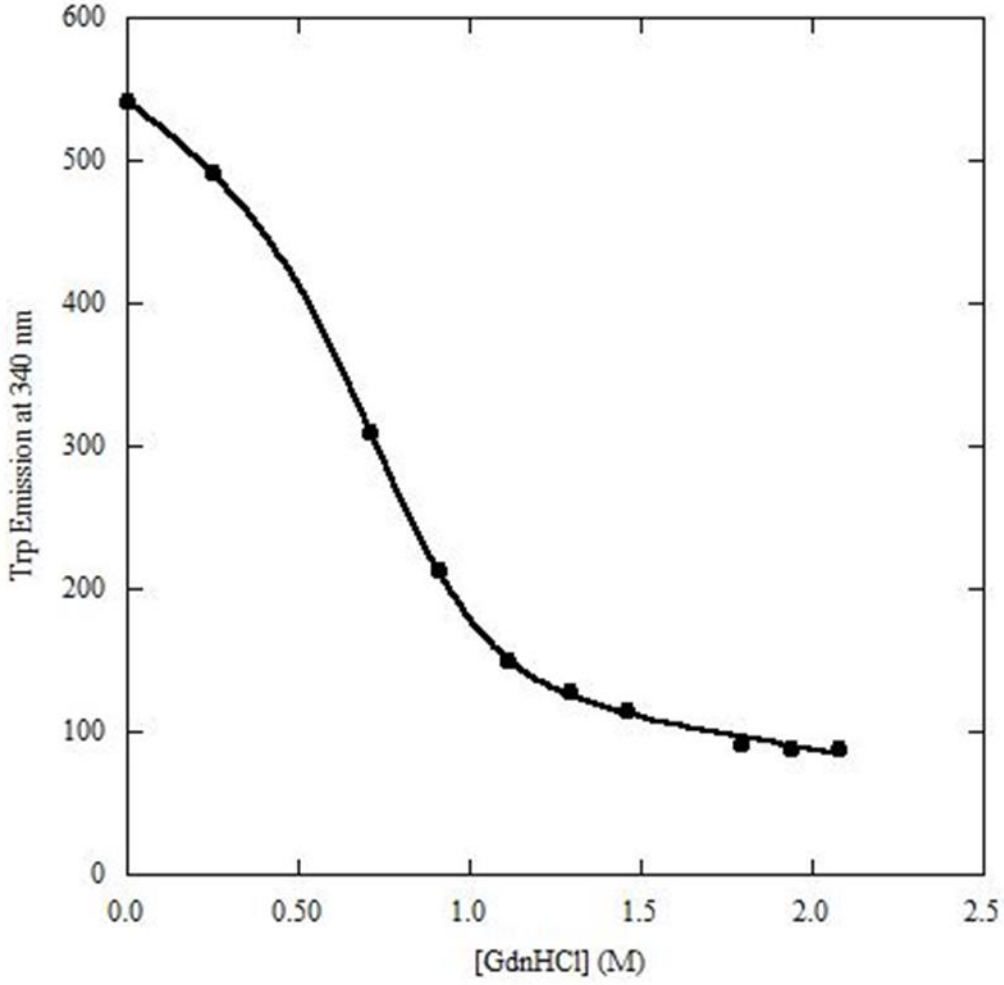

Figure 4.12 Tryptophan emission of as-isolated ChtB (30% heme loaded) as a function of GdnHCl concentration. The reaction was in 100 mM Tris-HCl, 150 mM NaCl, pH 8.0. The data points were recorded after chemical equilibration (10 min). Solid points represent the fluorescence intensity at the respective concentration of GdnHCl. The data were fit using the equation described in Section 4.2.9.

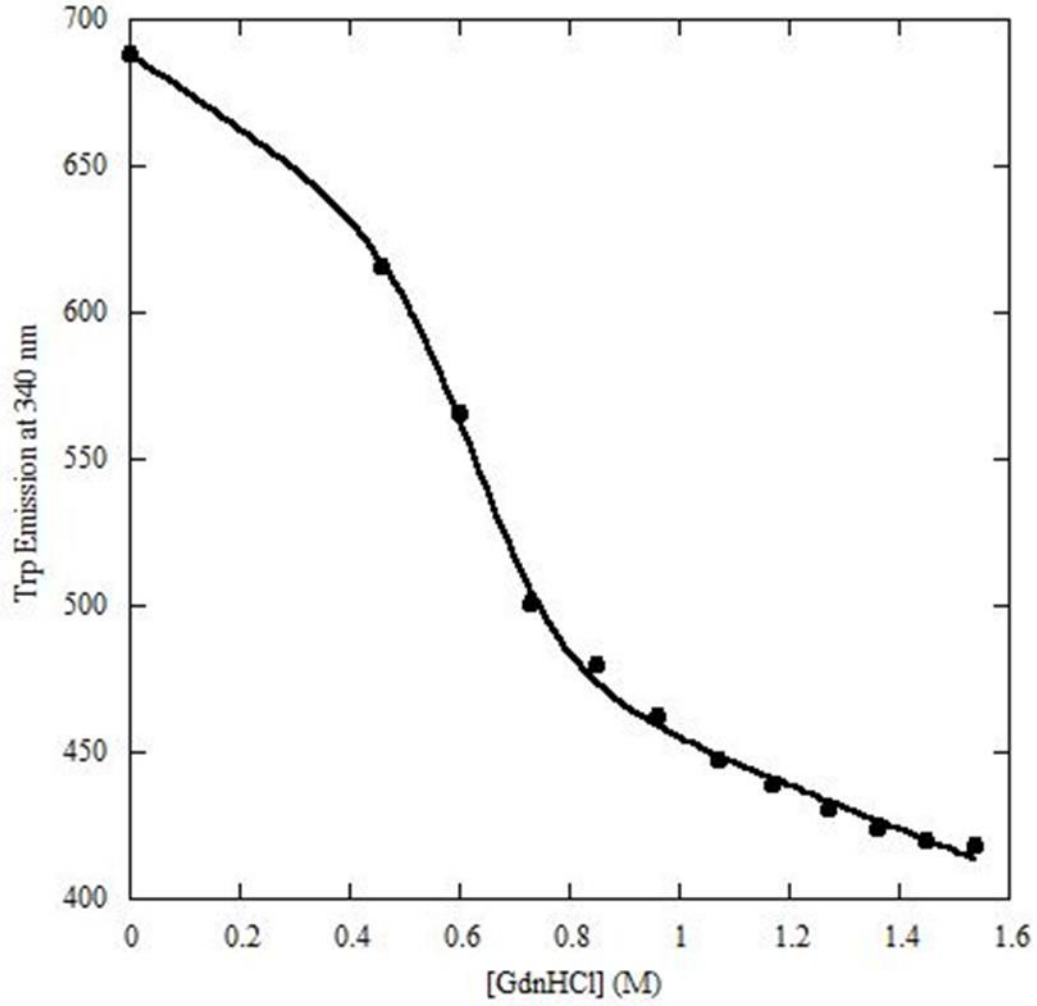

Figure 4.13 Tryptophan emission of fully heme-loaded ChtB as a function of GdnHCl concentration. The reaction was in 100 mM Tris-HCl, 150 mM NaCl, pH 8.0. The data points were recorded after chemical equilibration (10 min). Solid points represent the fluorescence intensity at the respective concentration of GdnHCl. The data were fit using the equation described in Section 4.2.9.

5 GENERAL CONCLUSIONS

Iron is an essential nutrient for many pathogenic bacteria. Invading pathogenic bacteria use the body's heme-containing proteins as sources of iron. This thesis analyzes a combination of the bioinformatics, biochemical, and biophysical properties of the HtaB and ChtB heme uptake proteins in *C. diphtheriae*.

As of this writing, a crystal structure of HtaA has not been published. There are two types of heme uptake systems utilized by Gram-positive pathogenic bacteria: the NEAT system and HtaA system. Our bioinformatics study indicates that for the two classifications of Gram-positive bacteria (Actinobacteria and Firmicutes), the Actinobacteria group utilize the HtaA system and Firmicutes utilize the NEAT system. The HtaA domains are consistently characterized by the conservation of two Tyr residues and one His residue. These domains also contain structural motifs that are similar to those found in the NEAT domains, such as the conserved SXXXY motif in the HtaA domains.

The heme uptake proteins HtaB and ChtB were previously proposed to function similarly and possibly be interchangeable for one another (Allen et al., 2013). A comparison of sequence alignments, UV-visible spectroscopy and resonance Raman studies of HtaB-WT and WT ChtB predict that both proteins utilize Tyr as the heme axial ligand. Resonance Raman data of ferrous-CO HtaB and ChtB shows that both contain two heme coordination forms: one with a Tyr *trans* to the CO group and the other with a His *trans* to the CO group. The data indicates that the first conserved Tyr and conserved His residues are near the bound heme. The Tyr-bound form of the ferrous-CO form of both HtaB and ChtB falls on the line on the resonance Raman correlation plot correlating with a single hydrogen bonding partner. These data are consistent with the

proposal that Tyr acts as the axial ligand with His acting as a hydrogen bonding partner to the Tyr.

HtaB and ChtB are nearly identical when analyzing their biochemical and biophysical properties. Both proteins have a T_m of 61°C in the presence of 1.0 M GdnHCl and both have half-lives of 39 min in the presence of 4.0 M GdnHCl at 25 °C. This substantial biophysical similarity of these proteins is consistent with their being able to substitute for one another in heme uptake, as has been proposed from microbiology studies (Allen and Schmitt, 2011; Allen et al., 2013)

The level of antibiotic resistant bacteria is continually on the rise. This makes it more difficult to treat patients infected with these pathogens. Heme uptake has been shown to play a critical role in the ability of some of these pathogens to obtain the necessary iron and survive. Due to the importance of these uptake systems in bacteria, understanding the heme uptake mechanism utilized by bacteria could allow for the development of alternative treatments for antibiotic-resistant bacteria.

REFERENCES

Akbas, N., Draganova, E.B., Block, D.R., Sook, B.R., Chan, Y.F., Zhuo, J., Eichenbaum, Z., Rodgers, K.R., Dixon, D.W., 2016. Heme-bound SiaA from *Streptococcus pyogenes*: Effects of mutations and oxidation state on protein stability. J. Inorg. Biochem. 158, 99-109.

Allen, C.E., Burgos, J.M., Schmitt, M.P., 2013. Analysis of novel iron-regulated, surface-anchored hemin-binding proteins in *Corynebacterium diphtheriae*. J. Bacteriol. 195, 2852-2863.

Allen, C.E., Schmitt, M.P., 2009. HtaA is an iron-regulated hemin binding protein involved in the utilization of heme iron in *Corynebacterium diphtheriae*. J. Bacteriol. 191, 2638-2648.

Allen, C.E., Schmitt, M.P., 2011. Novel hemin binding domains in the *Corynebacterium diphtheriae* HtaA protein interact with hemoglobin and are critical for heme iron utilization by HtaA. J. Bacteriol. 193, 5374-5385.

Allen, C.E., Schmitt, M.P., 2015. Utilization of host iron sources by *Corynebacterium diphtheriae*: Multiple hemoglobin-binding proteins are essential for the use of iron from the hemoglobin-haptoglobin complex. J. Bacteriol. 197, 553-562.

Alontaga, A.Y., Rodriguez, J.C., Schoenbrunn, E., Becker, A., Funke, T., Yukl, E.T., Hayashi, T., Stobaugh, J., Moenne-Loccoz, P., Rivera, M., 2009. Structural characterization of the hemophore HasAp from *Pseudomonas aeruginosa*: NMR spectroscopy reveals protein-protein interactions between holo-HasAp and hemoglobin. Biochemistry 48, 96-109.

Andrade, M.A., Ciccarelli, F.D., Perez-Iratxeta, C., Bork, P., 2002. NEAT: A domain duplicated in genes near the components of a putative Fe(3+) siderophore transporter from Gram-positive pathogenic bacteria. Genome Biol. 3, RESEARCH0047.

Antonini, E., Brunori, M., 1971. Hemoglobin and Myoglobin in their Reactions with Ligands. North-Holland Publishing Company, Amsterdam.

Anzaldi, L.L., Skaar, E.P., 2010. Overcoming the heme paradox: Heme toxicity and tolerance in bacterial pathogens. Infect. Immun. 78, 4977-4989.

Aranda, R., Worley, C.E., Liu, M., Bitto, E., Cates, M.S., Olson, J.S., Lei, B.F., Phillips, G.N., 2007. Bis-methionyl coordination in the crystal structure of the heme-binding domain of the streptococcal cell surface protein Shp. J. Mol. Biol. 374, 374-383.

Arnoux, P., Haser, R., Izadi, N., Lecroisey, A., Delepierre, M., Wandersman, C., Czjzek, M., 1999. The crystal structure of HasA, a hemophore secreted by *Serratia marcescens*. Nat. Struct. Biol. 6, 516-520.

Balderas, M.A., Nobles, C.L., Honsa, E.S., Alicki, E.R., Maresso, A.W., 2012. Hal is a *Bacillus anthracis* heme acquisition protein. J. Bacteriol. 194, 5513-5521.

Bassetti, M., Merelli, M., Temperoni, C., Astilean, A., 2013. New antibiotics for bad bugs: where are we? Ann. Clin. Microbiol. Antimicrob. 12.

Bates, C.S., Montañez, G.E., Woods, C.R., Vincent, R.M., Eichenbaum, Z., 2003. Identification and characterization of a *Streptococcus pyogenes* operon involved in binding of hemoproteins and acquisition of iron. Infect. Immun. 71, 1042-1055.

Benson, D.R., Rivera, M., 2013. Heme uptake and metabolism in bacteria. Met. Ions Life Sci. 12, 279-332.

Berry, E.A., Trumpower, B.L., 1987. Simultaneous determination of hemes *a*, *b*, and *c* from pyridine hemochrome spectra. Anal. Biochem. 161, 1-15.

Bibb, L.A., King, N.D., Kunkle, C.A., Schmitt, M.P., 2005. Analysis of a heme-dependent signal transduction system in *Corynebactetium diphtheriae*: Deletion of the chrA/S

genes results in heme sensitivity and diminished heme-dependent activation of the *hmuO* promoter. Infect. Immun. 73, 7406-7412.

Braun, V., Hantke, K., 2011. Recent insights into iron import by bacteria. Curr. Opin. Chem. Biol. 15, 328-334.

Brewitz, H.H., Goradia, N., Schubert, E., Galler, K., Kuhl, T., Syllwasschy, B., Popp, J., Neugebauer, U., Hagelueken, G., Schiemann, O., Ohlenschlager, O., Imhof, D., 2016. Heme interacts with histidine- and tyrosine-based protein motifs and inhibits enzymatic activity of chloramphenicol acetyltransferase from *Escherichia coli*. Biochimica Et Biophysica Acta-General Subjects 1860, 1343-1353.

Caillet-Saguy, C., Turano, P., Piccioli, M., Lukat-Rodgers, G.S., Czjzek, M., Guigliarelli, B., Izadi-Pruneyre, N., Rodgers, K.R., Delepierre, M., Lecroisey, A., 2008. Deciphering the structural role of histidine 83 for heme binding in hemophore HasA. J. Biol. Chem. 283, 5960-5970.

Chuang, W.J., Johnson, S., Van Wart, H.E., 1988. Resonance Raman spectra of bovine liver catalase: Enhancement of proximal tyrosinate vibrations. J. Inorg. Biochem. 34, 201-219.

Contreras, H., Chim, N., Credali, A., Goulding, C.W., 2014. Heme uptake in bacterial pathogens. Curr. Opin. Chem. Biol. 19, 34-41.

Cunningham, M.W., 2008. Pathogenesis of group A streptococcal infections and their sequelae. Adv. Exp. Med. Biol 609, 29-42.

DeLano, W., L., 2015. The PyMOL Molecular Graphics System, Version 1.7.4 Schrödinger, LLC. http://www. pymol. org.

Draganova, E.B., Adrian, S.A., Lukat-Rodgers, G.S., Keutcha, C.S., Schmitt, M.P., Rodgers, K.R., Dixon, D.W., 2016. *Corynebacterium diphtheriae* HmuT: Dissecting the roles of conserved residues in heme pocket stabilization. J. Biol. Inorg. Chem. 21, 875-886.

Draganova, E.B., Akbas, N., Adrian, S.A., Lukat-Rodgers, G.S., Collins, D.P., Dawson, J.H., Schmitt, M.P., Rodgers, K.R., Dixon, D.W., 2015. Heme binding by *Corynebacterium diphtheriae* HmuT: Function and heme environment. Biochemistry 54, 6598-6609.

Drazek, E.S., Hammack, C.A., Schmitt, M.P., 2000. *Corynebacterium diphtheriae* genes required for acquisition of iron from haemin and haemoglobin are homologous to ABC haemin transporters. Mol. Microbiol. 36, 68-84.

Du, J., Sono, M., Dawson, J.H., 2011. The H93G myoglobin cavity mutant as a versatile scaffold for modeling heme iron coordination structures in protein active sites and their characterization with magnetic circular dichroism spectroscopy. Coord. Chem. Rev. 255, 700-716.

Eakanunkul, S., Lukat-Rodgers, G.S., Sumithran, S., Ghosh, A., Rodgers, K.R., Dawson, J.H., Wilks, A., 2005. Characterization of the periplasmic heme-binding protein ShuT from the heme uptake system of *Shigella dysenteriae*. Biochemistry 44, 13179-13191.

Edelstein, S.J., Rehmar, M.J., Olson, J.S., Gibson, Q.H., 1970. Functional aspects of the subunit association-dissociation equilibria of hemoglobin. J. Biol. Chem. 245, 4372-4381.

Eichenbaum, Z., 2012. The streptococcal hemoprotein receptor. A moonlighting protein or a virulence factor? Virulence 3, 553-555.

Ekworomadu, M.T., Poor, C.B., Owens, C.P., Balderas, M.A., Fabian, M., Olson, J.S., Murphy, F., Balkabasi, E., Honsa, E.S., He, C., Goulding, C.W., Maresso, A.W., 2012. Differential function of lip residues in the mechanism and biology of an anthrax hemophore. PLoS Pathog. 8.

Farrand, A.J., Skaar, E.P., 2014. Heme and infectious diseases, in: Ferreira, G.C., Kadish, K.M., Smith, K.M., Guilard, R. (Eds.), Handbook of Porphyrin Science with Applications to Chemistry, Physics, Materials Science, Engineering, Biology and Medicine, Vol 26: Heme Biochemistry. World Scientific, Hackensack, NJ, pp. 317-377.

Fermi, G., Perutz, M.F., 1981. Haemoglobin and myoglobin. Clarendon Press, Oxford.

Gaudin, C.F.M., Grigg, J.C., Arrieta, A.L., Murphy, M.E.P., 2011. Unique heme-iron coordination by the hemoglobin receptor IsdB of *Staphylococcus aureus*. Biochemistry 50, 5443-5452.

Grigg, J.C., Ukpabi, G., Gaudin, C.F., Murphy, M.E., 2010. Structural biology of heme binding in the *Staphylococcus aureus* Isd system. J. Inorg. Biochem. 104, 341-348.

Grigg, J.C., Vermeiren, C.L., Heinrichs, D.E., Murphy, M.E., 2007. Heme coordination by *Staphylococcus aureus* IsdE. J. Biol. Chem. 282, 28815-28822.

Grinshtein, N., Bamm, V.V., Tsemakhovich, V.A., Shaklai, N., 2003. Mechanism of low-density lipoprotein oxidation by hemoglobin-derived iron. Biochemistry 42, 6977-6985.

Honsa, E.S., Fabian, M., Cardenas, A.M., Olson, J.S., Maresso, A.W., 2011. The five near-iron transporter (NEAT) domain anthrax hemophore, IsdX2, scavenges heme from hemoglobin and transfers heme to the surface protein IsdC. J. Biol. Chem. 286, 33652-33660.

Honsa, E.S., Johnson, M.D.L., Rosch, J.W., 2013a. The roles of transition metals in the physiology and pathogenesis of *Streptococcus pneumoniae*. Front. Cell. Infect. Microbiol. 3.

Honsa, E.S., Maresso, A.W., Highlander, S.K., 2014. Molecular and evolutionary analysis of NEAr-iron Transporter (NEAT) domains. PLoS One 9.

Honsa, E.S., Owens, C.P., Goulding, C.W., Maresso, A.W., 2013b. The near-iron transporter (NEAT) domains of the anthrax hemophore IsdX2 require a critical glutamine to extract heme from methemoglobin. J. Biol. Chem. 288, 8479-8490.

Hu, S.H., Kincaid, J.R., 1992. Resonance Raman studies of the carbonmonoxy form of catalase - Evidence for and effects of phenolate ligation. FEBS Lett. 314, 293-296.

Hu, S.Z., Smith, K.M., Spiro, T.G., 1996. Assignment of protoheme resonance Raman spectrum by heme labeling in myoglobin. J. Am. Chem. Soc. 118, 12638-12646.

Kristiansen, M., Graversen, J.H., Jacobsen, C., Sonne, O., Hoffman, H.J., Law, S.K.A., Moestrup, S.K., 2001. Identification of the haemoglobin scavenger receptor. Nature 409, 198-201.

Kumar, R., Lovell, S., Matsumura, H., Battaile, K.P., Moenne-Loccoz, P., Rivera, M., 2013. The hemophore HasA from *Yersinia pestis* ($HasA_{yp}$) coordinates hemin with a single residue, Tyr75, and with minimal conformational change. Biochemistry 52, 2705-2707.

Lei, B.F., Liu, M.Y., Prater, C.I., Kala, S.V., Deleo, F.R., Musser, J.M., 2003. Identification and characterization of HtsA, a second heme-binding protein made by *Streptococcus pyogenes*. Infect. Immun. 71, 5962-5969.

Li, T., Bonkovsky, H.L., Guo, J.T., 2011. Structural analysis of heme proteins: Implications for design and prediction. BMC Struct. Biol. 11.

Li, W.Z., Cowley, A., Uludag, M., Gur, T., McWilliam, H., Squizzato, S., Park, Y.M., Buso, N., Lopez, R., 2015. The EMBL-EBI bioinformatics web and programmatic tools framework. Nucleic Acids Res. 43, W580-W584.

Lu, C.M., Xie, G., Liu, M.Y., Zhu, H., Lei, B.F., 2012. Direct heme transfer reactions in the group A *Streptococcus* heme acquisition pathway. PLoS One 7.

Lukat-Rodgers, G.S., Rodgers, K.R., Caillet-Saguy, C., Izadi-Pruneyre, N., Lecroisey, A., 2008. Novel heme ligand displacement by CO in the soluble hemophore HasA and its proximal ligand mutants: Implications for heme uptake and release. Biochemistry 47, 2087-2098.

Müller-Hill, B., 1996. The lac Operon: A Short History of a Genetic Paradigm. Walter de Gruyter, Berlin ; New York.

Muraki, N., Aono, S., 2015. Structural basis for heme recognition by HmuT responsible for heme transport to the heme transporter in *Corynebacterium glutamicum*. Chem. Lett. 45, 24-26.

Naoe, Y., Nakamura, N., Rahman, M.M., Tosha, T., Nagatoishi, S., Tsumoto, K., Shiro, Y., Sugimoto, H., 2017. Structural basis for binding and transfer of heme in bacterial heme-acquisition systems. Proteins-Structure Function and Bioinformatics 85, 2217-2230.

Nobles, C.L., Maresso, A.W., 2011. The theft of host heme by Gram-positive pathogenic bacteria. Metallomics 3, 788-796.

Nygaard, T.K., Blouin, G.C., Liu, M.Y., Fukumura, M., Olson, J.S., Fabian, M., Dooley, D.M., Lei, B.F., 2006. The mechanism of direct heme transfer from the streptococcal cell surface protein Shp to HtsA of the HtsABC transporter. J. Biol. Chem. 281, 20761-20771.

Ouattara, M., Cunha, E.B., Li, X., Huang, Y.S., Dixon, D.W., Eichenbaum, Z., 2010. Shr of Group A streptococcus is a new type of composite NEAT protein involved in sequestering haem from methaemoglobin. Mol. Microbiol. 78, 739-756.

Ouattara, M., Pennati, A., Devlin, D.J., Huang, Y.S., Gadda, G., Eichenbaum, Z., 2013. Kinetics of heme transfer by the Shr NEAT domains of Group A Streptococcus. Arch. Biochem. Biophys. 538, 71-79.

Owens, C.P., Du, J., Dawson, J.H., Goulding, C.W., 2012. Characterization of heme ligation properties of Rv0203, a secreted heme binding protein involved in *Mycobacterium tuberculosis* heme uptake. Biochemistry 51, 1518-1531.

Ozaki, S., Sato, T., Sekine, Y., Migita, C.T., Uchida, T., Ishimori, K., 2014. Spectroscopic studies on HasA from *Yersinia pseudotuberculosis*. J. Inorg. Biochem. 138, 31-38.

Pace, C.N., Scholtz, J.M., 1997. Measuring the conformational stability of a protein, in: Creighton, T. (Ed.), Protein Structure: A Practical Approach, 2nd ed. Oxford University Press, Oxford, pp. 299-321.

Pilpa, R.M., Fadeev, E.A., Villareal, V.A., Wong, M.L., Phillips, M., Clubb, R.T., 2006. Solution structure of the NEAT (NEAr Transporter) domain from IsdH/HarA: The human hemoglobin receptor in *Staphylococcus aureus*. J. Mol. Biol. 360, 435-447.

Pilpa, R.M., Robson, S.A., Villareal, V.A., Wong, M.L., Phillips, M., Clubb, R.T., 2009. Functionally distinct NEAT (NEAr Transporter) domains within the *Staphylococcus aureus* IsdH/HarA protein extract heme from methemoglobin. J. Biol. Chem. 284, 1166-1176.

Rodgers, K.R., Lukat-Rodgers, G.S., 2014. Biophysical perspectives on the acquisition, transport, and trafficking of heme in bacteria, in: Ferreira, G.C., Kadish, K.M., Smith, K.M., Guilard, R. (Eds.), Handbook of Porphyrin Science with Applications to Chemistry, Physics, Materials Science, Engineering, Biology and Medicine, Vol. 30: Heme Proteins, Part II. World Scientific, Hackensack, N.J, pp. 251-309.

Rosano, G.L., Ceccarelli, E.A., 2014. Recombinant protein expression in *Escherichia coli*: Advances and challenges. Front Microbiol 5, 172.

Sachla, A.J., Le Breton, Y., Akhter, F., Mciver, K.S., Eichenbaum, Z., 2014. The crimson conundrum: Heme toxicity and tolerance in GAS. Front. Cell. Infect. Microbiol. 4.

Schmitt, M.P., Drazek, E.S., 2001. Construction and consequences of directed mutations affecting the hemin receptor in pathogenic *Corynebacterium species*. J. Bacteriol. 183, 1476-1481.

Schneider, S., Marles-Wright, J., Sharp, K.H., Paoli, M., 2007. Diversity and conservation of interactions for binding heme in *b*-type heme proteins. Nat. Prod. Rep. 24, 621-630.

Sharp, K.H., Schneider, S., Cockayne, A., Paoli, M., 2007. Crystal structure of the heme-IsdC complex, the central conduit of the Isd iron/heme uptake system in *Staphylococcus aureus*. J. Biol. Chem. 282, 10625-10631.

Sheldon, J.R., Heinrichs, D.E., 2015. Recent developments in understanding the iron acquisition strategies of gram positive pathogens. FEMS Microbiol. Rev. 39, 592-630.

Sievers, F., Wilm, A., Dineen, D., Gibson, T.J., Karplus, K., Li, W.Z., Lopez, R., McWilliam, H., Remmert, M., Soding, J., Thompson, J.D., Higgins, D.G., 2011. Fast, scalable generation of high-quality protein multiple sequence alignments using Clustal Omega. Mol. Syst. Biol. 7.

Silverstone, A.E., Arditti, R.R., Magasanik, B., 1970. Catabolite-insensitive revertants of lac promoter mutants. Proc. Natl. Acad. Sci. U. S. A. 66, 773-779.

Smith, A.D., Wilks, A., 2012. Extracellular heme uptake and the challenges of bacterial cell membranes. Curr. Top. Membr. 69, 359-392.

Smith, L.J., Kahraman, A., Thornton, J.M., 2010. Heme proteins - Diversity in structural characteristics, function, and folding. Proteins-Structure Function and Bioinformatics 78, 2349-2368.

Smulevich, G., Mauro, J.M., Fishel, L.A., English, A.M., Kraut, J., Spiro, T.G., 1988. Cytochrome *c* peroxidase mutant active site structures probed by resonance Raman and infrared signatures of the CO adducts. Biochemistry 27, 5486-5492.

Sook, B.R., Block, D.R., Sumithran, S., Montañez, G.E., Rodgers, K.R., Dawson, J.H., Eichenbaum, Z., Dixon, D.W., 2008. Characterization of SiaA, a streptococcal heme-binding protein associated with a heme ABC transport system. Biochemistry 47, 2678-2688.

Spiro, T.G., Soldatova, A.V., Balakrishnan, G., 2013. CO, NO and O_2 as vibrational probes of heme protein interactions. Coord. Chem. Rev. 257, 511-527.

Spiro, T.G., Wasbotten, I.H., 2005. CO as a vibrational probe of heme protein active sites. J. Inorg. Biochem. 99, 34-44.

Stano, N.M., Patel, S.S., 2004. T7 lysozyme represses T7 RNA polymerase transcription by destabilizing the open complex during initiation. J. Biol. Chem. 279, 16136-16143.

Streit, B.R., Blanc, B., Lukat-Rodgers, G.S., Rodgers, K.R., DuBois, J.L., 2010. How active-site protonation state influences the reactivity and ligation of the heme in chlorite dismutase. J. Am. Chem. Soc. 132, 5711-5724.

Studier, F.W., Moffatt, B.A., 1986. Use of bacteriophage T7 RNA polymerase to direct selective high-level expression of cloned genes. J. Mol. Biol. 189, 113-130.

Sun, X., Ge, R., Zhang, D., Sun, H., He, Q.Y., 2010. Iron-containing lipoprotein SiaA in SiaABC, the primary heme transporter of *Streptococcus pyogenes*. J. Biol. Inorg. Chem. 15, 1265-1273.

Swint, L., Robertson, A.D., 1993. Thermodynamics of unfolding for turkey ovomucoid third domain: Thermal and chemical denaturation. Protein Sci. 2, 2037-2049.

Tam, R., Saier, M.H., 1993. Structural, functional, and evolutionary relationships among extracellular solute-binding receptors of bacteria. Microbiol. Rev 57, 320-346.

Tiedemann, M.T., Stillman, M.J., 2011. Application of magnetic circular dichroism spectroscopy to porphyrins, phthalocyanines and hemes. J. Porph. Phthalo. 15, 1134-1149.

Tong, Y., Guo, M., 2009. Bacterial heme-transport proteins and their heme-coordination modes. Arch. Biochem. Biophys. 481, 1-15.

Trost, E., Blom, J., Soares, S.D., Huang, I.H., Al-Dilaimi, A., Schroder, J., Jaenicke, S., Dorella, F.A., Rocha, F.S., Miyoshi, A., Azevedo, V., Schneider, M.P., Silva, A., Camello, T.C., Sabbadini, P.S., Santos, C.S., Santos, L.S., Hirata, R., Mattos-Guaraldi, A.L., Efstratiou, A., Schmitt, M.P., Hung, T.T., Tauch, A., 2012. Pangenomic study of *Corynebacterium diphtheriae* that provides insights into the genomic diversity of pathogenic isolates from cases of classical diphtheria, endocarditis, and pneumonia. J. Bacteriol. 194, 3199-3215.

Uluisik, R.C., Akbas, N., Lukat-Rodgers, G.S., Adrian, S.A., Allen, C.E., Schmitt, M.P., Rodgers, K.R., Dixon, D.W., 2017. Characterization of the second conserved domain in the heme uptake protein HtaA from Corynebacterium diphtheriae. J. Inorg. Biochem. 167, 124-133.

Vogel, K.M., Kozlowski, P.M., Zgierski, M.Z., Spiro, T.G., 2000. Role of the axial ligand in heme-CO backbonding; DFT analysis of vibrational data. Inorg. Chim. Acta 297, 11-17.

Wardell, M., Wang, Z.M., Ho, J.X., Robert, J., Rüker, F., Ruble, J., Carter, D.C., 2002. The atomic structure of human methemalbumin at 1.9 Å. Biochem. Biophys. Res. Commun. 291, 813-819.

Watanabe, M., Tanaka, Y., Suenaga, A., Kuroda, M., Yao, M., Watanabe, N., Arisaka, F., Ohta, T., Tanaka, I., Tsumoto, K., 2008. Structural basis for multimeric heme complexation through a specific protein-heme interaction - The case of the third NEAT domain of IsdH from Staphylococcus aureus. J. Biol. Chem. 283, 28649-28659.

Wilks, A., Ikeda-Saito, M., 2014. Heme utilization by pathogenic bacteria: Not all pathways lead to biliverdin. Acc. Chem. Res. 47, 2291-2298.

Wilks, A., O'Neill, M.J., 2014. Extracellular heme uptake and metabolism in bacterial pathogenesis, in: Ferreira, G.C., Kadish, K.M., Smith, K.M., Guilard, R. (Eds.), Handbook of Porphyrin Science with Applications to Chemistry, Physics, Materials Science, Engineering, Biology and Medicine, Vol 26: Heme Biochemistry. World Scientific, Hackensack, NJ, pp. 267-315.

Yang, J.Y., Yan, R.X., Roy, A., Xu, D., Poisson, J., Zhang, Y., 2015. The I-TASSER Suite: Protein structure and function prediction. Nature Methods 12, 7-8.

Zunszain, P.A., Ghuman, J., Komatsu, T., Tsuchida, E., Curry, S., 2003. Crystal structural analysis of human serum albumin complexed with hemin and fatty acid. BMC Struct. Biol 3, 6.